Andean Geology 51 (1): 1-62. January, 2024
doi: 10.5027/andgeoV51n1-3633

Andean Geology
www.andeangeology.cl

Tracing hotspot traces in the Andes

Rex H. Pilger, Jr.[1]

[1] *Independent Researcher, 10630 W 66th Avenue, Arvada, Colorado 80004, United States of America.*
rexpilger@yahoo.com

ABSTRACT. Two segments of subduction of the Nazca plate beneath the South American plate occur at low angles based on seismic hypocenter locations, approaching nearly horizontal below ~100 km in depth. In contrast with most of the rest of the subduction zone, the two segments, beneath central Chile, and central and northern Peru, lack active volcanoes along the crest of the Andes and have more subdued topography to the east of the Andean crest. Each low-angle subduction segment occurs to the east of the intersection of inferred mantle hotspot traces on the Nazca plate with the Peru-Chile Trench: the Nazca ridge (at the southern part of the Peruvian segment), and the Juan Fernández island-seamount chain (offshore the Chilean segment). A third inferred trace, the Galápagos-Carnegie ridge, may be correlated with a zone on incipient low-angle subduction beneath Colombia.

The importance of such hotspot traces in contributing to low-angle subduction beneath the Andes is strengthened by updated South American-Nazca plate reconstructions, including three oceanic hotspot traces, in comparison with a new isotopic date compilation of igneous rocks from the mountain range. The Juan Fernández hotspot trace, reconstructed from Pacific-hotspot models to the Nazca-Farallon plate, encountered the subduction zone offshore southern Peru ~65 Ma, broadening arc volcanism to the east; the trace-trench intersection migrated gradually and then rapidly southward, widening the arc east to Bolivia and northern Argentina; it then stabilized about 13 Ma offshore central Chile, producing the contemporary low-angle Pampean segment. The Juan Fernández hotspot may also have been responsible for formation of the Manihiki Plateau on the Pacific plate much earlier, ~125 Ma. The Easter-Nazca hotspot trace intersected the subduction zone beneath Colombia before ~50 Ma and migrated southward beneath Ecuador beginning ~15 Ma, with progressive low-angle subduction implied by migrating volcanic cessation along the Andean crest to southern Peru. The Galápagos-Carnegie hotspot trace only recently encountered the subduction zone, apparently inducing a new low-angle segment and cessation of magmatism in Colombia. The reconstructions and magmatic history provided here strongly support a previously proposed genetic relationship of hotspot traces and low-angle subduction. Additionally, the reconstructions suggest remnants of older subducted traces in the asthenosphere may have sourced post-rift magmatism in eastern Brazil and Paraguay, which cannot be explained otherwise by simple hotspot mechanisms.

Keywords: Andes, Subduction, Volcanism, Hotspots, Plate reconstructions.

RESUMEN. Detección de rastros de puntos calientes en los Andes. La placa de Nazca, en su encuentro con la placa Sudamericana, presenta dos segmentos de subducción de bajo ángulo, ubicados en Chile central y el norte y centro de Perú. A diferencia del resto de la zona de subducción, estos segmentos coinciden con sectores carentes de volcanismo activo y regiones topográficamente más deprimidas al este de la cordillera de los Andes. Ambos se ubican geográficamente al este de la intersección de las dorsales oceánicas con la fosa Perú-Chile: la dorsal de Nazca, que se subduce bajo Perú, y la dorsal de Juan Fernández, que hace bajo Chile. Una tercera dorsal, la dorsal de Galápagos-Carnegie, puede tentativamente correlacionarse con una zona de subducción de bajo ángulo en el sur de Colombia.

La relación causal entre la subducción de estas dorsales oceánicas y zonas de subducción de bajo ángulo es reafirmada conforme aparecen nuevas reconstrucciones para las placas Nazca y Sudamericana, así como nuevas compilaciones de edades isotópicas para el volcanismo continental. Estos nuevos datos permiten también refinar la historia de migración de ambas dorsales con respecto a la fosa oceánica. La dorsal de Juan Fernández, por ejemplo, habría sido responsable a los ~125 Ma de la formación del *plateau* oceánico Manihiki en la placa Pacífico, mientras que entre los ~65 y los

~13 Ma habría migrado desde el sur de Perú hacia Chile central, y provocado un ensanchamiento transitorio del arco volcánico hacia el este. La dorsal de Nazca, en tanto, habría intersecado el margen continental colombiano previo a los ~50 Ma, para después, a los ~15 Ma, migrar hacia el sur, lo que produjo el cese momentáneo de la actividad volcánica hasta alcanzar el centro de Perú. Finalmente, se estima que la dorsal de Galápagos-Carnegie alcanzó hace poco tiempo la zona de subducción, y generó un nuevo segmento de subducción de bajo ángulo y un posible cese en la actividad magmática en Colombia.
Las reconstrucciones tectónicas y magmáticas provistas en este estudio sugieren una correlación evidente entre la subducción de dorsales oceánicas como responsables de las zonas de subducción de bajo ángulo observadas en el margen continental sudamericano. Además, se sugiere que la fusión de remanentes de antiguas dorsales subducidas y transportadas hacia el este dentro de la astenosfera podrían haber sido la fuente de volcanismo geoquímicamente anómalo en Paraguay y el este de Brasil.

Palabras clave: Andes, Subducción, Volcanismo, Puntos calientes, Reconstrucción de placas.

1. Introduction

The geometry and kinematics of subduction beneath the west coast of South America and the consequent tectono-magmatic evolution of the Andes continue to be explored by field and laboratory studies, physical and numerical modeling, and plate-to-plate and plate-to-hotspots reconstructions. Low-angle subduction of the Nazca Plate (first recognized by Barazangi and Isacks, 1976), the role of hotspot traces, and consequent volcanic gaps and deflections within the Andes (Fig. 1) are of particular interest even after more than forty years since such a functional role was initially proposed (Cross and Pilger, 1978a). Subsequent work via global plate and hotspot trace reconstructions showed correspondence with apparent gaps in the then limited Cenozoic magmatic record from Peru, Chile, Bolivia, and Argentina (Pilger, 1981, 1984), by analogy with contemporary intersection of such traces with two (and possibly three) low-angle zones within the subducting Nazca plate. Pilger's approach involved taking models of Pacific plate motion relative to hotspots (principally the Hawaiian-Emperor and Louisville hotspots) and extending them to the Nazca plate by relative plate reconstructions. The Nazca plate, including the modeled Easter-Nazca, Juan Fernández, and Galápagos-Carnegie hotspot traces, was then restored relative to the South American plate for several discrete times via global plate reconstructions. The 1981 global circuit was via Nazca-Pacific-Antarctic-Indian-African-South American plates; the 1984 circuit eliminated the connection through the Indian plate, replacing it with then newly published Antarctic to African plates reconstructions. Other workers subsequently calculated reconstructions of the Nazca to South American plates and Easter-Nazca and/or Juan Fernández hotspot traces relative to South America using a variety of approaches. Yáñez *et al.* (2001) utilized plate reconstructions relative to a fixed hotspot reference frame (rather than using a global plate circuit) as well as calculating the Juan Fernández hotspot trace in the same frame. Hampel (2002) reconstructed the projected Easter-Nazca trace relative to South America assuming mirror-imaging of the Tuamotu ridge on the Pacific plate (similar to Pilger, 1981), and updated relative plate motion parameters from Somoza (1998); however, Hampel did not calculate full relative reconstructions, but utilized Somoza's finite difference rotations assuming constant rotation rates. Martinod and Husson (2010) followed a methodology like Pilger's (1981, 1984), with updated reconstructions in a global circuit and a Pacific-hotspot model (along with other hotspot reference frames) for the Juan Fernández hotspot trace relative to South America. Bello-González *et al.* (2018) calculated the Juan Fernández trace relative to South America, using a software package that incorporates global circuits for relative motions assuming a global moving hotspot frame. In each of these cases, the observations of the positions of the two hotspot traces relative to South America are broadly consistent with those of Pilger (1981, 1984), but differ in calculated dates and precise positions for the encounter of the traces with the Andean subduction zone, possibly due to changes in geomagnetic timescales, resolution of relative plate reconstructions, and specific plate-hotspot models. In the current work, higher resolution relative plate reconstructions (largely similar to Martinod and Husson, 2010, but with revised South American-African-Antarctic reconstructions), and a combination

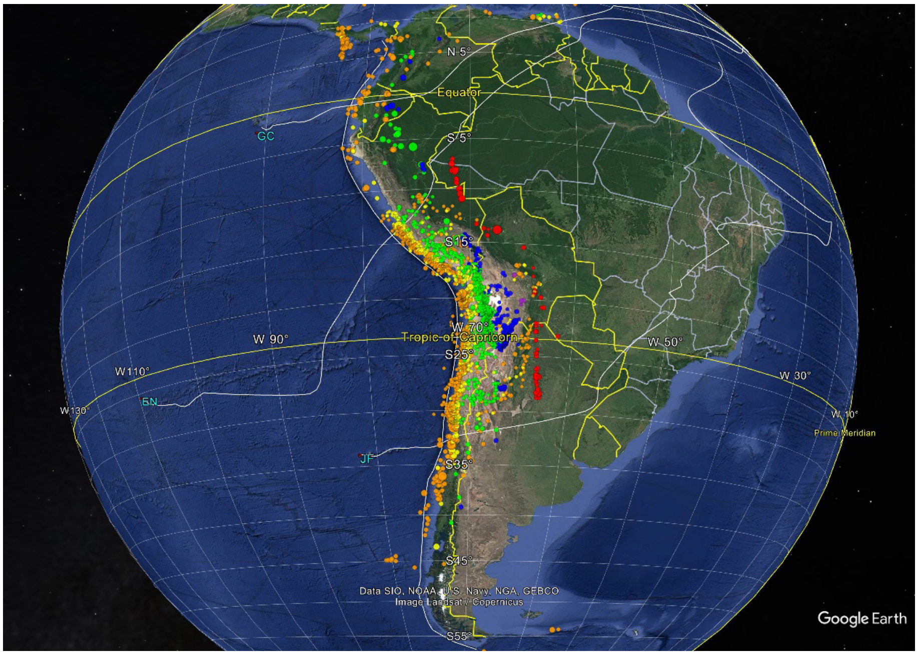

FIG. 1. Calculated traces of three hotspots, Juan Fernández (**JF**), Easter-Nazca (**EN**), and Galápagos-Carnegie (**GC**) relative to the contemporary Nazca plate with seismicity of the Andean subduction zone; the traces are not conformable to the inferred subduction zone. The calculations are based on a composite of several models of Pacific plate motion relative to hotspots, propagated to the Nazca plate by Pacific-Nazca plate motion, as discussed in the text. Parameters of Nazca/Farallon plate motion relative to the South American plate at 5 Myr increments are listed in table 1; parameters at 1 Myr increments are listed in Supplementary table 2.

of revised Pacific plate-hotspot models provide improved apparent correspondence with volcanic patterns in the Andes. (No other reconstruction study has addressed comparisons of modeled hotspot traces with documented Cenozoic magmatism patterns since the 1984 paper) As a byproduct of this revisitation of the role of hotspot trace subduction, the fate of previously subducted traces after passage beneath the Andes may explain anomalous magmatism well to the east along coastal Brazil and extending into the western South Atlantic Ocean.

1.1. Updated reconstructions across spreading centers

Plate-pair reconstructions in the ocean basins have greatly improved in resolution and confidence from denser magnetic and bathymetric coverage (especially over younger oceanic lithosphere) and satellite geoid measurements which constrain fracture zone locations. For example, Quiero *et al.* (2022) provide the most recent relative reconstructions of the Nazca and South American plates, although limited to ~30 Ma and younger, incorporating high resolution studies in the South Atlantic, Southwest Indian, and Southwest Pacific Oceans along with lower resolution studies in the East Pacific. While resolution over older portions of plates in the Atlantic and Indian oceans and East Pacific is reduced, largely due to less dense survey coverage, reconstructions extending to 80 Ma (for this study, reconstructions of the Pacific plate relative to the Atlantic-Indian Ocean plates are uncertain prior to ~84 Ma) are nevertheless improved relative to previous studies. Table A1 in the Appendix summarizes the source references for the plate-pair reconstructions used in this study (the source parameters are provided in Supplementary Table 1).

1.2. Plate-hotspot models

Beginning with Morgan (1972), numerous models of the motion of the Pacific plate relative to hotspots have been produced as more data have accumulated, especially with the replacement of potassium-argon by more accurate and precise argon-argon dating. Of particular relevance is the age of the Hawaiian-Emperor (HE) bend and its correlatives along other traces of the plate. Pacific-hotspot reconstruction parameters can be extrapolated to the Nazca plate by relative plate reconstructions, providing a means of distinguishing among the various Pacific-hotspot models by comparison with traces on the Nazca plate and patterns of subduction-related magmatism in the Andes. Figure 2 illustrates nine such models, applied to the Easter-Nazca, Juan Fernández, and Galápagos-Carnegie hotspots relative to the Nazca plate. As elaborated further below, a composite of several of the parameter sets over the last ~80 Myr (Fig. 3) appears to best correspond with the volcanic history of the Andes since ~30 Ma, while remaining conformable to Pacific and Nazca plate hotspot trace dates and patterns and global plate reconstructions. Table A2 in the Appendix summarizes the sources for the plate-hotspot reconstructions used in this study.

For the plates of the Atlantic and Indian oceans, the younger part of the classic model of Müller *et al.* (1993; "M93") for the hotspot traces corresponds well with the southward propagating wave of magmatism in east-central Africa from ~60 Ma to Present (Pilger, 2003) and with reconstructions of the Caribbean island arc over the same period of time (Müller *et al.*, 1999), neither of which were used in derivation of M93. M93 is utilized in the last part of this study, after examining several alternative "moving hotspot" models, beginning with O'Neill *et al.* (2005) and modified by Doubrovine *et al.* (2012); Torsvik *et al.* (2019) and Müller *et al.* (2019).

1.3. Magmatic history of the Andes

The author updated and expanded the compilation of radiometric dates from Andean igneous rocks providing for comparison with plate-to-plate and plate-hotspot reconstructions. The dataset, which incorporates previous regional compilations as well as numerous original publications, is particularly focused on the Andean crest from northern Peru to southern Chile and along the foreland from Peru through Bolivia and Argentina. Maps at 10 Myr intervals, 0-80 Ma, are provided in the Supplementary Data, along with a Supplementary File for display in Google Earth. For this study, sections parallel with the oceanic trench display the radiometric data projected normal to the sections. Figure 4 portrays the dates in two stacked views, in age versus latitude, for 0-100 Ma and 10° N to 60° S. Figures 5 and 6 are graphs of age versus latitude for 1° longitude segments together with reconstructed loci intersections.

2. Methodology

Global reconstructions of the motion of the subducting Nazca/Farallon plate (the Farallon plate fragmented into the Nazca and Cocos plates at ~23 Ma) relative to the upper, South American, plate follow the circuit Nazca/Farallon-Pacific-West Antarctic-East Antarctic-African-South American (plate-pair sources are indicated in the Table A1 in the Appendix, with parameter values in Supplementary Table 1), interpolated at 1 Myr increments from 0 to 80 Ma, using cubic-splined pseudovectors (converted from the original spherical coordinates) with magnitude equal to the total rotation rate (Pilger, 2003). The plate parameters are calibrated to the recent timescale of Ogg (2020), which is tied to the astronomically tuned timescale of Gradstein *et al.* (2020). Rotations are composed using quaternions transformed from the pseudovectors (Pilger, 2003), with further composition of the total reconstruction quaternions to rotate the (unit vector) points; the latter reconstructed vectors are inverted to spherical coordinates for display in Google Earth. Table 1 provides the calculated Nazca/Farallon-South America reconstruction parameters at 5 Myr increments (more detailed parameters at 1 Myr increments are provided in the Supplementary Data along with the source plate-pair reconstructions). Uncertainties are not provided because they cannot be legitimately calculated via interpolation (the rationale is provided in the Supplementary Data; see also discussion in Pilger, 2007). Instantaneous rotation rates are calculated at the same 1 Myr increments using the derivatives of the spline parameters (using the modified Smith, 1985, equation by Pilger, 2003) at several locations along the oceanic trench.

Three persistent hotspots appear to exist beneath the Nazca plate (Fig. 1), with traces extending to the east and northeast: the Juan Fernández (JF), Easter/Nazca (EN), and Galápagos/Carnegie (GC; this also appears to have an associated trace, the Cocos Ridge, on the Cocos plate). The motion of the Nazca (and its predecessor plate, the Farallon) relative to hotspots beneath the Pacific plate is calculated for eight Pacific-hotspot models (Table A2 in the Appendix),

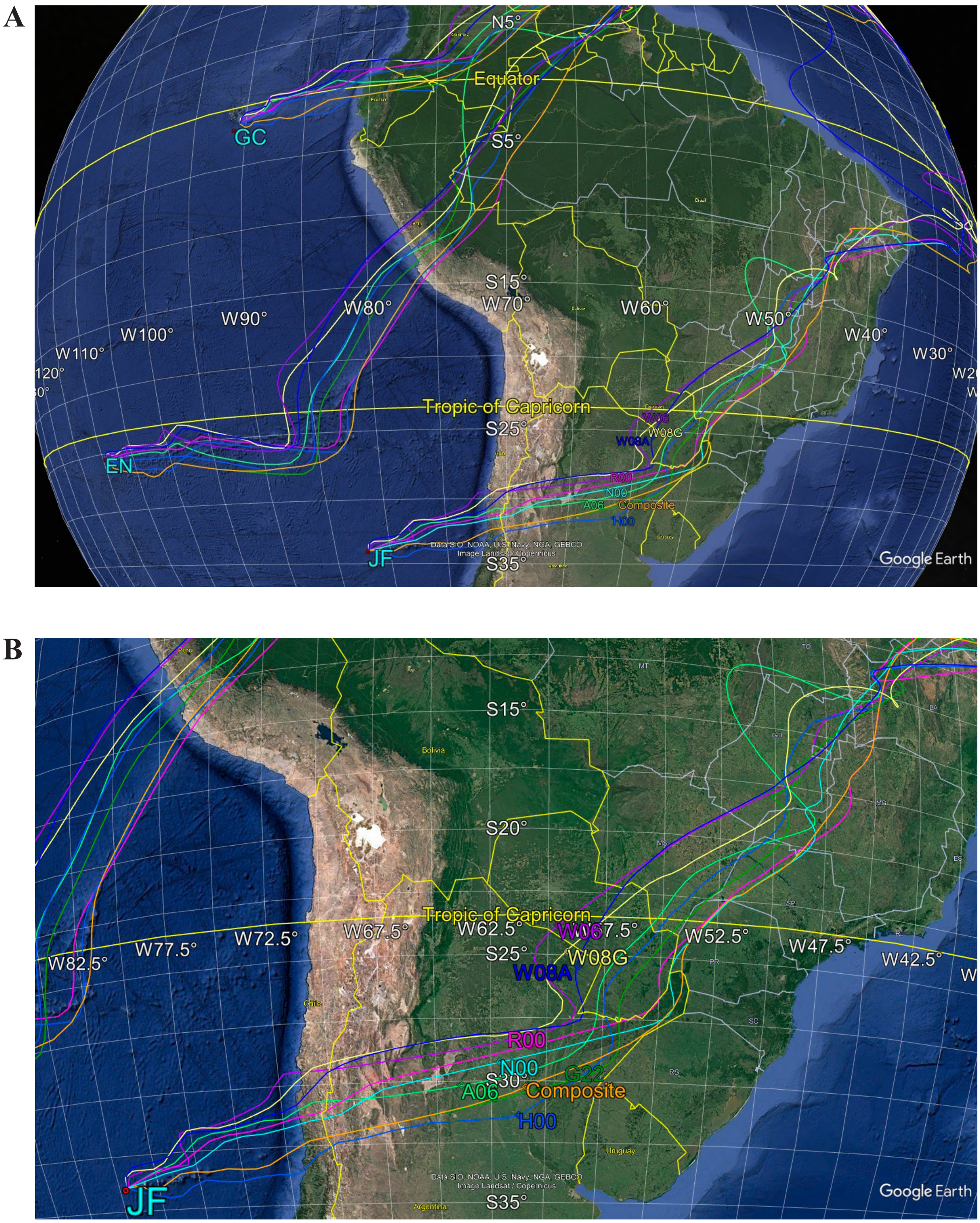

FIG. 2. **A.** Calculated loci of the Easter-Nazca (**EN**), Galápagos-Carnegie (**GC**), and Juan Fernández (**JF**) hotspot traces reconstructed relative to the Nazca Plate for eight Pacific-Hotspot models, plus composite model, modified to a Hawaiian-Emperor bend age of 50 Ma, propagated via Pacific-Nazca relative plate reconstructions (see text for details). **B.** Zoomed view of the JF trace as in **A**. Model key with sources: **A06:** Andrews *et al.* (2006; 10.9-80 Ma), **G22:** Gaastra *et al.* (2022; 1-80 Ma), **H00:** Harada and Hamano (2000; 2-70 Ma), **N00:** Norton (2000; 5-81 Ma), **R00:** Raymond *et al.* (2000 and personal communication, 2003; 5.81-78.78 Ma), **W06:** Wessel *et al.* (2006; 2.58-125 Ma), **W08A** and **W08G:** Wessel and Kroenke (2008; 2.58-140 and 3.36-140 Ma, respectively).

A

B

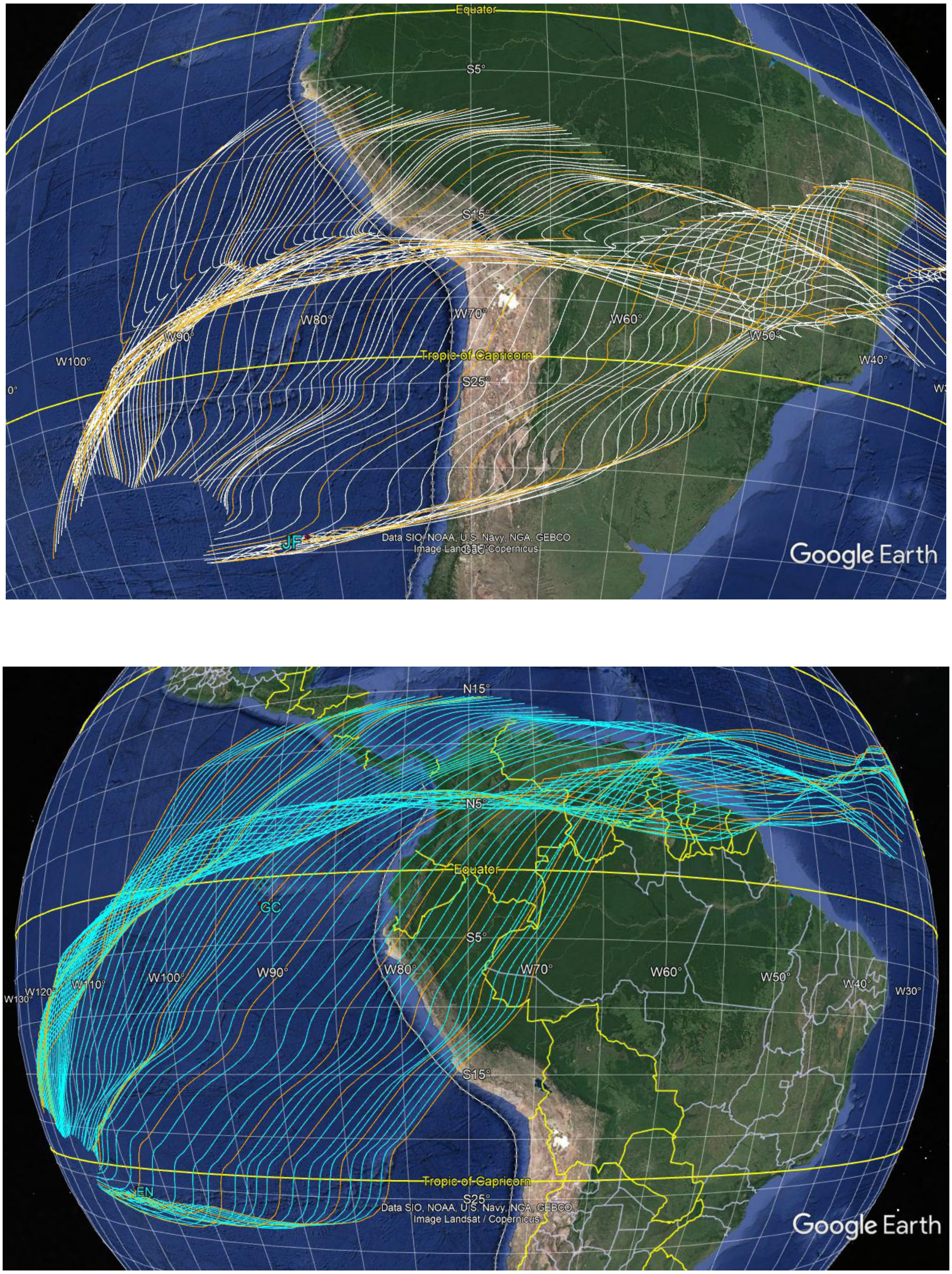

FIG. 3. **A**. Reconstruction of the Juan Fernández (**JF**) hotspot trace on the Nazca plate relative to the South American plate, 0-80 Ma, at 1 Myr increments; every fifth increment is colored gold. Parameters of Nazca/Farallon plate motion relative to the South American Plate are listed in table 1 at 5 Myr increments; the parameters at every 1 Myr are in Supplementary table 2. **B**. Reconstruction of the Easter-Nazca (**EN**) trace on the Nazca plate as in **A.** for 0-80 Ma.

TABLE 1. RECONSTRUCTION PARAMETERS FOR THE NAZCA/FARALLON PLATE RELATIVE TO THE SOUTH AMERICAN PLATE AT 5 MYR INCREMENTS, 0-80 MA.

Age (Ma)	Longitude (°)	Latitude (°)	Rotation Angle (°) / Rate* (°/Myr)
0	-34.300	63.900	*2.560
5	-101.675	61.272	3.976
10	-101.273	56.932	9.308
15	-105.993	61.667	15.010
20	-95.095	56.411	24.206
25	-92.144	57.979	29.777
30	-103.302	67.723	31.508
35	-118.546	73.114	36.245
40	-146.425	77.740	42.490
45	-169.253	76.334	49.270
50	175.994	74.227	53.191
55	163.328	72.353	57.494
60	154.621	70.058	61.002
65	150.151	67.537	64.340
70	145.954	65.092	69.811
75	143.316	62.397	75.513
80	139.403	59.161	79.847

(Parameters at 1 Myr increments are included in Supplementary Table 2). Timescale of Ogg (2020). Rotation rate at 0 Ma.

with dates for the parameters adjusted to an age of 50 Ma for the Hawaiian-Emperor (HE) bend (Pilger and Handschumacher, 1981; Sharp and Clague, 2006; O'Connor *et al.*, 2013; Wright *et al.*, 2015; Hu *et al.*, 2022), extended by relative plate reconstructions from the Pacific to the Nazca plate from 0 to 140 Ma at 1 Myr increments (some models do not cover the full 140 Ma, so the older part of the Wessel and Kroenke, 2008, model A is appended to them as shown in figure 2). The calculated traces relative to the Nazca plate are then reconstructed at 1 Myr increments relative to the South American plate to 80 Ma (Fig. 2), utilizing the global reconstruction circuit parameters and assuming symmetrical spreading across the Pacific-Farallon boundary between 53 and 83.65 Ma. A composite model was constructed by selecting segments of several models which best visually fit the bathymetry of the JF and GC traces, the seismicity onshore of JF, and the earliest intersection of the JF trace with the Andean crest. The selected model components are taken from Gripp and Gordon (2002; 0 Ma), Gaastra *et al.* (2022; 1-16 Ma), Norton (2000; 25-50 Ma), Raymond *et al.* (2000; 50-80 Ma), and Wessel and Kroenke (2008; Model A, 83.5-144 Ma), assuming an age of 50 Ma for the HE bend, spline-interpolated as with the relative plate reconstruction parameters. The Pacific-hotspot models can be extended to the Nazca/Farallon plate to 140 Ma or even earlier, but the motion of the Pacific, and thus Farallon, plates relative to South America cannot be confidently determined prior to the younger edge of magnetic isochron 34, that is, 83.65 Ma, because of uncertainty in the position of the Pacific plate relative to both Antarctica and Australia prior to this time. A spreading center between the Pacific and West Antarctic plates, permitting reconstructions, only came into existence at approximately isochron 34 time (*e.g.,* Wright *et al.*, 2015).

From the composite model, the calculated JF and EN hotspot traces on the Nazca plate were again reconstructed relative to the South American plate back to 80 Ma, at 1 Myr increments (Fig. 3, with 5 Myr increments highlighted). The traces are not conformed to an inferred three-dimensional subduction zone configuration in either map views or graphical sections.

In figure 4, all isotopic dates <80 Ma are projected onto a graph of age versus latitude arranged by longitudinal distance from the trench. The dates farthest from the trench are progressively "on top" of dates closer to the trench in figure 4A, and viceversa in figure 4B.

The isotopic dates are further analyzed in comparison with the reconstructed hotspot traces using projected sections of width one degree of arc from and parallel with the trench (Figs. 5 and 6; Google Earth map views of the dates in 10 Myr intervals are provided in the Supplementary File). Most of the dates are concentrated along the crest of the Andes, approximately two to three degrees of arc from the contemporary trench. Some dates are observed along the east and west flanks of the range, extending into the respective foreland and hinterland.

3. Results

3.1. Reconstructions of the Nazca/Farallon and South American plates and the hotspot traces

As previously inferred from sparse radiometric dates (*e.g.,* Pilger, 1981, 1984), in Peru (5° to 18° S) there is a northwest-to-southeast, time-transgressive, narrowing gap in young igneous dates along the Andean crest, implying cessation of volcanism from ~13 Ma to the Present (Figs. 5C and 6C). The cessation pattern is parallel with and slightly younger than the calculated intersection of the reconstructed EN trace (Figs. 5C and 6C), and consistent with the progressive onset of low-angle subduction from northwest to southeast.

The patterns of magmatism farther south beginning at 20°S indicate near continuous activity since 80 Ma, although varying in longitudinal position, to 32° S (Figs. 4-6). Along the Andean crest, a gap in volcanism is apparent between 32 and 33° S especially over the last 10 Myr, widening at younger ages (Fig. 6C), again strengthening the inferences of Pilger (1981, 1984). The gap corresponds well with the calculated intersections of the JF hotspot trace, beginning at about 13 Ma, and with the Pampean low-angle subduction segment (*e.g.,* Ramos *et al.*, 2002).

What is the significance of the correlation of isotopic dates and loci intersections of hotspot traces? It is inferred that after passage of the JF trace to the south, magmatism increased and spread farther to the east (*e.g.,* Kay and Coira, 2009). In other words, a southward-shifting, short-lived period of low-angle subduction (depending on the width of the segment, perhaps 2 to 4 Myr in duration between 25 and 15 Ma) interrupted normal subduction and was quickly followed by resumption of, perhaps even increase in magmatism, after passage of the trace (*e.g.,* de Silva and Kay, 2018). Note that the older (>50 Ma) parts of the JF locus intersections lack obvious correspondence with observed isotopic dates (Fig. 5); this is also the least certain part of the Pacific-hotspot motion (Wessel and Kroenke, 2008) due to the scarcity of dates from the Pacific traces older than 80 Ma, although Gaastra *et al.* (2022) have shown that a fixed hotspot model can fit available data for the past 80 Myr. For the younger parts of both hotspot traces, especially <40 Ma, the projected dates are a bit older than the calculated intersections; because of the two-dimensionality of the graphs, the differences are uncertain. This may be a function of errors in the Pacific-Nazca reconstructions, especially between 10 and 25 Ma, for which magnetic survey coverage is sorely lacking. It is possible that the JF trace encountered the trench several million years earlier than calculated here. Given the sparse magnetic surveys over the Nazca and east-central Pacific plates, and reliance upon assumptions of symmetric spreading based on one-sided reconstructions of the Farallon-Pacific spreading center, there is room for significant variation in the calculated reconstructions (for example, compare the parameters from Rowan and Rowley, 2014, used in this study, with those from Wright *et al.*, 2015). Also, given the oblique encounter of the JF trace with the subduction zone from 25 to 15 Ma, the cessation of trace subduction, as the ridge-subduction intersection migrates southbound, would produce a propagating window with possible "leakage" into the overlying South American plate ahead of the actual deeper trace intersection; that is, possible propagating tears or gaps in the subducting slab accompanying both flanks of the low-angle segment (cf. Báez *et al.*, 2023).

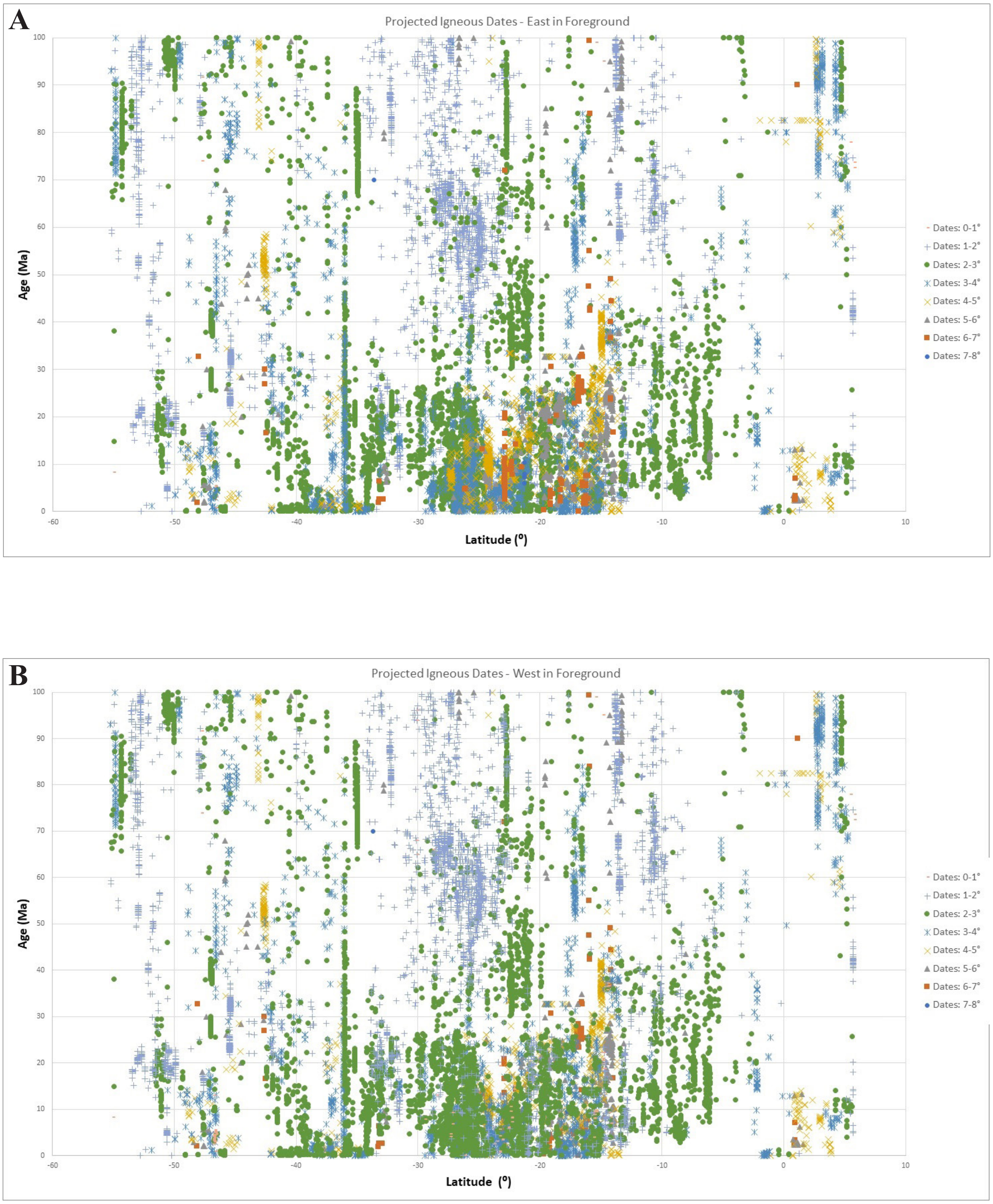

FIG. 4. Isotopic dates (Ma) from the Andes, versus latitude, along sections parallel with the oceanic trench. Distance from trench in longitudinal segments, by indicated symbol. **A**. "View" is from the east. **B**. "View" from the west. The data, from 0-100 Ma silicic and intermediate igneous rocks, are provided in the Supplementary File. The full compilation can be accessed via GEOROC (Pilger, 2022).

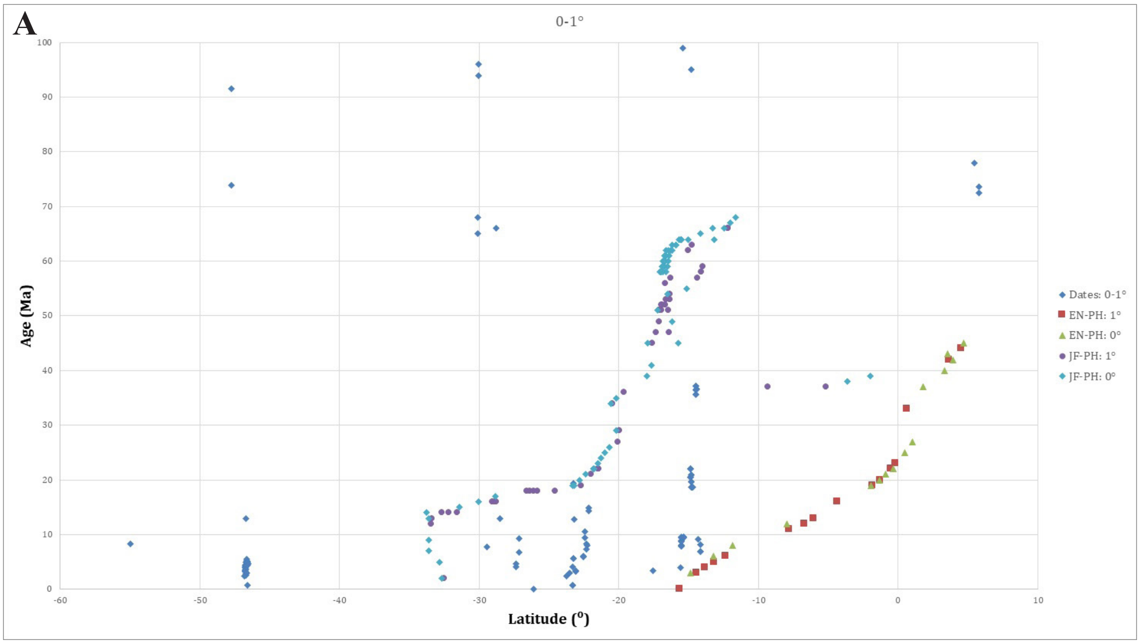
A
0-1°
Age (Ma)
Latitude (°)
Dates: 0-1°
EN-PH: 1°
EN-PH: 0°
JF-PH: 1°
JF-PH: 0°

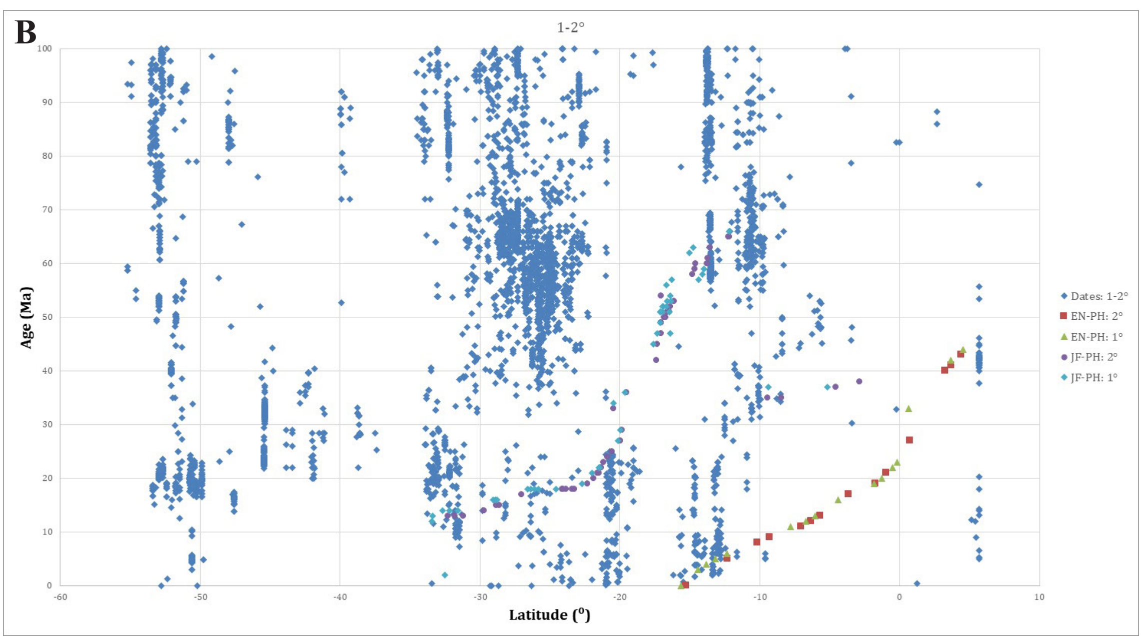
B
1-2°
Age (Ma)
Latitude (°)
Dates: 1-2°
EN-PH: 2°
EN-PH: 1°
JF-PH: 2°
JF-PH: 1°

C

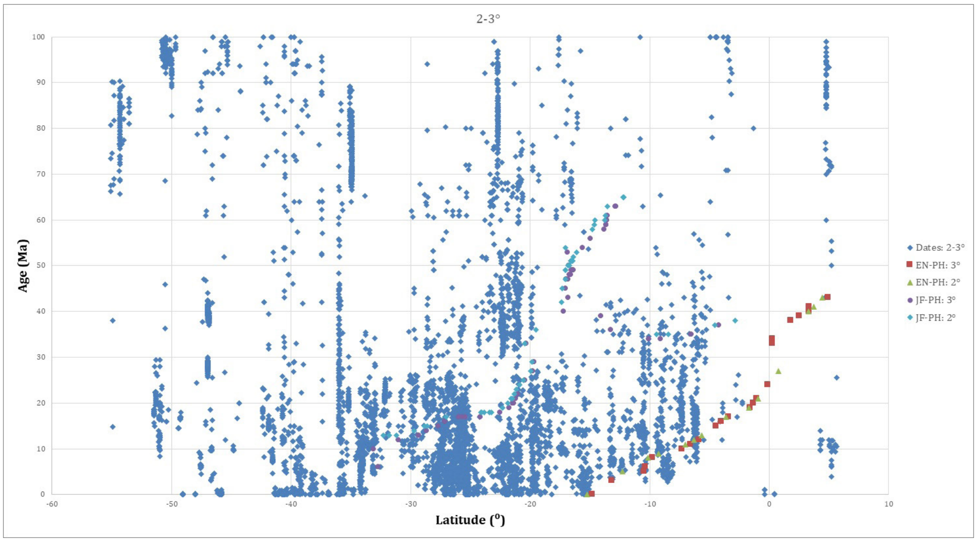
2-3°
Age (Ma)
Latitude (°)
Dates: 2-3°
EN-PH: 3°
EN-PH: 2°
JF-PH: 3°
JF-PH: 2°

D

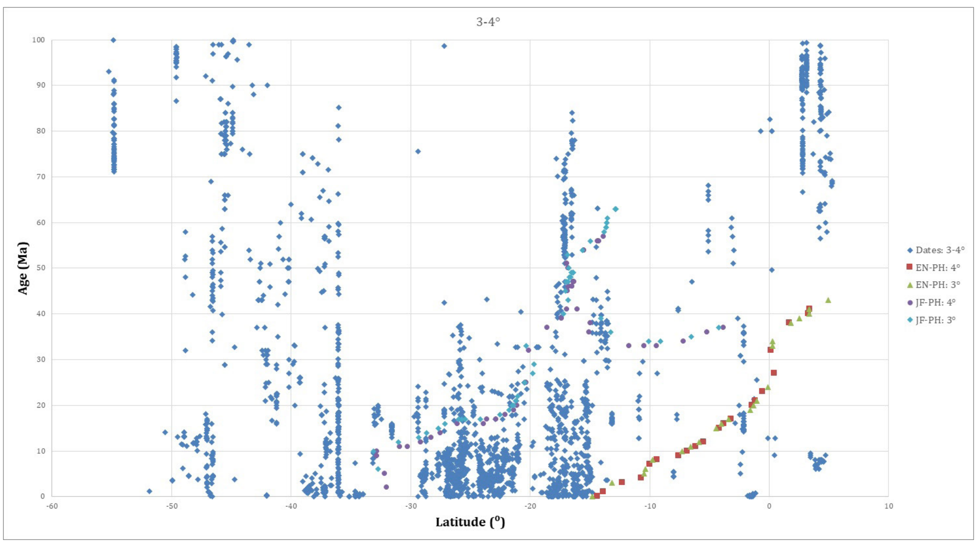
3-4°
Age (Ma)
Latitude (°)
Dates: 3-4°
EN-PH: 4°
EN-PH: 3°
JF-PH: 4°
JF-PH: 3°

E

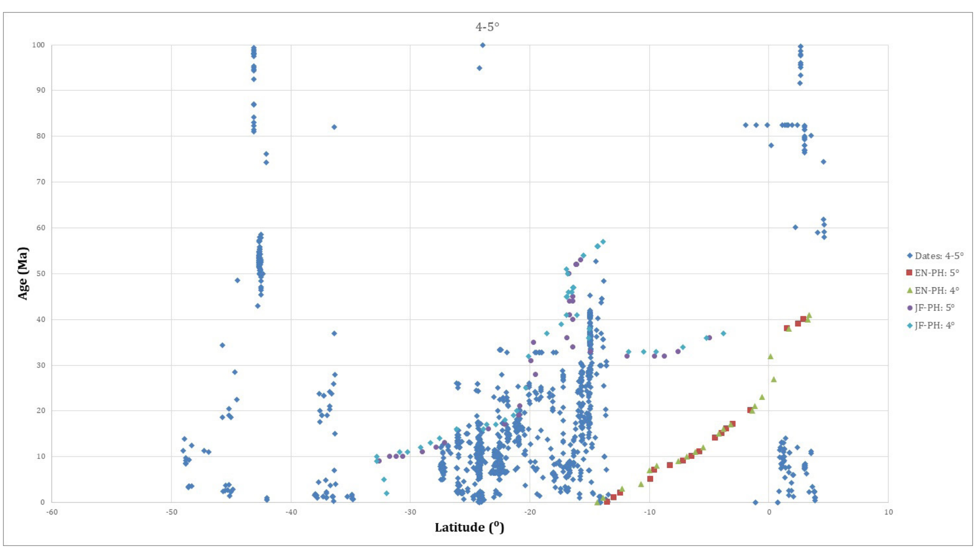
4-5°
Age (Ma)
Latitude (°)
Dates: 4-5°
EN-PH: 5°
EN-PH: 4°
JF-PH: 5°
JF-PH: 4°

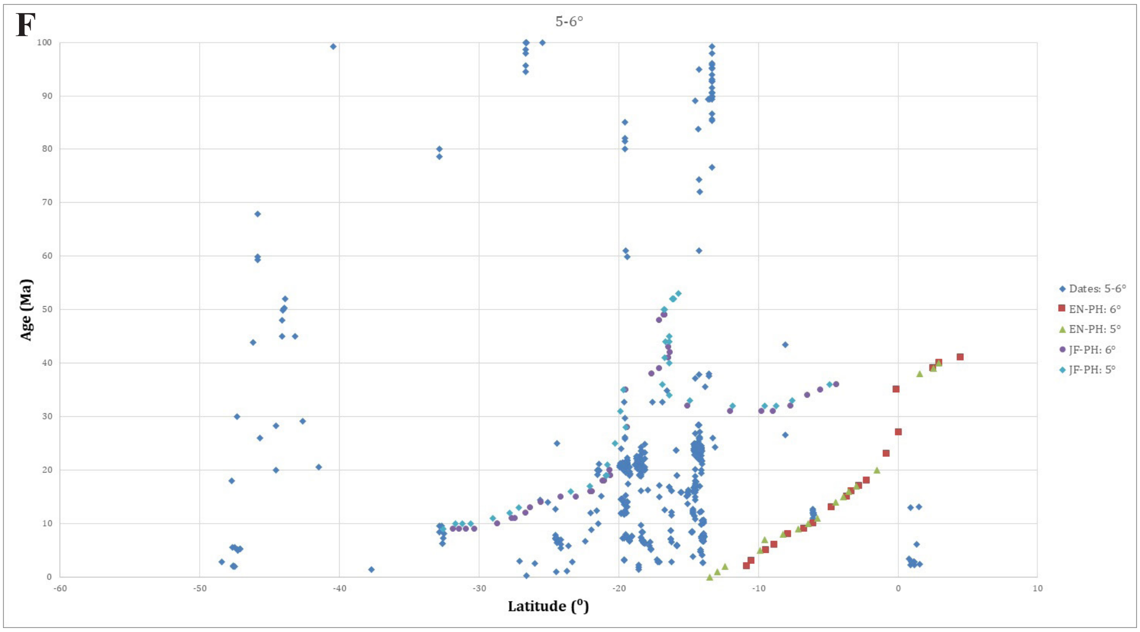

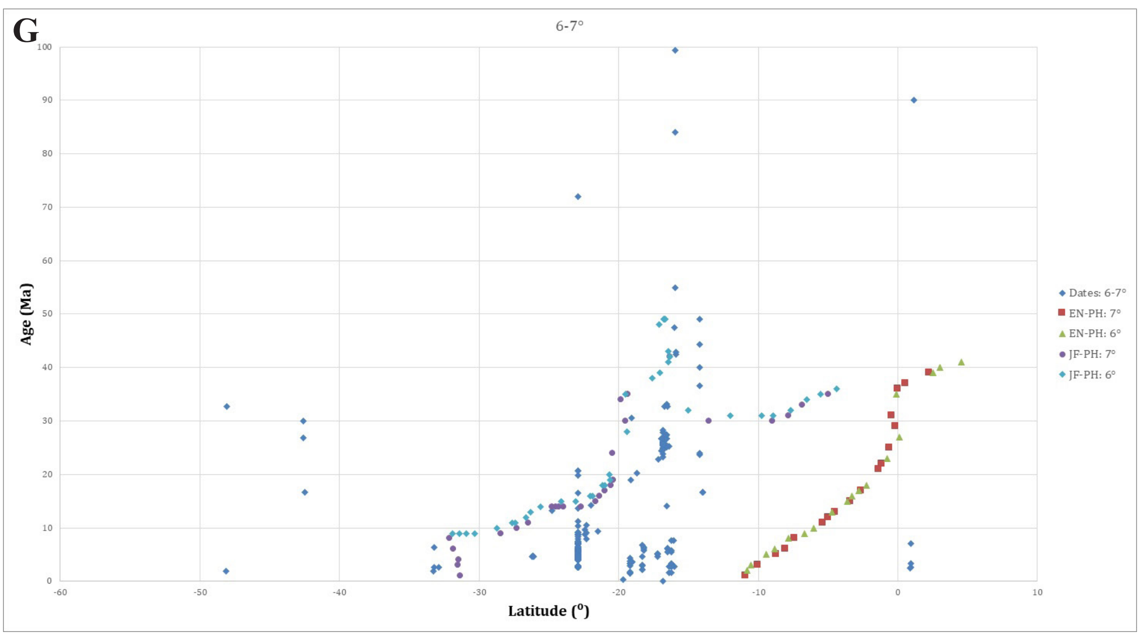

FIG. 5. Projection of isotopic dates ranging from 0 to 100 Ma and 10°N-60°S latitude from the Andes and adjacent foreland in arc segments at increments of 1° of arc separation from the contemporary Andean trench, from 0-1° (**A**) to 6-7° (**G**) of arc, with intersections of reconstructed hotspot locus at 1° increments. **JF**: Juan Fernández, **EN**: Easter-Nazca, **PH**: Pacific Hotspot model.

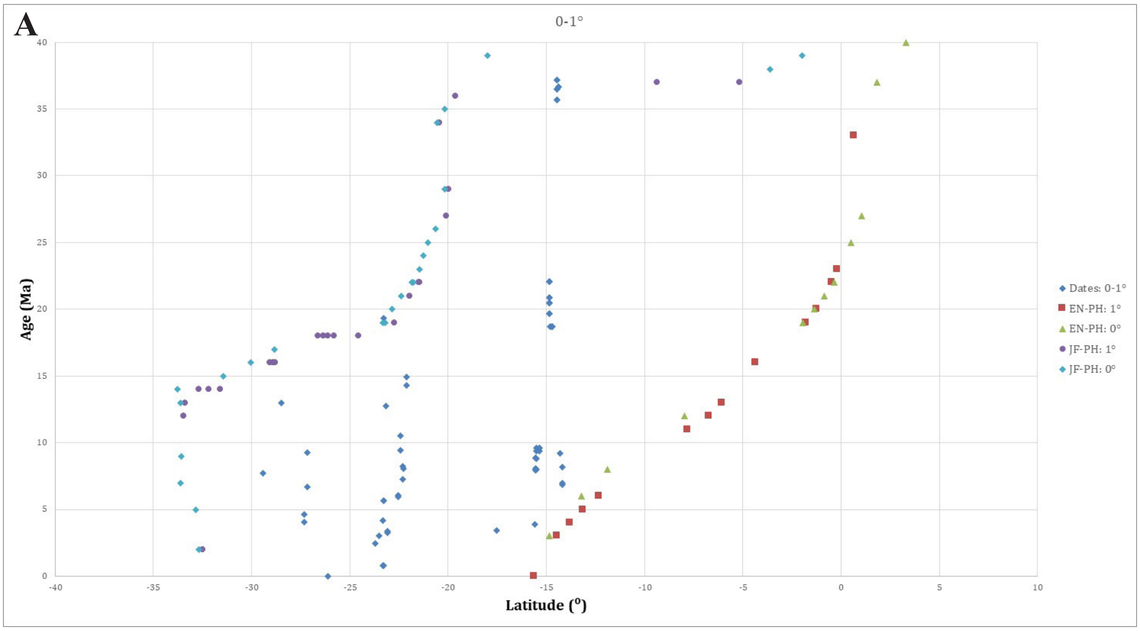
A
0-1°
Age (Ma)
Latitude (°)
Dates: 0-1°
EN-PH: 1°
EN-PH: 0°
JF-PH: 1°
JF-PH: 0°

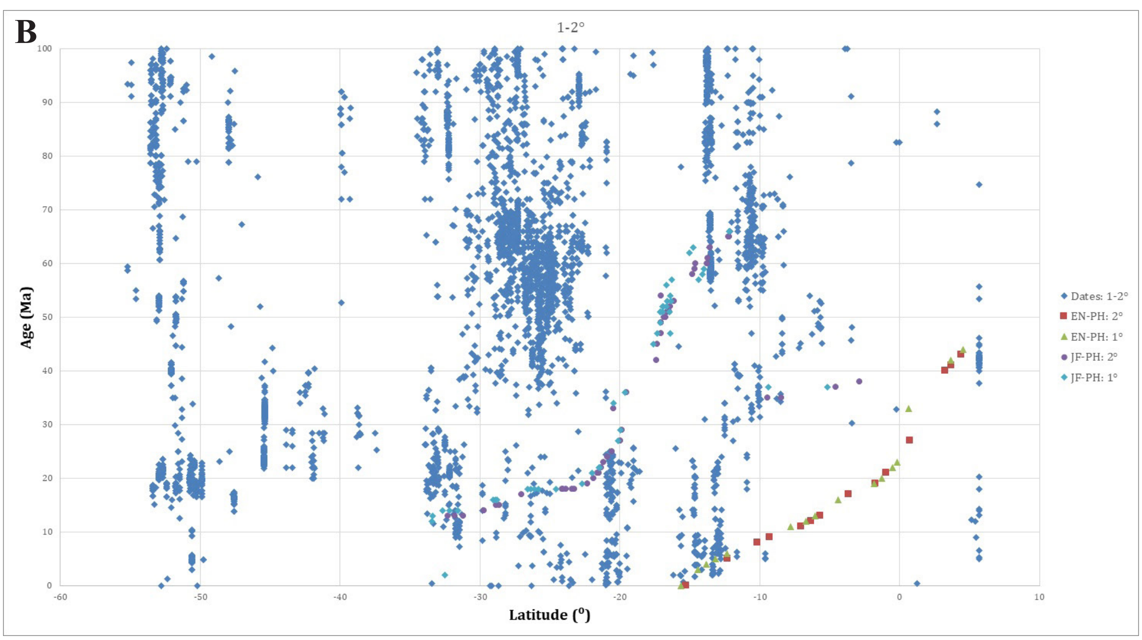
B
1-2°
Age (Ma)
Latitude (°)
Dates: 1-2°
EN-PH: 2°
EN-PH: 1°
JF-PH: 2°
JF-PH: 1°

C

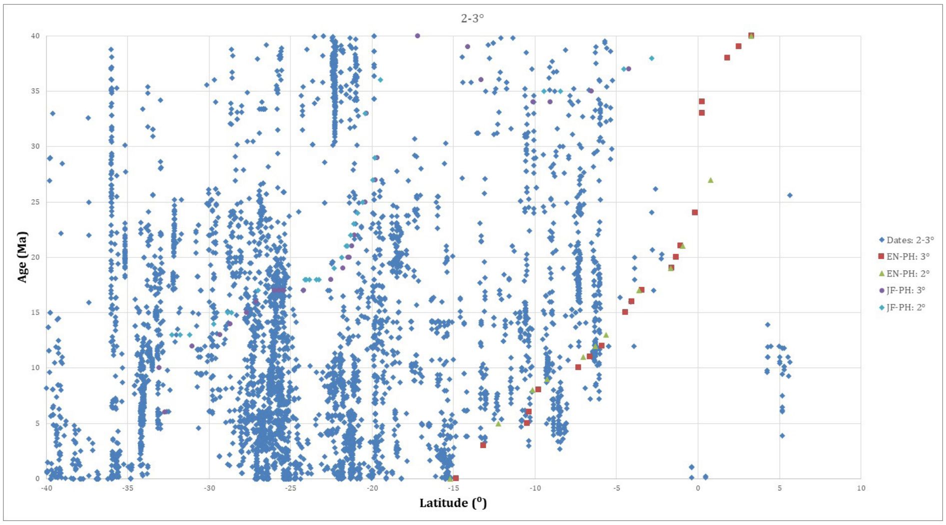
2-3°
Age (Ma)
Latitude (°)
Dates: 2-3°
EN-PH: 3°
EN-PH: 2°
JF-PH: 3°
JF-PH: 2°

D

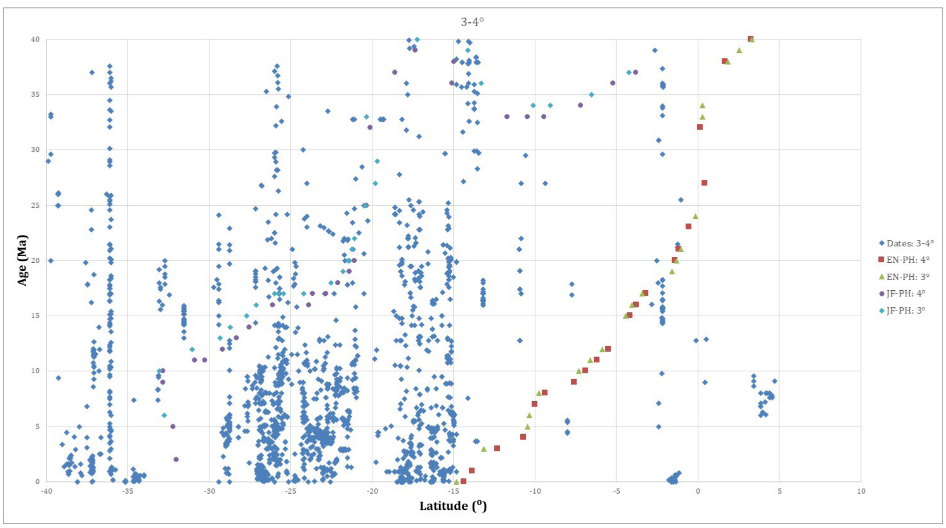
3-4°
Age (Ma)
Latitude (°)
Dates: 3-4°
EN-PH: 4°
EN-PH: 3°
JF-PH: 4°
JF-PH: 3°

E

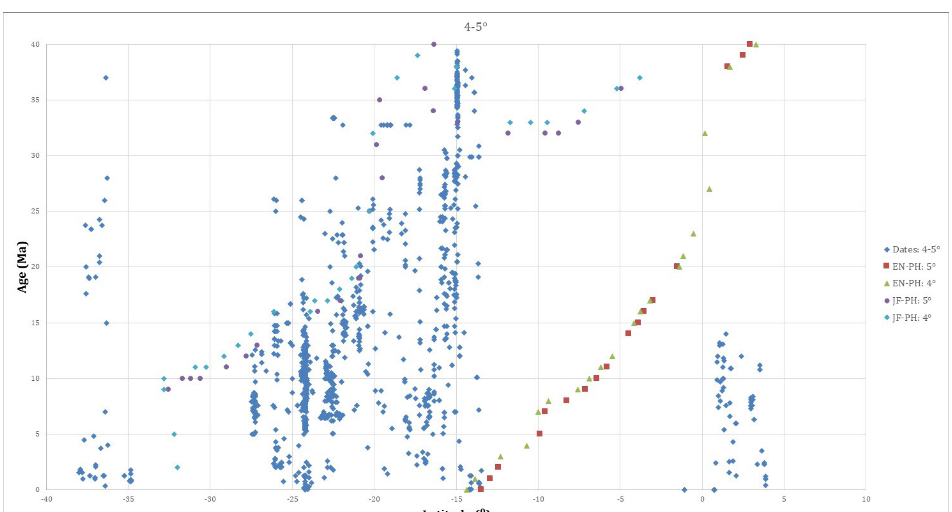
4-5°
Age (Ma)
Latitude (°)
Dates: 4-5°
EN-PH: 5°
EN-PH: 4°
JF-PH: 5°
JF-PH: 4°

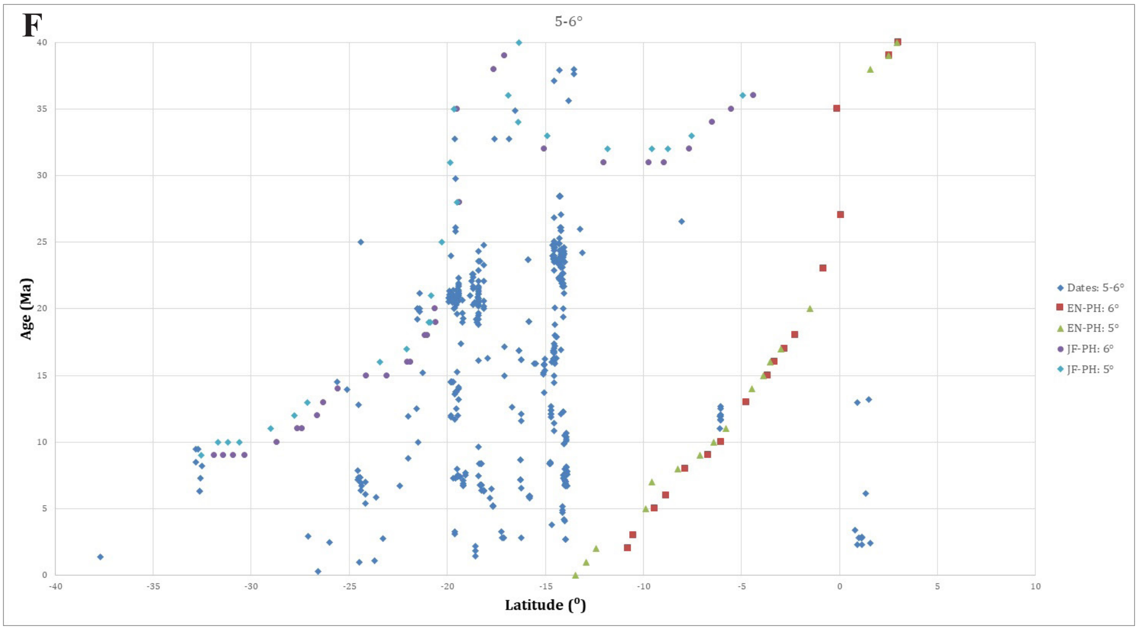

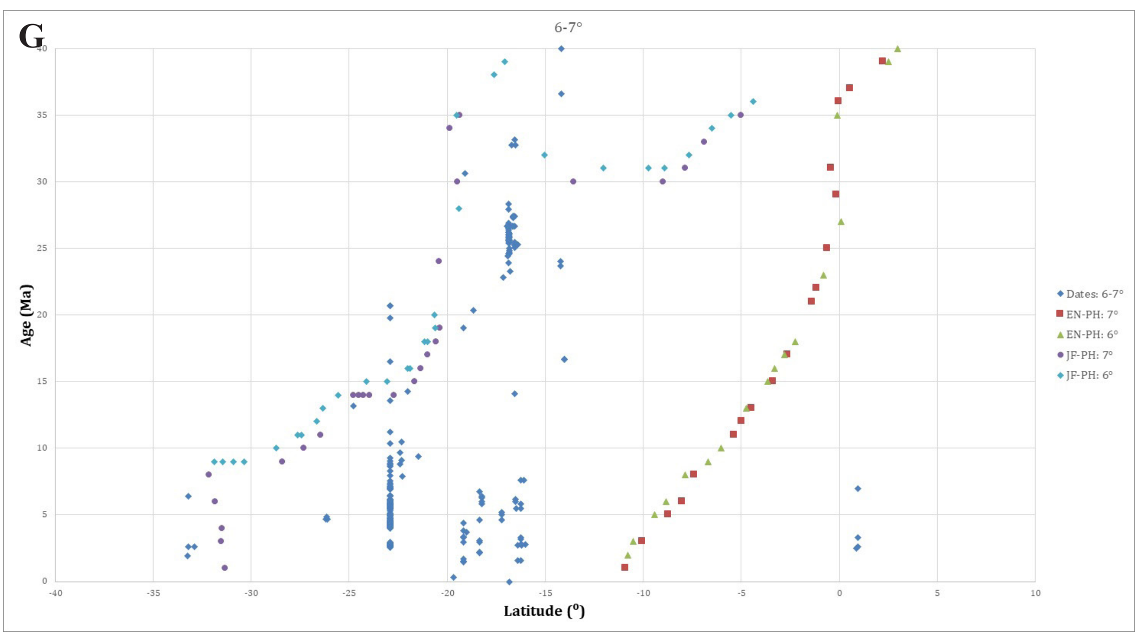

FIG. 6. Zoomed projections of isotopic dates and intersections of hotspot traces as in figure 5, for 0-40 Ma and 10° N-40° S latitude. Symbols as in figure 5.

Figure 7 is a sketch of the postulated sequence of events involved with the change from normal subduction (Time 0) to the encounter with the hotspot trace (Time 1) and return to normal subduction (Time 2). The replacement of normal by low-angle subduction would likely result in a transient reduction, if not extinguishment, of magmatism (*e.g.,* Kay and Coira, 2009). With the resumption of normal subduction, a “window” develops, resulting in widening of the magmatic arc, perhaps enhanced by delamination of the mantle portion of the South American plate (*e.g.,* Kay and Kay, 1993; Risse *et al.*, 2013) above the window. Time 3 represents a later period in which normal subduction has continued while the remnant of the trace is eventually under the thinner eastern edge of the South American plate (for the current traces, this is far into the future; long subducted, older traces could have been responsible for observed anomalous magmatism along the east coast of Brazil - see below).

Juan Fernández ridge subduction has also been inferred to produce rotation of the region of the Andes north and south of ~15° S, (*i.e*., oroclinal bending; Isacks, 1988), as proposed by a number of workers (*e.g.,* Yáñez *et al.*, 2001; McQuarrie, 2002; Martinod *et al.*, 2010; Arriagada *et al.*, 2013; Schepers *et al.*, 2017). The correspondence of the reconstruction timing with the geological observations, as they noted, is supported by paleomagnetic evidence as well (*e.g.,* Dupont-Nivet *et al.*, 1996; Arriagada *et al.*, 2008; Puigdomenech *et al.*, 2021).

3.2. Convergence rate and direction

Figure 8 illustrates instantaneous Nazca to South American convergence rates and directions calculated at 1 Myr increments at locations along the Andean trench, via spline interpolation of rotation pseudovectors. The angles are measured clockwise from the trench. Resolution of source data is denser over the past 25 Myr, because of the greater resolution of source plate pairs in the South Atlantic, Southwest Indian, and Southwest Pacific oceans.

Comparison of the convergence rates (Fig. 8A) with the isotopic date sections shown in figures 5 and 6 is not easily characterized. However, there does appear to be a correlation of the greater density of dates between 45 to 30 Ma and 25 to 15 Ma in parts

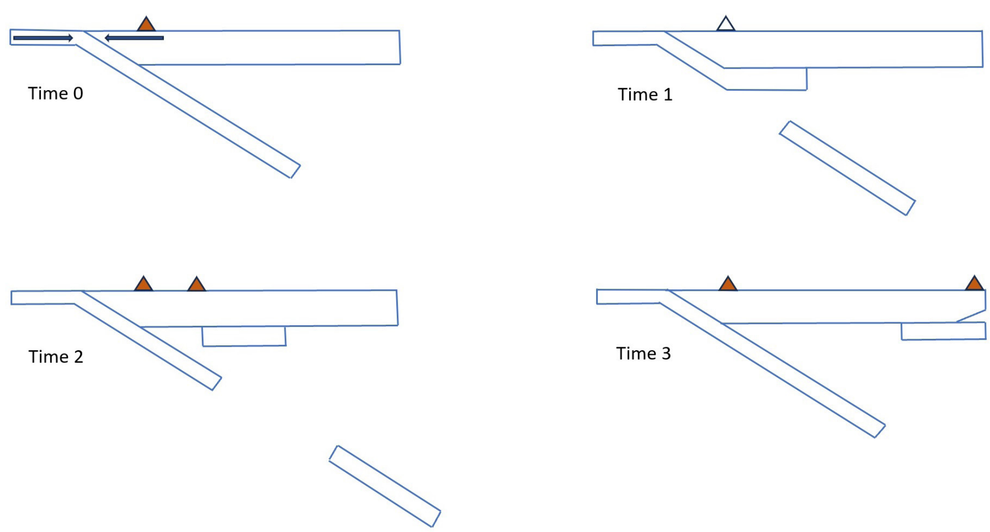

FIG. 7. Schematic illustration of the transitory interaction of a hotspot trace with the Andean subduction zone. Volcanic zone is indicated by triangles (**filled:** active, **empty:** inactive). **Time 0:** Subduction of normal oceanic plate. **Time 1:** Subduction of part of a hotspot trace. **Time 2:** Resumption of normal subduction after trace migration. **Time 3:** Prolonged normal subduction, with trace remnant under thinner upper plate, producing anomalous volcanism. At Time 1, supply of magma to the volcanic arc is suppressed, so that remaining volcanism is from previous magma chambers. Note development of a “window” during Time 2 as the trace segment is overridden by the upper plate, allowing for widening of the volcanic arc. Interruption of normal subduction produces the detached lower oceanic plate, resulting in separation of seismic zones within the subduction zone.

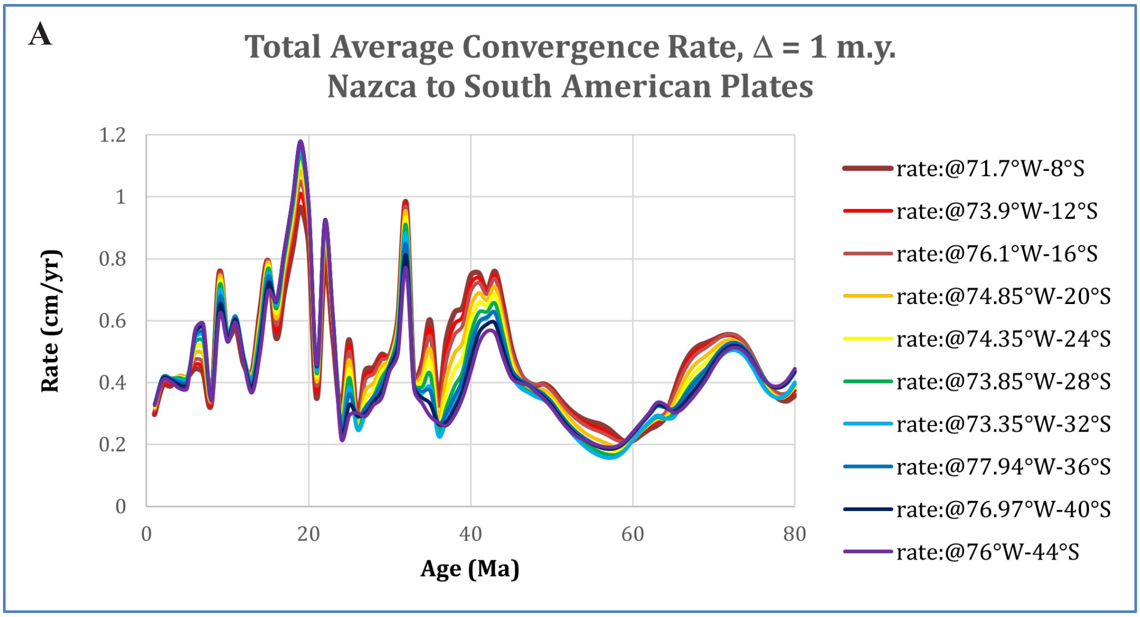

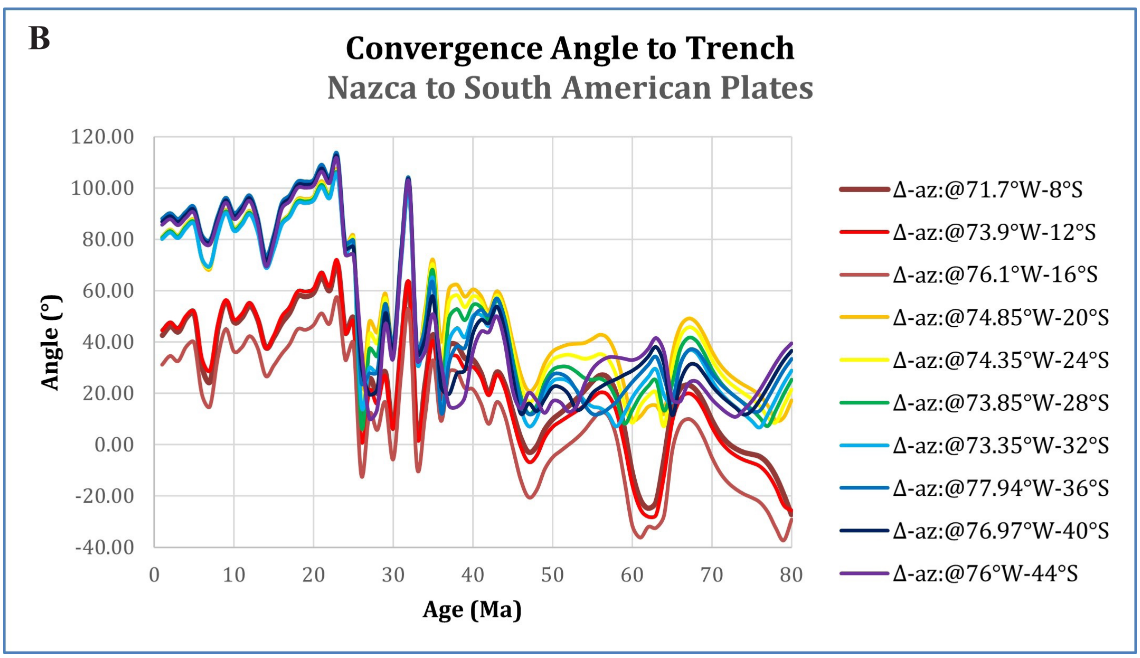

FIG. 8. Incremental average rates and angles. **A.** Instantaneous Nazca/Farallon to South American plate convergence rates calculated at indicated locations along the Andean Trench, as described in the text. **B.** Instantaneous angle between convergence direction and Andean trench, measured clockwise at same points as A.

of the Andes with the observed higher convergence rates (*e.g.,* Figs. 5C and 6C). In addition, gaps in magmatism in the Peruvian Andes prior to 45 Ma appear to correlate with highly oblique subduction. A short pulse of oblique convergence between 30 and 25 Ma may also correlate with reduced density of dates over much of the Andes. The variations in the convergence angle and rate over time may have implications for the tectonics of the Andes, as shown recently in some studies (*e.g.,* Bello-González *et al.*, 2018; Quiero *et al.*, 2022). The principal variations in rate and direction, now quantifiable at higher resolution were, nevertheless, implicit in the earliest studies, (*e.g.,* Pilger, 1983; Cande, 1985; and Pardo-Casas and Molnar, 1987), although apparent errors in the early geomagnetic time scales used then may have resulted in artificial variations in the calculated convergence rates. It is worth mentioning that the Pacific-Nazca plate pair is still poorly documented due to low density of magnetic surveys (*e.g.,* Wilder, 2003; Seton *et al.*, 2014), so it is likely that further improvement in the rate/angle calculations could result from future, higher density coverage of the region.

3.3. Complications and alternative models

A spectrum of models to explain the Peruvian and Pampean low-angle subduction zones have been advanced since these zones were first recognized. In addition to subduction of hotspot traces, these models have included the absolute motion of the upper (continental) plate, convergence rate, cycles of upper plate thickening due to crustal shortening, trench erosion, and/or magmatism. In support of such models, physical and numerical modeling as well as empirical observations have been utilized. As background to such investigations, a comprehensive study of subduction zone configuration, updating Jarrard's (1986) original study, by Lallemand *et al.* (2005) showed that increased absolute motion rate of the upper plate toward the trench may be an important factor in systematically reducing the subduction dip angle. However, they did not consider the effect of hotspot trace subduction in their global synthesis.

Martinod *et al.* (2005, 2013) applied analog modeling to testing the role of aseismic ridge subduction without success in producing low-angle inclination of the descending slab. Numerical modeling by van Hunen *et al.* (2004) supported the absolute motion effect, as Cross and Pilger (1978a, b) had earlier proposed. Physical analog modeling by Espurt *et al.* (2008) suggested that low-angle subduction of a thickened oceanic feature like the Nazca Ridge would require ~7 Myr to develop, assuming the thickened portion retains continuity with previously subducted normal, denser oceanic lithosphere. They also supported the inferred absolute motion effect but did not test the subduction of thickened oceanic plate detached from previously subducted normal oceanic plate. DeCelles *et al.* (2009) advanced a grand model which emphasize inferred cyclicity in Andean-type subduction relative to tectonic effects within and along the magmatic arc, while incorporating the role of subducting hotspot traces as rare factors independent of the cyclicity, producing not only low-angle subduction but also internal deformation of the foreland of the mountain belt, such as the central Chile-Argentina low-angle subduction segment and the Laramide Rocky Mountains of the United States.

Gerya *et al.* (2009) interpreted their numerical modeling to imply the aseismic ridge effect on subduction was transient and unstable. However, they did not consider the absolute motion of the upper plate. Skinner and Clayton (2010, 2013) argued against the hotspot trace subduction effect based on an interpreted seamount chain on the Nazca plate, unlike the Easter/Nazca or Juan Fernández traces, whose extension into the subduction zone has no apparent effect on the inclined seismic zone (in the 2010 paper they also cited examples of similar subducting traces in the western Pacific, but did not consider the role of absolute motion as an additional factor). Their 2013 study is discussed further, below.

Rodríguez-González *et al.* (2012) suggested the thermal state of the upper plate is an important factor in low-angle subduction, through numerical modeling and comparisons of subduction zones beneath Mexico and southern Central America; however, they did not consider the contrasting absolute motions of the upper plates in either environment (*e.g.,* Cross and Pilger, 1982). Manea *et al.* (2012, 2017) applied numerical modeling with results supporting trenchward absolute motion and thickness of the upper plate as important factors in low-angle subduction, while ruling out hotspot traces based on Skinner and Clayton's (2010) evidence. Antonijevic *et al.* (2015), in studying the configuration of the low-angle subduction segment beneath Peru, supported a combination of the subducting Nazca Ridge, trenchward movement of the upper plate, and suction. Huangfu *et al.* (2016)

applied numerical modeling to subducting oceanic plate and produced lower angle subduction with thickened lithosphere; absolute motion of the upper plate toward the trench also could contribute to low-angle subduction in their work. Hu *et al.* (2016) were able also to produce low-angle subduction from the aseismic ridge effect and increased thickness of the upper plate without taking trenchward motion of the upper plate into account.

Schepers *et al.* (2017) emphasized absolute motion of the upper plate (in a moving hotspot reference frame) as a primary factor in low-angle subduction beneath Peru, excluding a Nazca ridge effect, based on Skinner and Clayton's (2013) inferences. Flórez-Rodríguez *et al.* (2019), from analog modeling, inferred that aseismic ridges can produce low-angle subduction in some circumstances; they also contrasted their modeling with that of Martinod *et al.* (2005, 2013) to explain their differing results. Bishop *et al.* (2017), from seismicity and velocity modeling, detected an apparent low-velocity layer beneath the crustal part of the subducting Nazca ridge which they infer may represent serpentinized lower oceanic lithosphere, which would contribute to the buoyancy of the ridge, a factor which dynamic modelers may want to incorporate in future work (Kopp *et al.*, 2004 previously inferred possible serpentinization of the lithosphere beneath the Juan Fernández seamount chain). Yan *et al.* (2020), from numerical modeling, inferred that subduction of an oceanic plateau in combination with trenchward displacement of the upper plate leads to low-angle subduction (they did not deal with the origin of such a *plateau*). Schellart (2020), based on numerical and analog modeling and a global synthesis, argued against the roles of subducting ridges and/or trenchward migration of the upper plate, and ruled out their role in combination by one example, Mexico, where no aseismic ridge is observed.

For the most part a combination of subduction of aseismic ridges and trenchward motion of the upper plate appear to be the most consistent mechanisms the numerical and analog modeling studies have inferred. With few exceptions, most of the studies did not consider the evidence from plate reconstructions (*e.g.,* Pilger, 1981, 1984; Yáñez *et al.*, 2001; Bello-González *et al.*, 2018) that show correspondences with Andean tectonism and volcanic patterns.

Some other observations involving aseismic ridge models also can be addressed. For example, subduction of a Manihiki Plateau (MP) fragment in the late Paleocene-early Eocene may have formed the Bolivian orocline at ~18-22° S (O'Driscoll *et al.*, 2012; Saylor *et al.*, 2023). Interestingly, calculated loci for three models of the JF hotspot relative to the Pacific plate for 140-80 Ma (Fig. 9, calculated from the parameters of Wessel and Kroenke, 2006, and 2008, their models A and B) intersect the region to the west of the MP where O'Driscoll *et al.* (2012) postulated a Farallon plate complement existed at approximately 125 Ma. Given the variations in the positions between the three modeled loci (Fig. 9), it seems plausible that the existing JF hotspot is a remnant of the plume that O'Driscoll *et al.* (2012) and others postulated produced the MP and the Ontong Java plateau. In contrast, the modeled loci from the parameters of Torsvik *et al.* (2019) place the calculated JF locus well to the east of the MP (Fig. 9), which is inconsistent with the association of the MP and the JF. Also, the calculated locus of the Foundation (FN) hotspot relative to the Pacific plate, calculated from the composite Wessel and Kroenke (2008) Model A utilized here, falls just north of the MP at about 100 Ma. The composite Torsvik *et al.* (2019) model intersects the northern flank of the MP (Fig. 9). Ages as young as the locus predicts (~100 Ma) have not been reported, but this part of the plateau may be yet unsampled. In sum, the proposal of O'Driscoll *et al.* (2012) is consistent only in part with the results presented here. The Manihiki Plateau may have been produced by the same hotspot (or plume) that produced the Juan Fernández trace; however, the reconstructed portion of the trace that intersected the Peru-Chile trench offshore southern Peru and northern Chile (responsible for the Bolivian orocline), is younger than the Plateau (Fig. 3A). The complement to the Plateau on the Nazca plate, if it indeed existed, would have encountered the trench earlier (*i.e.*, >40 Ma) than the formation of the orocline. Alternatively, the complement to the Manihiki Plateau may have been displaced onto the now subducted Phoenix plate (beneath Antarctica; Hochmuth and Gohl, 2017), rather than becoming part of the Nazca plate, but this does not obviate a common origin of the Plateau, its complement, and the Juan Fernández hotspot.

As noted above, Skinner and Clayton (2013) suggested another subducting aseismic ridge exists offshore southern Peru and northern Chile (17° to 19° S), previously interpreted as a propagating

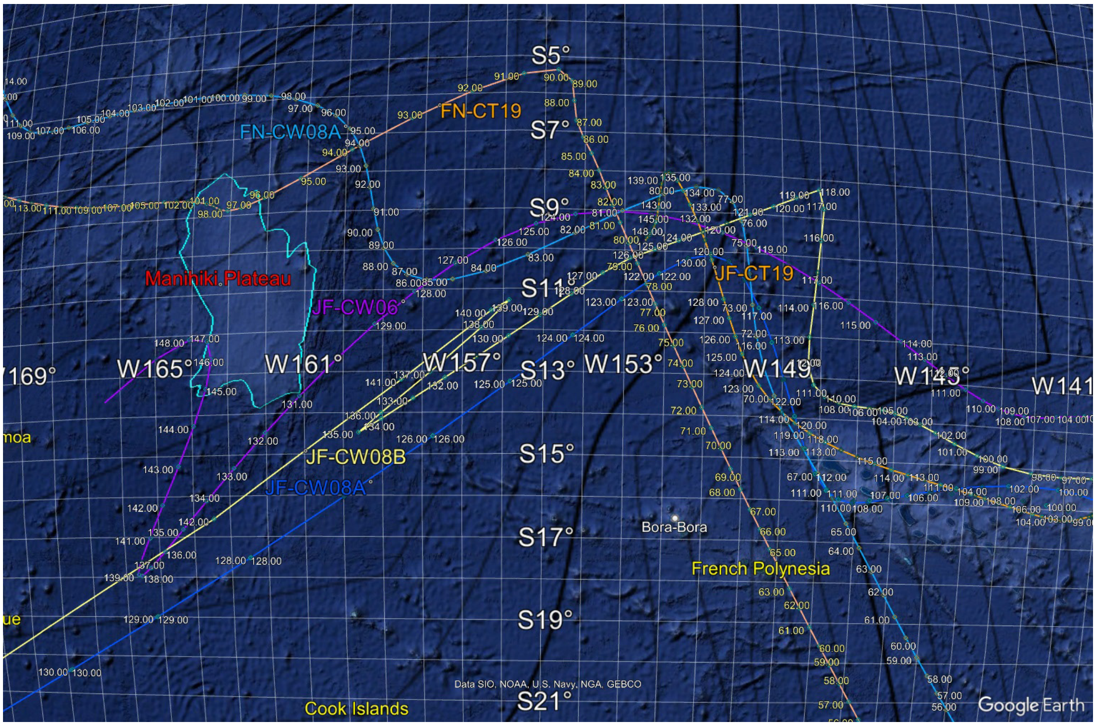

FIG. 9. Region around Manihiki Plateau with loci from proposed Juan Fernández (**JF**) and Foundation (**FN**) hotspots, relative to a Pacific hotspot frame, based on three composite model with various parameters for 80-140 Ma as indicated. **CT19:** Torsvik *et al.* (2019). **CW06:** Wessel *et al.* (2006). **CW08A** and **CW08B:** Wessel and Kroenke (2008).

spreading center (Cande and Haxby, 1991). Where the inferred ridge encounters the trench there is no obvious effect on the subduction configuration, which argues against the hypothetical correlation of hotspot traces with low-angle subduction; this observation has been cited by several workers as an argument for other mechanisms for low-angle subduction (as mentioned above). A candidate for this ridge's hotspot is the same melting center assumed to have produced the Foundation seamount chain on the young Pacific plate (Bello-González *et al.*, 2018, see also Contreras-Reyes *et al.*, 2021). Utilizing the composite Pacific-hotspot model of Pacific and Nazca/Farallon plate motion, loci of the Foundation hotspot on each plate are calculated (Fig. 10) and come close to observed ridge segments on each plate, including that which Skinner and Clayton (2013) recognized, as well as that by Cande and Haxby (1991) on the Pacific plate. When the age of the hypothetical hotspot trace on the Pacific plate is compared to the age of the underlying plate, the portion of the locus >50 Ma is younger than the plate (Fig. 10A). Conversely the corresponding part of the locus on the Nazca/Farallon plate is older than the underlying plate (Fig. 10B). This implies that, prior to ~50 Ma the Foundation hotspot was beneath the Pacific plate, not the Farallon plate. Only after ~50 Ma until ~25 Ma was the hotspot beneath the Farallon plate (Bello-González *et al.*, 2018). Then it began forming the younger Foundation seamount chain on the Pacific plate. If this model is approximately correct, a limited section of the Foundation hotspot trace formed on the Nazca plate (Fig. 10B). This implies that an aseismic ridge within this segment of the Andean subduction zone, as postulated by the model of Skinner and Clayton (2013), is not present.

Báez *et al.* (2023), using Bello-González *et al.*'s (2018) reconstructions and extensive field data, proposed that the late Cenozoic volcanic history of the Southern Puna region (~24-27° S) reflected fracturing of the subducting plate along flexures controlled by subducting aseismic ridges (two lesser Nazca plate features as well as the Juan Fernández trace).

A

B

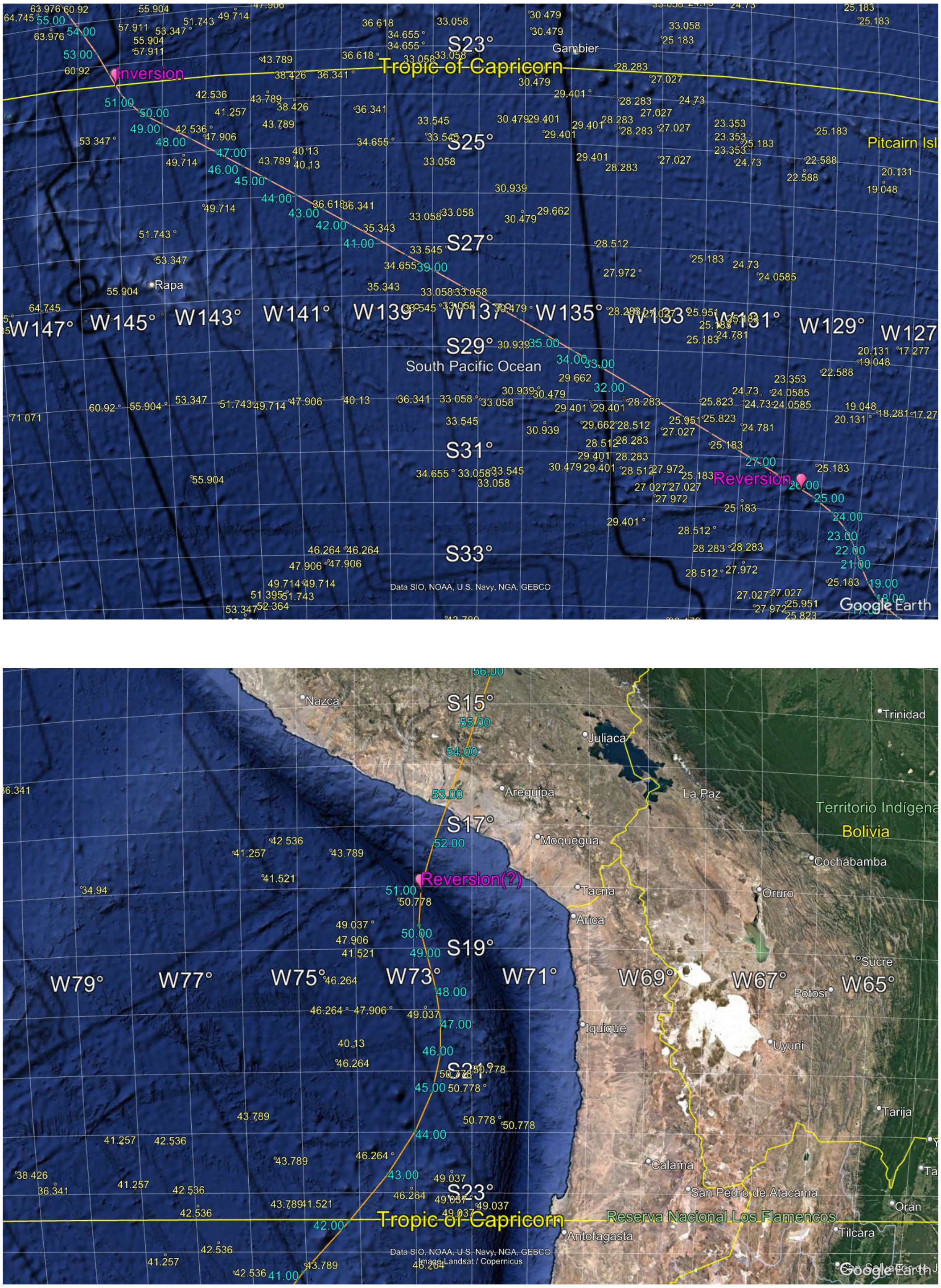

FIG. 10. Foundation hotspot loci (Composite model) compared with the Global Seafloor Fabric and Magnetic Lineation (GSFML) magnetic isochron identification ages (Seton *et al.*, 2014). **A.** Locus over Pacific plate. **B.** Locus over Nazca plate. Inversion: Transition of younging locus age from younger to older than plate age. Reversion: Transition of younging locus age from older to younger than plate age.

They did not attempt to reconstruct these features beyond projections into the subduction zone. Whether they represent small hotspots or alternative features of the Nazca plate is uncertain.

4. Discussion

4.1. Implications for low-angle subduction

This empirical study shows that one reconstructed hotspot trace (Juan Fernández) undergoing subduction is consistent with magmatic patterns in the Andes since at least ~50 Ma, and a second trace (Easter-Nazca) since ~15 Ma. Physical and numerical models discussed above, which involve non-hotspot trace explanations for the two contemporary low-angle subduction segments beneath the Andes, have not been tested against Cenozoic magmatic patterns and/or are inconsistent with plate reconstructions. As also noted, variations in the Nazca/Farallon convergence rate over the last 80 Myr do not indicate a clear correspondence with the formation of the low-angle subduction segments. Insofar as upper (*e.g.,* South American) plate-to-hotspot motion is concerned, displacement of the upper plate toward the trench (and relative to the underlying asthenosphere) appears to be necessary, if not sufficient, for the existence of a volcanic arc on the upper plate and the absence of significant back-arc extension (*e.g.,* Cross and Pilger, 1982; Jurdy, 1983; Jarrard, 1986). There may be a dynamic effect on the angle of normal subduction observed beneath the Andes (*e.g.,* Lallemand *et al.*, 2005; Schellart, 2017), typically a maximum of 45° to a depth of 300 km, in contrast with near vertical subduction observed beneath some island arcs of the western Pacific which are experiencing back-arc extension. Where motion relative to hotspots is calculable, the upper plate appears to be stationary or moving away from the trench (*e.g.,* Jurdy, 1983; Jarrard, 1986). Other factors may contribute to low-angle subduction without aseismic ridge subduction: *e.g.,* young age of the subducting plate, convergence rate, and motion of the upper plate toward the trench (Cross and Pilger, 1982). The latter two such controls are relevant to an entire subduction system and/or for long periods of time, and do not necessarily explain short-duration, anomalous low-angle subduction such as that observed in this study.

4.2. Implications for the fixed hotspot hypothesis

In addition to strengthening the proposal that hotspot traces may contribute to low-angle subduction, this study also provides support for an expanded distinct Pacific hotspot reference frame. This domain extends from Hawaii in the northwest to Juan Fernández in the southeast and includes Louisville to the southwest and the Gulf of Alaska and Yellowstone to the northeast. Figure 11 illustrates the reconstructed Yellowstone trace beneath the northwestern United States, including the Basin and Range Province (after McQuarrie and Wernicke, 2005), in the Hawaiian reference frame (using the composite model), and a reconstructed trace relative to the M93 Atlantic-Indian Ocean frame model. Isotopic dates along the reconstructed trace in figure 11 correspond relatively well with the trace in the Hawaiian frame (volcanism began after the arrival of the trace for a given longitude). The Hawaiian and Tristan (Atlantic-Indian Oceans) frames appear to deviate from one another (*e.g.,* Duncan, 1981; Norton, 1995; Raymond *et al.*, 2000). The moving-hotspot reference frames (*e.g.,* O'Neill *et al.*, 2005; Doubrovine *et al.*, 2012) are rooted in a mantle convection model based on seismic tomography, with velocity converted to density, and radial, but not spherical, viscosity variations. The hotspots deviation from the convection model is then globally averaged over the last 80 Myr with dates from four traces to produce final models. Gaastra *et al.* (2022) showed that two of the traces, the Hawaiian-Emperor and Louisville, from the Pacific plate, do not require significant motion between their source hotspots over the same period based on more recent dating, modeling incorporating data from other Pacific plate traces, and treating the hotspot locations as variables. Similarly, the two hotspot traces from the Atlantic and Indian oceans are consistent with a separate reference frame as Müller *et al.* (1993) defined (modifying Duncan, 1981; see also Maher *et al.*, 2015). Perhaps, instead of globally moving hotspots (such as in the Atlantic-Indian frame), there are the two geographically restricted reference frames: Hawaiian (beneath the plates of the Pacific Ocean and western North America) and Tristan (beneath the Indian and the South and central North Atlantic oceans and bordering continents), with perhaps a third, Iceland, which includes most of Eurasia (Pilger, 2003).

A

B

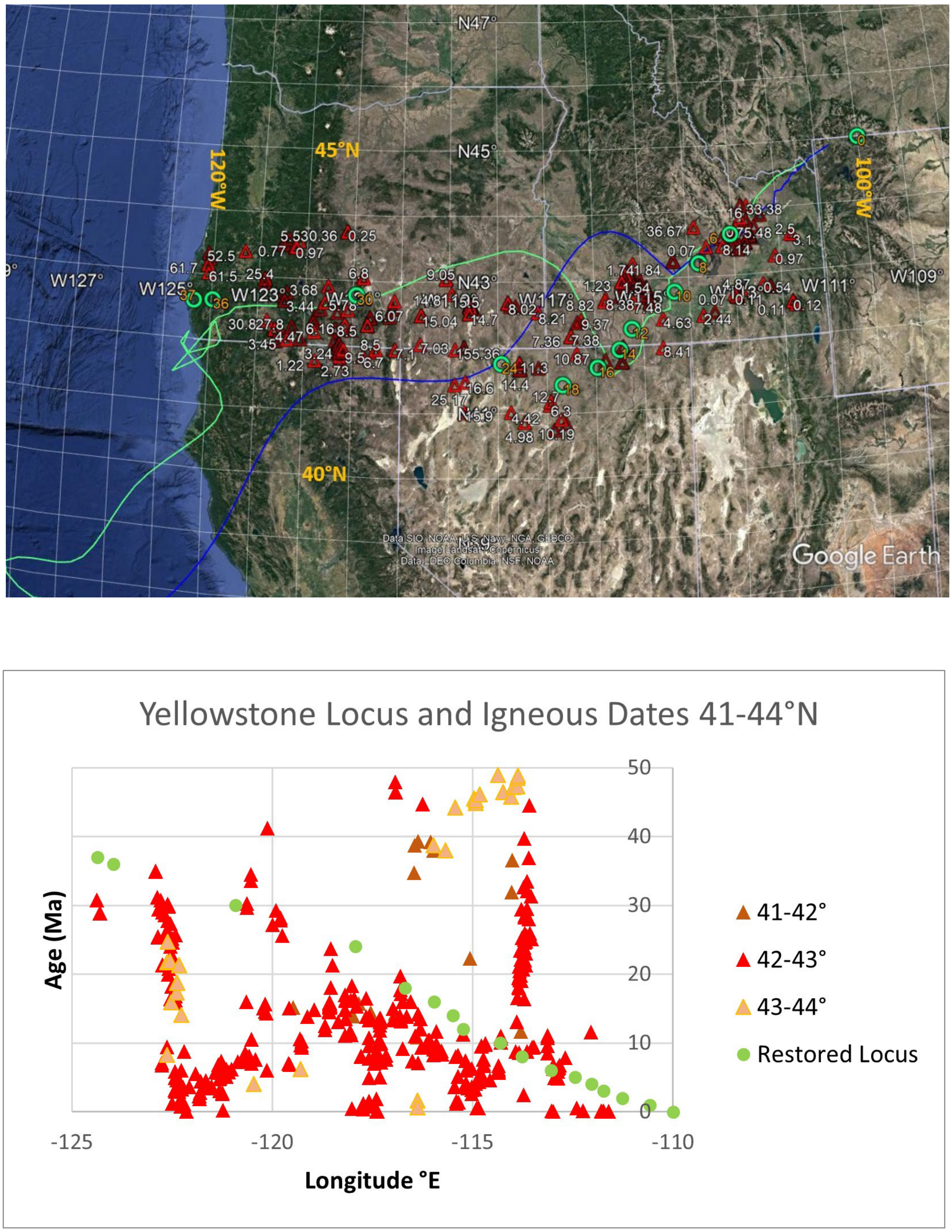

FIG. 11. Basalt isotopic dates between 42° and 43°N latitude, western North America, with points along the calculated locus of the Yellowstone hotspot trace. The calculated locus incorporates the composite Pacific-hotspot model with the crustal extension model of McQuarrie and Wernicke (2005) for the Basin and Range Province relative to the North American plate. **A.** Google Earth view - **red triangles:** isotopic date locations (dates in white); **green circles:** *restored* Yellowstone hotspot trace locations (ages in orange). **Curves:** calculated loci relative to stable North American plate (Hawaiian hotspot frame, green; Tristan hotspot frame, blue). **B.** Plot of isotopic ages (Ma) versus longitude for basalts (red triangles) with restored locations of the Yellowstone hotspot trace (green circles) in the Hawaiian reference frame. Isotopic data from Hillenbrand *et al.* (2023).

4.3. Byproduct of hotspot trace subduction: post-rifting magmatism in Paraguay and Eastern Brazil?

The distribution of volcanism from the Andean crest to the east, and its relationship to inferred hotspot traces within the underlying Nazca/Farallon plate, prompts a question regarding the fate of subducted hotspot traces beneath the South American plate (Fig. 7). Does a subducted trace segment, perhaps detached from the subducted plate, itself sink into the deeper mantle? Or, alternatively, might it be incorporated into the shallow asthenosphere, especially if the trace lithosphere is extensively serpentinized?

In Paraguay and northeast and southeast Brazil there are two seemingly anomalous magmatic zones significantly younger than volcanics associated with rifting and initial spreading of the South Atlantic Ocean (*e.g.,* Gomes *et al.*, 1990, 2013; Gibson *et al.*, 1995; Mizusaki *et al.*, 2002; Perlingeiro *et al.*, 2013; Souza *et al.*, 2013). Two hotspots (perhaps underlain by plumes) have been suggested to be responsible for the Fernando de Noronha and Martin Vaz archipelagos. However, the age patterns onshore do not provide an obvious age progression, especially for Fernando de Noronha (*e.g.,* Knesel *et al.*, 2011). One explanation for the younger volcanism is that it represents edge-effect convection in the asthenosphere along the zone of progressive thinning of the lithosphere from the Amazonian craton to the oceanic lithosphere of the South Atlantic, like what has been observed on the African margin to the east (*e.g.,* Knesel *et al.*, 2011; Belay *et al.*, 2019). Other explanations invoke deviated plumes from the presumed Tristan da Cunha plume in the South Atlantic or extensional stresses propagating through the lithosphere, tapping hot asthenosphere at depth (*e.g.,* Geraldes *et al.*, 2022). Guimarães *et al.* (2020) propose a complex model, involving pre-South Atlantic rifting asthenosphere, having experienced extended heating, which slowly flows into rifted or thinned lithosphere for a prolonged period after the South Atlantic Ocean began to open. This model requires decompression melting as the asthenospheric material reaches shallower depths, either through previous crustal-scale structures or induced by intraplate extension. Stanton *et al.* (2022) also invoke decompression melting above a postulated thermal anomaly.

It is proposed here that the anomalous zones involve older, shallowly subducted hotspot traces (originally from the Farallon or other Pacific oceanic plate; that is, from the west) in the upper asthenosphere. As they initially pass beneath the progressively thickened South American lithosphere of the Amazon craton, melting ceases. Further passage to the east, where the lithosphere is thinner, may allow for decompression and resumed partial melting of the subducted remnant blocks to produce the eastern Brazil/Paraguay magmatism. Two or more hotspot traces on the Farallon (or another Pacific) plate, older than the existing Easter-Nazca and Juan Fernández traces, are required in this model to explain the anomalous magmatism observed in Paraguay and eastern Brazil.

There are two tests for the hypothesis outlined above. In the first, the distribution of Paraguayan and east Brazilian age dates (see Appendix for age references) is plotted on a map of calculated lithospheric thicknesses beneath continental South America (Fig. 12; see Supplementary File for the geospatial data). The isotopic ages utilized in this study occur along boundaries between thick and thin lithosphere (subjectively inferred at ~150 km), consistent with the depressurization hypothesis, that is, magmatism does not occur within the thickest parts of the South American plate (decompression melting is also part of some the alternative models as noted above). Second, the various date sample locations are restored back in time relative to the Müller *et al.* (1993) African hotspot reference frame (Fig. 13) extended to South America. Many of the restored loci extending as early as 130 Ma are proximal to the Andean foreland front where igneous bodies of that age and older are present. Were one to further transform the loci into a Pacific plate frame (from earlier subduction of the postulated older Pacific plate and the included older hotspot traces), the loci would be restored further to the west into the paleo-Pacific Ocean. These reconstructions indicate the plausibility of the plate kinematics required, despite uncertainty in the South Atlantic plate-hotspot model used, as well as in the proposed hotspot sources for the inferred subducted traces.

The possible role of shallow subduction of hotspot traces in sourcing magmatism to the far east, in Brazil and Paraguay (1,500-3,000 km from the current oceanic trench), is not inconsistent with the analysis of Speziale *et al.* (2020a, b), or with the model of Ferreira *et al.* (2022, and references therein), in which crustal extension, shallow

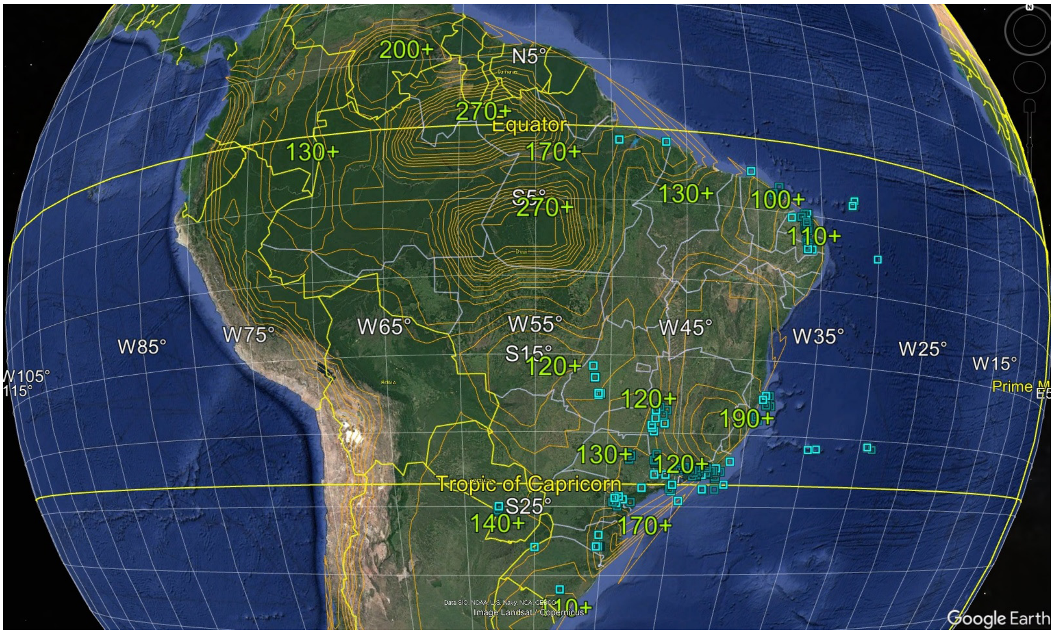

FIG. 12. Calculated thickness in km of the South American continental lithosphere after Artemieva (2006; data provided by author) with dated sample points (blue squares; geospatial data provided in Supplementary File). Note how most onshore samples in east Brazil and Paraguay occur along boundaries between thin (<150 km) and thick (>150 km) lithosphere. Oceanic plate lithosphere thickness is on the order of 90 km (*e.g.,* Niu, 2021).

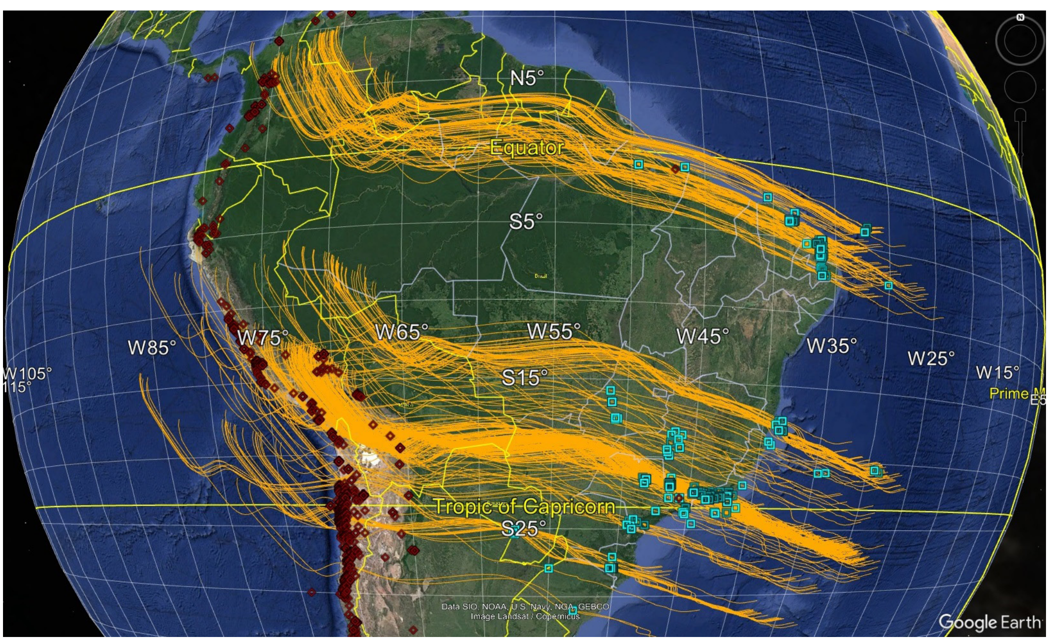

FIG. 13. Full loci of isotopic dates from eastern Brazil and Paraguay (blue squares) backtracked with respect to the Tristan hotspot reference frame using (spline interpolated) parameters of Müller *et al.* (1993) for 0-130 Ma and Maher *et al.* (2015) for 130-150 Ma. Also shown are Jurassic and Cretaceous dates (red diamonds) in Colombia, Peru, Bolivia, Argentina, and Chile. (Note how many back-tracked loci come close to the data points in the Andes.) Data points and loci provided in Supplementary File.

convection, and variations in lithospheric thickness are invoked as contributors to that anomalous igneous activity. The proposal advanced herein provides potentially predictable heterogeneities in the shallow asthenosphere (for example, introducing eclogite which originated as oceanic hotspot trace crust as well as serpentinite) that melted and mixed with shallower continental lithospheric sources. Additional magmatic studies might provide a potential record of passage of South American lithosphere over older subducted hotspot traces like that of ridges undergoing contemporary subduction. Such a model may also be pertinent to other zones of anomalous magmatism which do not clearly fit hotspot trace models (cf. Gianni *et al.*, 2023), including those beneath the African plate, which may represent previously subducted traces formed on the Tethys plate.

4.4. Additional considerations

Three recent contributions, Gianni and Navarrete (2022); Gianni *et al.* (2023) and Mather *et al.* (2023) invoke low-angle subduction or its remnants, in some cases produced by anomalous thick lithosphere, as responsible for distinctive igneous events in the geologic record. Such possible features are compatible with the hypotheses put forward in this contribution. Gianni *et al.* (2023) and Mather *et al.* (2023) propose that asthenosphere remnants of low-angle subduction persist for long and would be responsible for some peculiar geochemical magmatic patterns. Gianni and Navarrete (2022) suggest that slab loss by detachment of normal lithosphere from newly subducted, thickened oceanic lithosphere produced a gap in the igneous record of part of southwestern Pangea, by a mechanism distinct from those proposed here.

As with any scientific study, more data are desirable, not only for improved understanding of hotspots and their products and the tectono-magmatic evolution of the Andes, but their global implications for plate reconstructions for the Mesozoic and Cenozoic. Perhaps new technology, such as multiple solar-powered magnetometers in GPS-guided drones could obtain more detailed surveys of the east-central Pacific, at much lower cost than conventional marine surveying. From such surveys, significant improvement in characterization of the kinematics of the Pacific-Nazca/Farallon plate boundary since ~84 Ma, including microplates, could be accomplished.

Significant progress in the study of island-seamount chains and aseismic ridges of the world oceans has been made. However, many such features have not been dated or have had only potassium-argon measurements made. The composite plate-hotspot model constructed in this work can be improved upon by additional dating, especially adding the traces on the Nazca and Cocos plates to those on the Pacific plate in future modeling.

Insofar as on-land studies are concerned, it is quite possible that additional relevant published dates have been overlooked in this study. Dating of known volcanics and intrusive bodies which have not been analyzed here, particularly where apparent gaps exist, would be most valuable. Like several hotspot studies, this work has not incorporated geochemical implications for the origin and evolution of volcanic arc and intraplate magmas, so the context of hotspot trace subduction could be enhanced by incorporating ages with petrological models.

5. Conclusions

This study strengthens the inferences that (1) the Pacific hotspots form a relatively fixed reference frame beneath the Pacific, Nazca, and Cocos plates, and (2) traces formed from the hotspots beneath the Nazca plate, especially those produced by the Juan Fernández and Easter-Nazca hotspots, produce low-angle subduction segments and profoundly influence subduction-related magmatism in and adjacent to the Andes. In addition, it is inferred that remnants of long-subducted hotspot traces may be responsible for anomalous magmatism in Paraguay, eastern Brazil, and offshore in the western South Atlantic Ocean. Uncertainties in the details of these correlations and inferences persist, especially because of sparse magnetic surveys of the eastern Pacific Ocean, far-from-complete studies of the seamounts of the Pacific and Atlantic, and the derivative plate-hotspot models. Some of the most rapid seafloor spreading in the world ocean occur along perhaps the least surveyed young ocean floor, that of the east-central Pacific, so future studies are recommended in that direction.

Acknowledgements

Comments by an anonymous reviewer and the editor were very helpful in suggesting areas for clarification and are appreciated.

References

Andrews, D.L.; Gordon, R.G.; Horner-Johnson, B.C. 2006. Uncertainties in plate reconstructions relative to the hotspots; Pacific-hotspot rotations and uncertainties for the past 68 million years. Geophysical Journal International 166: 939-951. doi: https://doi.org/10.1111/j.1365-246X.2006.03029.x

Antonijevic, S.K.; Wagner, L.S.; Kumar, A.; Beck, S.L.; Long, M.D.; Zandt, G.; Tavera, H.; Condori, C. 2015. The role of ridges in the formation and longevity of flat slabs. Nature 524: 212-215.

Arriagada, C.; Roperch, P.; Mpodozis, C.; Cobbold, P.R. 2008. Paleogene building of the Bolivian Orocline: Tectonic restoration of the central Andes in 2-D map view. Tectonics 27: TC6014. doi: https://doi.org/10.1029/2008TC002269

Arriagada, C.; Ferrando, R.; Córdova, L.; Morata, D.; Roperch, P. 2013. Andean Geology, The Maipo Orocline: A first scale structural feature in the Miocene to Recent geodynamic evolution in the central Chilean Andes. Andean Geology 40 (3): 419-437. doi: http://dx.doi.org/10.5027/andgeoV40n3-a02

Artemieva, I.M. 2006. Global 1° x 1° thermal model TC1 for the continental lithosphere: implications for lithosphere secular evolution. Tectonophysics 416 (1-4): 245-277. doi: https://doi.org/10.1016/j.tecto.2005.11.022

Báez, W.; Bustos, E.; Chiodi, A.; García, H.P.A.; Álvarez, O.; Simón, V.; Folguera, A. 2023. Reviewing the geodynamic impact of aseismic ridges subduction on the tectonic-magmatic evolution of the Southern Puna plateau. Journal of South American Earth Sciences 129: 104520. doi: https://doi.org/10.1016/j.jsames.2023.104520.

Barazangi, M.; Isacks, B.L. 1976. Spatial distribution of earthquakes and subduction of the Nazca plate beneath South America. Geology 4: 686-692. doi: https://doi.org/10.1130/0091-7613(1976)4%3C686:SDOEAS%3E2.0.CO;2

Belay, I.G.; Tanaka, R.; Kitagawa, H.; Kobayashi, K.; Nakamura, E. 2019. Origin of ocean island basalts in the West African passive margin without mantle plume involvement. Nature Communications 10: 1-12. doi: https://doi.org/10.1038/s41467-019-10832-7.

Bello-González, J.P.; Contreras-Reyes, E.; Arriagada, C. 2018. Predicted path for hotspot tracks off South America since Paleocene times: Tectonic implications of ridge-trench collision along the Andean margin. Gondwana Research 64: 216-234. doi: https://doi.org/10.1016/j.gr.2018.07.008

Bishop, B.T.; Beck, S.L.; Zandt, G.; Wagner, L.; Long, M.D.; Antonijevic, S.K.; Kumar, A.; Tavera, H. 2017. Geosphere, Causes and consequences of flat-slab subduction in southern Peru. Geosphere 13: 1392-1407. doi: https://doi.org/10.1130/GES01440.1

Cande, S.C. 1985. Nazca-South America plate interactions since 50 My B.P. *In* Ocean Margin Drilling Program, (Hussong, D.M.; Dang, S.P.; Kulm, L.D.; Couch, R.W.; Hilde, T.W.C.; editors). Regional Atlas Series, Atlas 9, Peru-Chile Trench off Peru.

Cande, S.C.; Haxby, W.F. 1991. Eocene propagating rifts in the southwest Pacific and their conjugate features on the Nazca Plate. Journal of Geophysical Research 96 (B12): 19609-19622. doi: https://doi.org/10.1029/91JB01991

Contreras-Reyes, E.; Obando-Orrego, S.; Geersen, J.; Bello-González, J.P. 2021. Density structure, flexure, and tectonics of the Iquique Ridge, northern Chile. Journal of South American Earth Sciences 111: 103423. doi: https://doi.org/10.1016/j.jsames.2021.103423

Cross, T.A.; Pilger, R.H.Jr. 1978a. Tectonic controls of Late Cretaceous sedimentation, western interior, U.S.A. Nature 274: 653-657. doi: https://doi.org/10.1038/274653a0

Cross, T.A.; Pilger, R.H.Jr. 1978b. Constraints on absolute motion and plate interactions inferred from Cenozoic igneous activity in the western United States. American Journal of Science 278: 865-902. doi: https://doi.org/10.2475/ajs.278.7.865

Cross, T.A.; Pilger, R.H.Jr. 1982. Geological Society of America Bulletin, Controls of subduction geometry, location of magmatic arcs, and tectonics of arc and back-arc regions. Geological Society of America Bulletin 93 (6): 545-562. doi: https://doi.org/10.1130/0016-7606(1982)93%3C545:COSGLO%3E2.0.CO;2

de Silva, S.; Kay, S.M. 2018. Turning up the Heat: High-Flux Magmatism in the Central Andes. Elements 14 (4): 245-250. doi: https://doi.org/10.2138/gselements.14.4.245

DeCelles, P.G.; Ducea, M.N.; Kapp, P.; Zandt, G. 2009. Cyclicity in Cordilleran orogenic systems. Nature Geoscience 2: 251-257. doi: https://doi.org/10.1038/ngeo469

Doubrovine, P.V.; Steinberger, B.; Torsvik, T.H. 2012. Absolute plate motions in a reference frame defined by moving hotspots in the Pacific, Atlantic and Indian Oceans. Journal of Geophysical Research 117: B09101. doi: https://doi.org/10.1029/2011JB009072

Duncan, R.A. 1981. Hotspots in the southern oceans; an absolute frame of reference for motion of the Gondwana continents. Tectonophysics 74 (1-2): 29-42. doi: https://doi.org/10.1016/0040-1951(81)90126-8

Dupont-Nivet, G.; Roperch, P.; Gautier, P.; Chauvin, A.; Gerard, M.; Carlier, G. 1996. Clockwise rotations in northern Chile: oroclinal bending and in situ tectonic rotations. Third International Symposium on Andean Geodynamics: 355-358. St. Malo.

Espurt, N.; Funiciello, F.; Martinod, J.; Guillaume, B.; Regard, V.; Faccenna, C.; Brusset, S. 2008. Flat subduction dynamics and deformation of the South American plate: Insights from analog modeling. Tectonics 27: TC3011. doi: https://doi.org/10.1029/2007TC002175

Ferreira, A.C.D.; Conceição, R.; Vieira, M.; Pimentel, A.M. 2022. Mesozoic to Cenozoic alkaline and tholeiitic magmatism related to West Gondwana break-up and dispersal. Gondwana Research 106: 15-33. doi: https://doi.org/10.1016/j.gr.2022.01.005

Flórez-Rodríguez, A.G.; Schellart, W.P.; Strak, V. 2019. Impact of aseismic ridges on subduction systems: Insights from analog modeling. Journal of Geophysical Research: Solid Earth 124: 5951-5969. doi: https://doi.org/10.1029/2019JB017488

Gaastra, K.M.; Gordon, R.G.; Woodworth, D.T. 2022. Quantification of Pacific plate hotspot tracks since 80 Ma. Tectonics 41 (7): e2021TC006772. doi: https://doi.org/10.1029/2021TC006772

Geraldes, M.C.; Mohriak, W.U.; Bonifácio, J.F.; Cardoso, L.M.C.; Moura, S.C. 2022. The role of the Rio Grande Rise on the continental Meso-Cenozoic alkaline magmatism in southwest Brazil. *In* Meso-Cenozoic Brazilian Offshore Magmatism. Geochemistry, Petrology and Tectonics, Chapter 8: 257-292. doi: https://doi.org/10.1016/B978-0-12-823988-9.00005-8

Gerya, T.V.; Fossati, D.; Cantieni, C.; Seward, D. 2009. Dynamic effects of aseismic ridge subduction: numerical modelling. European Journal Mineralogy 21 (3): 649-661.

Gianni, G.M.; Navarrete, C.R. 2022. Catastrophic slab loss in southwestern Pangea preserved in the mantle and igneous record. Nature Communications 13: 698. doi: https://doi.org/10.1038/s41467-022-28290-z

Gianni, G.M.; Likerman, J.; Navarrete, C.R.; Gianni, C.R.; Zlotnik, S. 2023. Ghost-arc geochemical anomaly at a spreading ridge caused by supersized flat subduction. Nature Communications 14: 2023. doi: https://doi.org/10.1038/s41467-023-37799-w

Gibson, S.A.; Thompson, R.N.; Leonardos, O.H.; Dickin, A.P.; Mitchell, J.G. 1995. The Late Cretaceous impact of the Trindade mantle plume: Evidence from large-volume, mafic, potassic magmatism in SE Brazil. Journal of Petrology 36 (1): 189-229. doi: https://doi.org/10.1093/petrology/36.1.189

Gomes, C.B.; Ruberti, E.; Morbidelli, L. 1990. Carbonatite complexes from Brazil: a review. Journal of South American Earth Sciences 3: 51-63. doi: https://doi.org/10.1016/0895-9811(90)90017-U

Gomes, C.B.; Comin-Chiaramonti, P.; Velázquez, V.F. 2013. A synthesis on the alkaline magmatism of Eastern Paraguay. Brazilian Journal of Geology 43: 745-761. doi: https://doi.org/10.5327/Z2317-488920130004000012

Gradstein, F.M.; Ogg, J.G.; Schmitz, M.D.; Ogg, G.M. 2020. Geologic Time Scale 2020. Elsevier BV. Amsterdam. doi: https://doi.org/10.1016/B978-0-12-824360-2.00032-2

Gripp, A.E.; Gordon, R.G. 2002. Young tracks of hotspots and current plate velocities. Geophysical Journal International 150 (2): 321-361. doi: https://doi.org/10.1046/j.1365-246X.2002.01627.x

Guimarães, A.R.; Fitton, J.G.; Kirstein, L.A.; Barfod, D.N. 2020. Contemporaneous intraplate magmatism on conjugate South Atlantic margins: A hotspot conundrum. Earth and Planetary Science Letters 536: 116147. doi: https://doi.org/10.1016/j.epsl.2020.116147

Hampel, A. 2002. The migration history of the Nazca Ridge along the Peruvian active margin: a re-evaluation. Earth and Planetary Science Letters 203 (2): 665-679. doi: https://doi.org/10.1016/S0012-821X(02)00859-2.

Harada, Y.; Hamano, Y. 2000. Recent progress on plate motions relative to hot spots. *In* The History and Dynamics of Global Plate Motions, Geophysical Monograph Series, 121 (Richards, M.A.; Gordon, R.G.; van der Hilst, R.D.; editors). American Geophysical Union: 327-338, Washington, D.C.

Hillenbrand, I.W.; Thomson, K.D.; Morgan, L.E.; Gilmer, A.K.; Dombrowski, A.D.; Warrell, K.F.; Malone, J.R.; Souders, A.K.; Hudson, A.M.; Cosca, M.A.; Paces, J.B.; Thompson, R.A.; Park, A.J. 2023. USGS Geochron: A Database of Geochronological and Thermochronological Dates and Data. United States Geological Survey data release. doi: https://doi.org/10.5066/P9RZNPIF

Hochmuth, K.; Gohl, K. 2017. Collision of Manihiki Plateau fragments to accretional margins of northern Andes and Antarctic Peninsula. Tectonics 36 (2): 229-240. doi: https://doi.org/10.1002/2016TC004333

Hu, J.; Liu, L.; Hermosillo, A.; Zhou, Q. 2016. Simulation of late Cenozoic South American flat-slab subduction using geodynamic models with data assimilation. Earth and Planetary Science Letters, 438: 1-13. doi: https://doi.org/10.1016/j.epsl.2016.01.011

Hu, J.; Gurnis, M.; Rudi, J.; Stadler, G.; Müller, R.D. 2022. Dynamics of the abrupt change in Pacific Plate motion around 50 million years ago. Nature Geoscience 15: 74-78. doi: https://www.nature.com/articles/s41561-021-00862-6

Huangfu, P.; Wang, Y.; Cawood, P.A.; Li, Z.-H.; Fan, W.; Gerya, T.V. 2016. Thermo-mechanical controls of flat subduction: Insights from numerical modeling. Gondwana Research. doi: https://doi.org/10.1016/j.gr.2016.08.012

Isacks, B.L. 1988. Uplift of the Central Andean Plateau and Bending of the Bolivian Orocline. Journal of Geophysical Research: Solid Earth 93 (B4): 3211-3231. doi: https://doi.org/10.1029/JB093iB04p03211.

Jarrard, R.D. 1986. Relations among subduction parameters. Reviews of Geophysics 24 (2): 217-284. doi: https://doi.org/10.1029/RG024i002p00217

Jurdy, D.M. 1983. Early Tertiary subduction zones and hot spots. Journal of Geophysical Research-Solid Earth 88 (B8): 6395-6402. doi: https://doi.org/10.1029/JB088iB08p06395

Kay, S.M.; Coira, B.L. 2009. Shallowing and steepening subduction zones, continental lithospheric loss, magmatism, and crustal flow under the Central Andean Altiplano-Puna Plateau. *In* Backbone of the Americas: Shallow Subduction, Plateau Uplift, and Ridge and Terrane Collision (Kay, S.M.; Ramos, V.A.; Dickinson, W.R.; editors). Memoir of the Geological Society of America 204: 229-259. doi: https://doi.org/10.1130/2009.1204(11)

Kay, R.W.; Kay, S.M. 1993. Delamination and delamination magmatism. Tectonophysics 219 (1-3): 177-189. doi: https://doi.org/10.1016/0040-1951(93)90295-U

Knesel, K.M.; Souza, Z.S.; Vasconcelos, P.M.; Cohen, B.E.; Silveira, F.V. 2011. Young volcanism in the Borborema Province, NE Brazil, shows no evidence for a trace of the Fernando de Noronha plume on the continent. Earth and Planetary Science Letters 302 (1-2): 38-50. doi: https://doi.org/10.1016/j.epsl.2010.11.036

Kopp, H.; Flueh, E.R.; Papenberg, C.; Klaeschen, D. 2004. Seismic investigations of the O'Higgins Seamount Group and Juan Fernández Ridge: Aseismic ridge emplacement and lithosphere hydration. Tectonics 23: 21 p. doi: https://doi.org/10.1029/2003TC001590

Lallemand, S.; Heuret, A.; Boutelier, D. 2005. On the relationships between slab dip, back-arc stress, upper plate absolute motion, and crustal nature in subduction zones. Geochemistry, Geophysics, Geosystems 6 (9): Q09006. doi: https://doi.org/10.1029/2005GC000917

Maher, S.M.; Wessel, P.; Müller, R.D.; Williams, S.E.; Harada, Y. 2015. Absolute plate motion of Africa around Hawaii-Emperor bend time. Geophysical Journal International 201 (3): 1743-1764. doi: https://doi.org/10.1093/gji/ggv104

Manea, V.C.; Pérez-Gussinyé, M.; Manea, M. 2012. Chilean flat slab subduction controlled by overriding plate thickness and trench rollback. Geology 40: 35-38. doi: https://doi.org/10.1130/G32543.1

Manea, V.C.; Manea, M.; Ferrari, L.; Orozco-Esquivel, T.; Valenzuela, R.W.; Husker, A.; Kostoglodov, V. 2017. A review of the geodynamic evolution of flat slab subduction in Mexico, Peru, and Chile. Tectonophysics 695: 27-5.

Martinod, J.; Husson, N. 2010. Horizontal subduction zones, convergence velocity and the building of the Andes. Earth and Planetary Science Letters 299 (3-4): 299-309. doi: https://doi.org/10.1016/j.epsl.2010.09.010

Martinod, J.; Funiciello, F.; Faccenna, C.; Labanieh, S.; Regard, V. 2005. Dynamical effects of subducting ridges: Insights from 3-D laboratory models. Geophysical Journal International 163 (3): 1137-1150. doi: https://doi.org/10.1111/j.1365-246X.2005.02797.x

Mather, B.R.; Müller, R.D.; Alfonso, C.P.; Seton, M.; Wright, N.M. 2023. Kimberlite eruptions driven by slab flux and subduction angle. Scientific Report 13: 9216. doi: https://doi.org/10.1038/s41598-023-36250-w

McQuarrie, N. 2002. Initial plate geometry, shortening variations, and evolution of the Bolivian orocline. Geology 30 (10): 867-870. doi: https://doi.org/10.1130/0091-7613(2002)030%3C0867:IPGSVA%3E2.0.CO;2

McQuarrie, N.; Wernicke, B.P. 2005. An animated tectonic reconstruction of southwestern North America since 36 Ma. Geosphere 1 (3): 147-172. doi: https://doi.org/10.1130/GES00016.1

Mizusaki, A.M.P.; Thomaz-Filho, A.; Milani, E.J.; de Cesero, P. 2002. Mesozoic and Cenozoic igneous activity and its tectonic control in northeastern Brazil. Journal of South American Earth Sciences 15 (2) 183-198. doi: https://doi.org/10.1016/S0895-9811(02)00014-7

Morgan, W.J. 1972. Plate motions and deep mantle convection. Geological Society of America Memoir 132: 7-22.

Müller, R.D.; Royer, J.-Y.; Lawver, L.A. 1993. Revised plate motions relative to the hotspots from combined Atlantic and Indian Ocean hotspot tracks. Geology 21 (3): 275-278. doi: https://doi.org/10.1130/0091-7613(1993)021%3C0275:RPMRTT%3E2.3.CO;2

Müller, R.D.; Cande, S.C.; Royer, J.-Y.; Roest, W.R.; Maschenkov, S. 1999. New constraints on the Late

Cretaceous/Tertiary plate tectonic evolution of the Caribbean. *In* Caribbean Basins (Mann, P.; editor). Elsevier: 39-55. Amsterdam.

Müller, R.D.; Zahirovic, S.; Williams, S.E.; Cannon, J.; Seton, M.; Bower, D.J.; Tetley, M.G.; Heine1, C.; Le Breton, E.; Liu, S.; Russell, S.H.J.; Yang, T.; Leonard, J.; Gurnis, M. 2019. A global plate model including lithospheric deformation along major rifts and orogens since the Triassic. Tectonics 38 (6): 1884-1907. doi: https://doi.org/10.1029/2018TC005462

Niu, Y. 2021. Lithosphere thickness controls the extent of mantle melting, depth of melt extraction and basalt compositions in all tectonic settings on Earth-A review and new perspectives. Earth-Science Reviews 217: 103614. doi: https://doi.org/10.1016/j.earscirev.2021.103614

Norton, I.O. 1995. Plate motions in the North Pacific: the 43 Ma nonevent. Tectonics 14 (5): 1080-1094. doi: https://doi.org/10.1029/95TC01256

Norton, I.O. 2000. Global hotspot reference frames and plate motion. *In* The History and Dynamics of Global Plate Motions (Richards, M.A.; Gordon, R.G.; van der Hilst, R.D.; editors). American Geophysical Union, Geophysical Monograph Series 121: 339-357.

O'Connor, J.M.; Steinberger, B.; Regelous, M.; Koppers, A.A.P.; Wijbrans, J.R.; Haase, K.M.; Stoffers, P.; Jokat, W.; Garbe-Schönberg, D. 2013. Constraints on past plate and mantle motion from new ages for the Hawaiian-Emperor Seamount Chain. Geochemistry, Geophysics, Geosystems 14 (10): 4564-4584. doi: https://doi.org/10.1002/ggge.20267

O'Driscoll, L.J.; Richards, M.A.; Humphreys, E.D. 2012. Nazca-South America interactions and the late Eocene-late Oligocene flat-slab episode in the central Andes. Tectonics 31 (2): TC2013. doi: https://doi.org/10.1029/2011TC003036

O'Neill, C.; Müller, R.D.; Steinberger, B. 2005. On the uncertainties in hot spot reconstructions and the significance of moving hot spot reference frames. Geochemistry, Geophysics, Geosystems 6 (4). doi: https://doi.org/10.1029/2004GC000784

Ogg, J.G. 2020. Geomagnetic Polarity Time Scale. *In* Geologic Time Scale 2020 (Gradstein, F.M.; Ogg, J.G.; Schmitz, M.D.; Ogg, G.M.; editors). Elsevier, Amsterdam 1: 159-192.

Pardo-Casas, F.; Molnar, P.; 1987. Relative motion of the Nazca (Farallon) and South American Plates since Late Cretaceous time. Tectonics 6 (3): 233-248. doi: https://doi.org/10.1029/TC006i003p00233

Perlingeiro, G.; Vasconcelos, P.M.; Knesel, K.M.; Thiede, D.S.; Cordani, U.G. 2013. ^{40}Ar/^{39}Ar geochronology of the Fernando de Noronha Archipelago and implications for the origin of alkaline volcanism in the NE Brazil. Journal of Volcanology and Geothermal Research 249: 140-154. doi: https://doi.org/10.1016/j.jvolgeores.2012.08.017

Pilger, R.H.Jr. 1981. Plate reconstructions, aseismic ridges, and low-angle subduction beneath the Andes. Geological Society of America Bulletin 92 (7): 448-456. doi: https://doi.org/10.1130/0016-7606(1981)92<448:PRARAL>2.0.CO;2

Pilger, R.H.Jr. 1983. Kinematics of the South American subduction zone from global plate reconstructions. *In* Geodynamics of the Eastern Pacific Region, Caribbean and Scotia Arcs Geodynamics of the Eastern Pacific Region, Caribbean and Scotia Arcs, 9 (Ramón-Cabré, S.J.; editor). doi: https://doi.org/10.1029/GD009p0113

Pilger, R.H.Jr. 1984. Cenozoic plate kinematics. subduction and magmatism: South American Andes. Journal of the Geological Society 141 (5): 793-802. doi: https://doi.org/10.1144/gsjgs.141.5.0793

Pilger, R.H.Jr. 2003. Geokinematics-Prelude to Geodynamics. Springer, New York. doi: https://doi.org/10.1007/978-3-662-07439-8

Pilger, R.H.Jr. 2007. The Bend: Origin and significance. Geological Society of America Bulletin 119 (3-4): 302-313. doi: https://doi.org/10.1130/B25713.1

Pilger, R.H.Jr. 2022. Radiometric ages from the South American Andes and adjacent areas: A compilation hosted by GEOROC. doi: http://dx.doi.org/10.25625/NGG0Q7

Pilger, R.H.Jr.; Handschumacher, D. 1981. The fixed-hotspot hypothesis and origin of the Easter-Sala y Gómez-Nazca trace. Geological Society of America Bulletin 92 (7): 437-446. doi: https://doi.org/10.1130/0016-7606(1981)92<437:TFHAOO>2.0.CO;2

Puigdomenech, C.; Alarcón, S.; Ruiz González, V.; Rossel, P.; Orts, D.; Zaffarana, C. 2021. Tectonic rotations in central Chile: New insights on the southern limit of the Maipo Orocline. Journal of South American Earth Sciences 106: 103012. doi: https://doi.org/10.1016/j.jsames.2020.103012

Quiero, F.; Tassara, A.; Iaffaldano, G.; Rabbia, O. 2022. Growth of Neogene Andes linked to changes in plate convergence using high-resolution kinematic models. Nature Communications 13: 1339. doi: https://doi.org/10.1038/s41467-022-29055-4

Ramos, V.A.; Cristallini, E.O.; Pérez, D.J. 2002. The Pampean flat-slab of the Central Andes. Journal of South American Earth Sciences 15 (1): 59-78. doi: https://doi.org/10.1016/S0895-9811(02)00006-8

Raymond, C.A.; Stock, J.M.; Cande, S.C. 2000. Fast Paleogene motion of the Pacific hotspots from revised global plate circuit constraints. *In* History and Dynamics of Plate Motions (Richards, M.A.; Gordon, R.G.; van der Hilst, R.D.; editors). American Geophysical Union, Geophysical Monograph Series 121: 359-375.

Risse, A.; Trumbull, R.B.; Kay, S.M.; Coira, B.; Romer, R.L. 2013. Multi-stage evolution of Late Neogene mantle-derived magmas from the Central Andes back-arc in the southern Puna Plateau of Argentina. Journal of Petrology 54 (10): 1963-1995. doi: https://doi.org/10.1093/petrology/egt038

Rodríguez-González, J.; Negredo, A.M.; Billen, M.I. 2012. The role of the overriding plate thermal state on slab dip variability and on the occurrence of flat subduction. Geochemistry, Geophysics, Geosystems 13 (1): Q01002. doi: http://dx.doi.org/10.1029/2011GC003859

Rowan, C.J.; Rowley, D.B. 2014. Spreading behaviour of the Pacific-Farallon ridge system since 83 Ma. Geophysical Journal International 197 (3): 1273-1283. doi: https://doi.org/10.1093/gji/ggu056

Saylor, J.E.; Sundell, K.E.; Pérez, N.D.; Hensley, J.B.; McCain, P.; Runyon, B.; Álvarez, P.; Cárdenas, J.; Usnayo, W.P.; Valer, C.S. 2023. Basin formation, magmatism, and exhumation document southward migrating flat-slab subduction in the central Andes. Earth and Planetary Science Letters 606: 118050. doi: https://doi.org/10.1016/j.epsl.2023.118050

Schellart, W.P. 2017. Andean mountain building and magmatic arc migration driven by subduction-induced whole mantle flow. Nature Communications 8: 2010. doi: https://doi.org/10.1038/s41467-017-01847-z

Schellart, W.P. 2020. Frontiers in Earth Science, Control of subduction zone age and size on flat slab subduction. Frontiers in Earth Science 8 (26). doi: https://doi.org/10.3389/feart.2020.00026

Schepers, G.; van Hinsbergen, D.; Spakman, W.; Kosters, M.E.; Boschman, L.M.; McQuarrie, N. 2017. South-American plate advance and forced Andean trench retreat as drivers for transient flat subduction episodes. Nature Communications 8: 15249. doi: https://doi.org/10.1038/ncomms15249

Seton, M.; Whittaker, J.; Wessel, P.; Müller, R.D.; DeMets, C.; Merkouriev, S.; Cande, S.; Gaina, C.; Eagles, G.; Granot, R.; Stock, J.; Wright, N.; Williams, S. 2014. Community infrastructure and repository for marine magnetic identifications. Geochemistry, Geophysics, Geosystems 15 (4): 1629-1641. doi: https://doi.org/10.1002/2013GC005176

Sharp, W.D.; Clague, D.A. 2006. 50-Ma Initiation of Hawaiian-Emperor Bend records major change in Pacific plate motion. Science 313 (5791): 1281-1284. doi: https://doi.org/10.1126/science.1128489

Skinner, S.M.; Clayton, R.W. 2010. An evaluation of proposed mechanisms of slab flattening on central Mexico. Pure and Applied Geophysics 168: 1461-1474. doi: https://doi.org/10.1007/s00024-010-0200-3

Skinner, B.; Clayton, R.W. 2013. The lack of correlation between flat slabs and bathymetric impactors in South America. Earth and Planet Science Letters 371-372: 1-5. doi: 10.1016/j.epsl.2013.04.013

Smith, E.G.C. 1985. Calculations of poles of instantaneous rotation from poles of finite rotation. Geophysical Journal of the Royal Astronomical Society 65 (1): 223-227. doi: https://doi.org/10.1111/j.1365-246X.1981.tb02710.x

Somoza, R. 1998. Updated Nazca (Farallon)-South America relative motions during the last 40 My: implications for mountain building in the central Andean region. Journal of South American Earth Sciences 11 (3): 211-215. doi: https://doi.org/10.1016/S0895-9811(98)00012-1

Souza, Z.S.; Vasconcelos, P.M.; Knesel, K.M.; da Silveira Dias, L.G.; Roesner, E.H.; Cordeiro de Farias, P.R.; de Morais Neto, J.M. 2013. The tectonic evolution of Cenozoic extensional basins, northeast Brazil: Geochronological constraints from continental basalt $^{40}Ar/^{39}Ar$ ages. Journal of South American Earth Sciences 48: 159-172. doi: https://doi.org/10.1016/j.jsames.2013.09.008

Speziale, S.; Castorina, F.; Censi, P.; de Barros Gomes, C.; Marques, L.S.; Comin-Chiaramonti, P. 2020a. Carbonatites from the Southern Brazilian platform: I. Open Geosciences 12 (1): 452-478. doi: https://doi.org/10.1515/geo-2020-0050

Speziale, S.; Castorina, F.; Censi, P.; de Barros Gomes, C.; Marques, L.S.; Comin-Chiaramonti, P. 2020b. Carbonatites from the Southern Brazilian Platform: A review. II: Isotopic evidences. Open Geosciences 12 (1): 678-702. doi: https://doi.org/10.1515/geo-2020-0032

Stanton, N.; Gordon, A.C.; Valente, S.C.; Mohriak, W.U.; Maia, T.H.; Arena, M. 2022. The Abrolhos Magmatic Province, the largest post breakup magmatism of the Eastern Brazilian margin: a geological, geophysical, and geochemical review. *In* Meso-Cenozoic Brazilian Offshore Magmatism: Geochemistry, Petrology, and Tectonics (Costa dos Santos, A.; Hackspacher, P.C.; editors). Academic Press 6: 189-230. doi: https://doi.org/10.1016/B978-0-12-823988-9.00014-9

Torsvik, T.H.; Steinberger, B.; Shephard, G.E.; Doubrovine, P.V.; Gaina, C.; Domeier, M.; Conrad, C.P.; Sager, W.W. 2019. Pacific-Panthalassic reconstructions: Overview, errata and the way forward. Geochemistry, Geophysics, Geosystems 20 (7): 3659-3689. doi: https://doi.org/10.1029/2019GC008402

van Hunen, J.; van der Berg, A.P.; Vlaar, N.J. 2004. Various mechanisms to induce present-day flat subduction and implications for the younger Earth: A numerical parameter study. Physics of the Earth and Planetary Interiors 146: 179-194. doi: https://doi.org/10.1016/j.pepi.2003.07.027

Wessel, P.; Kroenke, L.W. 2008. Pacific absolute plate motions since 145 Ma. Journal of Geophysical Research 113: B06101. doi: https://doi.org/10.1029/2007JB005499

Wessel, P.; Harada, Y.; Kroenke, L.W. 2006. Toward a self-consistent, high-resolution absolute plate motion model for the Pacific. Geochemistry, Geophysics, Geosystems 7: Q03L12. doi: https://doi.org/10.1029/2005GC001000.

Wilder, D.T. 2003. Relative motion history of the Pacific-Nazca (Farallon) plates since 30 million years ago. M.Sc. Thesis, University of South Florida.

Wright, N.; Müller, R.D.; Seton, M.; Williams, S. 2015. Revision of Paleogene plate motions in the Pacific and implications for the Hawaiian-Emperor bend. Geology 43 (5): 455-458. doi: https://doi.org/10.1130/G36303.1

Yan, Z.; Chen, L.; Xiong, X.; Wang, K.; Xie, R.; Hsu, H.T. 2020. Observations and modeling of flat subduction and its geological effects. Science China Earth Sciences 63: 1069-1091. doi: https://doi.org/10.1007/s11430-019-9575-2

Yáñez, G.A.; Ranero, C.R.; von Huene, R.; Díaz, J. 2001. Journal of Geophysical Research, Magnetic anomaly interpretation across the southern central Andes (32°-34°S): The role of the Juan Fernández Ridge in the late Tertiary evolution of the margin. Journal of Geophysical Research 106 (B4): 6325- 6345. doi: https://doi.org/10.1029/2000JB900337

Manuscript received: November 01, 2022; revised/accepted: September 27, 2023; available online: September 29, 2023.

Appendix

TABLE A1. SOURCES FOR PLATE-PAIR RECONSTRUCTION MODELS BETWEEN THE SOUTH AMERICAN AND NAZCA PLATES.

Plate pairs	References	Notes
South America-Africa	Müller *et al*. (1999); Pérez-Díaz and Eagles (2014); DeMets and Merkouriev (2019)	-
Africa-East Antarctica	Nankivell (1997); Bernard *et al*. (2005); Cande *et al*. (2010); Cande and Patriat (2015); DeMets *et al*. (2015)	-
East-West Antarctica	Granot *et al*. (2013); Matthews *et al*. (2015); Granot and Dyment (2018)	-
West Antarctica-Pacific	Croon *et al*. (2008); Wright *et al*. (2015, 2016)	-
West Antarctica-Nazca	Tebbens and Cande (1997)	Replaces West Antarctic-Pacific-Nazca with West Antarctic-Nazca for two isochrons in global circuit
Pacific-Nazca	Wilder (2003); Rowan and Rowley (2014)	-
Pacific-Farallon	Seton *et al*. (2012); Rowan and Rowley (2014); Wright *et al*. (2015, 2016)	Assuming symmetrical spreading prior to ~25 Ma

TABLE A2. SOURCES FOR PLATE-HOTSPOT RECONSTRUCTION MODELS.

Plate - Hotspot reference frame	References	Notes
Pacific-Hawaiian	Harada and Hamano (2000); Norton (2000); Raymond *et al*. (2000); Andrews *et al*. (2006); Wessel *et al*. (2006); Wessel and Kroenke (2008); Torsvik *et al*. (2019); Gaastra *et al*. (2022)	"Hawaiian" refers to the hotspot set beneath the Pacific plate, extended to the Nazca plate in this paper. Selected segments from Norton (2000); Raymond *et al*. (2000); Wessel and Kroenke (2008); Torsvik *et al*. (2019); and Gaastra *et al*. (2022) as described in text and in Supplementary Data
African-Tristan	Müller *et al*. (1993); Maher *et al*. (2015)	"Tristan" refers to the hotspot set beneath the Central and South Atlantic and Indian Oceans, with African, Indian, and East Antarctic plates, plus the South American east of the Andes, and North American plate east of the Cordillera
African-Moving Hotspots	O'Neill *et al*. (2005); Müller *et al*. (2019); Torsvik *et al*. (2019)	There are a number of other moving hotspot models, some of which, according to Torsvik *et al*. (2019), incorporate erroneous calculations

Age sources for late Cretaceous and Cenozoic igneous rocks in Brazil and Paraguay (alphabetically)

Bustamante *et al*. (2016); Coelho *et al*. (2022); Comin-Chiaramonti *et al*. (1991); Conceição *et al*. (2020); Costa dos Santos and Hackspacher (2020); de Oliveira Amaral Quaresma *et al*. (2023); Fodor *et al*. (1983, 1998); Geraldes *et al*. (2013); Gibson *et al*. (1994, 1995); Guedes *et al*. (2005); Guimarães *et al*. (2020); Hansen *et al*. (1998); Hartmann *et al*. (2019); Knesel *et al*. (2011); Mizusaki *et al*. (2002; compilation); Motoki *et al*. (2018); Omarini *et al*. (2016); Perlingeiro *et al*. (2013); Riccomini *et al*. (1991); Siebel *et al*. (2000); Skolotnev *et al*. (2011); Sonoki and Grada (1998) and Souza *et al*. (2013).

References

Andrews, D.L.; Gordon, R.G.; Horner-Johnson, B.C. 2006. Uncertainties in plate reconstructions relative to the hotspots; Pacific-hotspot rotations and uncertainties for the past 68 million years. Geophysical Journal International 166: 939-951. doi: https://doi.org/10.1111/j.1365-246X.2006.03029.x

Bernard, A.; Munschy, M.; Rotstein, Y.; Sauter, D. 2005. Refined spreading history at the Southwest Indian Ridge for the last 96 Ma, with the aid of satellite gravity data. Geophysical Journal International 162: 765-778. doi: https://doi.org/10.1111/j.1365-246X.2005.02672.x

Bustamante, C.; Archanjo, C.J.; Cardona, A.; Vervoort, J.D. 2016. Late Jurassic to Early Cretaceous plutonism in the Colombian Andes: A record of long-term arc maturity. Geological Society of America Bulletin 128 (11-12): 1762-1779. doi: https://doi.org/10.1130/B31307.1

Cande, S.C.; Patriat, P. 2015. The anticorrelated velocities of Africa and India in the Late Cretaceous and early Cenozoic. Geophysical Journal International 200 (1): 227-243. doi: https://doi.org/10.1093/gji/ggu392

Cande, S.C.; Patriat, P.; Dyment, J. 2010. Motion between the Indian, Antarctic and African plates in the early Cenozoic. Geophysical Journal International 183: 127-149. doi: https://doi.org/10.1111/j.1365-246X.2010.04737.x

Coelho, M.H.P.; Martins, M.V.A.; Tavares, A.D.Jr.; Armando, D.; Muniz, L.; Romero, L.F.; Paiva, G.A.; Zan, W.G.; Weska, R.K.; Geraldes, M.C. 2022. U-Pb and Lu-Hf in zircon deciphering magmatic pulses of the Juína Kimberlite: Implications for the lithospheric mantle isotopic composition of the Amazonian Craton. Boletim Paranaense de Geociências 80 (2): 129-153. doi: http://dx.doi.org/10.5380/geo.v80i2.88628

Comin-Chiaramonti, P.; Civeta, L.; Petrini, R.; Piccirillo, E.M.; Bellieni, G.; Censi, P.; Bitschene, P.; Demarchi, G.; De Min, A.; Gomes, C.B.; Castilho, A.M.; Velázquez, J.C. 1991. Tertiary nephelinitic magmatism in Eastern Paraguay: petrology, Sr-Nd isotopes and genetic relationships. European Journal of Mineralogy 3: 507-525.

Conceição, F.T.; Vasconcelos, P.M.; Godoy, L.H.; Navarro, G.R.B. 2020. $^{40}Ar/^{39}Ar$ geochronological evidence for multiple magmatic events during the emplacement of Tapira alkaline-carbonatite complex, Minas Gerais, Brazil. Journal of South American Earth Sciences 97: 102416. doi: https://doi.org/10.1016/j.jsames.2019.102416

Costa dos Santos, A.; Hackspacher, P.C. 2020. Trindade Island Revisited: constraints based on Isotopes, $^{40}Ar/^{39}Ar$ dating, mineral and whole-rock chemistry of a metasomatized-CO_2-garnet-lherzolite mantle: the role of a shallow secondary plume. Goldschmidt Abstracts. doi: https://doi.org/10.46427/gold2020.2277

Croon, M.B.; Cande, S.C.; Stock, J.M. 2008. Geochemistry Geophysics Geosystems, Revised Pacific-Antarctic plate motions and geophysics of the Menard Fracture Zone. Geochemistry, Geophysics, Geosystems 9 (7): Q07001. doi: https://doi.org/10.1029/2008GC002019

de Oliveira Amaral Quaresma, G.; Costa dos Santos, A.; Rocha-Júnior, E.R.V.; Bonifácio, J.; Queiroz R.; Caio A.; Mata, J.; de Morisson, V.C.; Jourdan, F.; Mattielli, N.; Geraldes, M.C. 2023. Isotopic Constraints on Davis Bank, Vitória-Trindade Ridge: A Revisited Petrogenetic Model. Journal of South American Earth Sciences 122: 104099. doi: https://doi.org/10.1016/j.jsames.2022.104099

DeMets, C.; Merkouriev, S. 2019. Geophysical Journal International, High-resolution reconstructions of Nubia, North America, and Antarctic plate motions relative to South America: 34 Ma to present. Geophysical Journal International 217 (3): 1821-1853. doi: https://doi.org/10.1093/gji/ggz087

DeMets, C.; Merkouriev, S.; Sauter, D. 2015. Geophysical Journal International, High-resolution estimates of Southwest Indian Ridge plate motions, 20 Ma to present. Geophysical Journal International 203 (3): 1495-1527. doi: https://doi.org/10.1093/gji/ggv366

Fodor, R.V.; McKee, E.H.; Asmus, H.E. 1983. K-Ar ages and the opening of the South Atlantic Ocean: basaltic rock from the Brazilian margin. Marine Geology 54 (1-2): M1-M8. doi: https://doi.org/10.1016/0025-3227(83)90002-6

Fodor, R.V.; Mukasa, S.B.; Sial, A.N. 1998. Isotopic and trace-element indications of lithospheric and asthenospheric components in Tertiary alkalic basalts, northeastern Brazil. Lithos 43 (4): 197-217. doi: https://doi.org/10.1016/S0024-4937(98)00012-7

Gaastra, K.M.; Gordon, R.G.; Woodworth, D.T.; 2022. Quantification of Pacific Plate Hotspot Tracks Since 80 Ma. Tectonics 41 (7): e2021TC006772. doi: https://doi.org/10.1029/2021TC006772

Geraldes, M.C.; Motoki, A.; Costa, A.; Mota, C.E.; Mohriak, W.U. 2013. Geochronology (Ar/Ar and K-Ar) of the South Atlantic post breakup magmatism, Conjugate Divergent Margins. Geological Society, London, Special Publications 369 (1): 41-74. doi: http://dx.doi.org/10.1144/SP369.21

Gibson, S.A.; Thompson, R.N.; Leonardos, O.H.; Turner, S.E.; Mitchell, J.G.; Dickin, A.P. 1994. The Serra do Bueno Potassic Diatreme: A Possible Hypabyssal Equivalent of the Ultramafic Alkaline Volcanics in the Late Cretaceous

Alto Paranaíba Igneous Province, SE Brazil. Mineralogical Magazine 58 (392): 357-373. doi: https://doi.org/10.1180/minmag.1994.058.392.02

Gibson, S.A.; Thompson, R.N.; Leonardos, O.H.; Dickin, A.P.; Mitchell, J.G. 1995. The Late Cretaceous impact of the Trindade mantle plume: Evidence from large-volume, mafic, potassic magmatism in SE Brazil. Journal of Petrology 36 (1): 189-229. doi: https://doi.org/10.1093/petrology/36.1.189

Granot, R.; Dyment, J. 2018. Late Cenozoic unification of East and West Antarctica. Nature Communications 9: 3189. doi: https://doi.org/10.1038/s41467-018-05270-w

Granot, R.; Cande, S.C.; Stock, J.M.; Damaske, D. 2013. Revised Eocene-Oligocene kinematics for the West Antarctic rift system. Geophysical Research Letters 40 (2): 279-284. doi: https://doi.org/10.1029/2012GL054181

Guedes, E.; Heilbron, M.; Vasconcelos, P.M.; de Morisson Valeriano, C.; Horta de Almeida, J.; Teixeira, W.; Thomaz Filho, A. 2005. K-Ar and $^{40}Ar/^{39}Ar$ ages of dikes emplaced in the onshore basement of the Santos Basin, Resende area, SE Brazil: implications for the south Atlantic opening and Tertiary reactivation. Journal of South American Earth Sciences 18 (3-4): 371-382. doi: https://doi.org/10.1016/j.jsames.2004.11.008

Guimarães, A.R.; Fitton, J.G.; Kirstein, L.A.; Barfod, D.N. 2020. Contemporaneous intraplate magmatism on conjugate South Atlantic margins: A hotspot conundrum. Earth and Planetary Science Letters 536: 116147. doi: https://doi.org/10.1016/j.epsl.2020.116147

Hansen, M.A.F.; Viramonte, J.G.; Troian, F.L.; Mizusaki, A.M.P.; Becchio, R.; Fensterseifer, H.C. 1998. Nuevas edades para el volcanismo de las islas Trindade y Martín Vaz, Brasil. *In* International Meeting: Colima Volcano, Mexico, No. 6, Abstracts: p. 125.

Harada, Y.; Hamano, Y. 2000. Recent progress on plate motions relative to hot spots. *In* The History and Dynamics of Global Plate Motions. Geophysical Monograph Series, 121, (Richards, M.A.; Gordon, R.G.; van der Hilst, R.D.; editors). American Geophysical Union: 327-338. Washington, D.C.

Hartmann, L.A.; Baggio, S.B.; Brückmann, M.P.; Knijnik, D.B.; Lana, C.; Massonne, H.-J.; Opitz, J.; Pinto, V.M.; Sato, K.; Tassinari, C.C.G.; Arena, K.R. 2019. U-Pb geochronology of Paraná volcanics combined with trace element geochemistry of the zircon crystals and zircon Hf isotope data. Journal of South American Earth Sciences 89: 219-226. doi: https://doi.org/10.1016/j.jsames.2018.11.026

Knesel, K.M.; Souza, Z.S.; Vasconcelos, P.M.; Cohen, B.E.; Silveira, F.V. 2011. Young volcanism in the Borborema Province, NE Brazil, shows no evidence for a trace of the Fernando de Noronha plume on the continent. Earth and Planetary Science Letters 302 (1-2): 38-50. doi: https://doi.org/10.1016/j.epsl.2010.11.036

Maher, S.M.; Wessel, P.; Müller, R.D.; Williams, S.E.; Harada, Y. 2015. Absolute plate motion of Africa around Hawaii-Emperor bend time. Geophysical Journal International 201 (3): 1743-1764. doi: https://doi.org/10.1093/gji/ggv104

Matthews, K.J.; Williams, S.E.; Whittaker, J.M.; Müller, R.D.; Seton, M.; Clarke, G.L. 2015. Geologic and kinematic constraints on Late Cretaceous to mid Eocene plate boundaries in the southwest Pacific. Earth-Science Reviews 140: 72-107. doi: https://doi.org/10.1016/j.Earscirev.2014.10.008

Mizusaki, A.M.P.; Thomaz-Filho, A.; Milani, E.J.; de Cesero, P. 2002. Mesozoic and Cenozoic igneous activity and its tectonic control in northeastern Brazil. Journal of South American Earth Sciences 15 (2) 183-198. doi: https://doi.org/10.1016/S0895-9811(02)00014-7

Motoki, A.; Motoki, K.; Costa dos Santos, A.; Cardoso Nogueira, C.; Holanda dos Santos, W.; Geraldes, M.C.; Sichel, S.; Vargas, T. 2018. Geology, Petrology and Magmatic Evolution of the Felsic Alkaline Rocks of the Vitória Island, São Paulo State, Brazil. Anuário do Instituto de Geociências-Federal University of Rio de Janeiro (UFRJ) 41: 125-136. doi: http://dx.doi.org/10.11137/2018_3_125_136

Müller, R.D.; Royer, J.-Y.; Lawver, L.A. 1993. Revised plate motions relative to the hotspots from combined Atlantic and Indian Ocean hotspot tracks. Geology 21 (3): 275-278. doi: https://doi.org/10.1130/0091-7613(1993)021%3C0275:RPMRTT%3E2.3.CO;2

Dietmar-Müller, R.; Royer, J.-Y.; Cande, S.C.; Roest, W.R.; Maschenkov, S. 1999. New constraints on the late cretaceous/tertiary plate tectonic evolution of the caribbean, Sedimentary Basins of the World (Mann, P.; editor), Elsevier, Chapter 2: 33-59. doi: https://doi.org/10.1016/S1874-5997(99)80036-7

Müller, R.D.; Zahirovic, S.; Williams, S.E.; Cannon, J.; Seton, M.; Bower, D.J.; Tetley, M.G.; Heine1, C.; Le Breton, E.; Liu, S.; Russell, S.H.J.; Yang, T.; Leonard, J.; Gurnis, M. 2019. A global plate model including lithospheric deformation along major rifts and orogens since the Triassic. Tectonics 38 (6): 1884-1907. doi: https://doi.org/10.1029/2018TC005462

Nankivell, A.P. 1997. Tectonic evolution of the southern ocean between Antarctica, South America and Africa over the last 84 Ma. PhD thesis, University of Oxford: 303 p. Oxford.

Norton, I.O. 2000. Global hotspot reference frames and plate motion. *In* The History and Dynamics of Global Plate Motions (Richards, M.A.; Gordon, R.G.; van der Hilst, R.D.; editors). American Geophysical Union, Geophysical Monograph Series 121: 339-357.

O'Neill, C.; Müller, R.D.; Steinberger, B. 2005. On the uncertainties in hot spot reconstructions and the significance of moving hot spot reference frames. Geochemistry, Geophysics, Geosystems 6 (4): Q04003. doi: https://doi.org/10.1029/2004GC000784.

Omarini, R.H.; Gasparon, M.; De Min, A.; Comin-Chiaramonti, P. 2016. An overview of the Mesozoic-Cenozoic magmatism and tectonics in Eastern Paraguay and central Andes (Western Gondwana): Implications for the composition of mantle sources. Journal of South American Earth Sciences 72: 302-314. doi: https://doi.org/10.1016/j.jsames.2016.10.002

Pérez-Díaz, L.; Eagles, G. 2014. Constraining South Atlantic growth with seafloor spreading data. Tectonics 33 (9): 1848-1873. doi: https://doi.org/10.1002/2014TC003644

Perlingeiro, G.; Vasconcelos, P.M.; Knesel, K.M.; Thiede, D.S.; Cordani, U.G. 2013. $^{40}Ar/^{39}Ar$ geochronology of the Fernando de Noronha Archipelago and implications for the origin of alkaline volcanism in the NE Brazil. Journal of Volcanology and Geothermal Research 249: 140-154. doi: https://doi.org/10.1016/j.jvolgeores.2012.08.017

Raymond, C.A.; Stock, J.M.; Cande, S.C. 2000. Fast Paleogene motion of the Pacific hotspots from revised global plate circuit constraints. *In* History and Dynamics of Plate Motions (Richards, M.A.; Gordon, R.G.; van der Hilst, R.D.; editors). American Geophysical Union, Geophysical Monograph 121: 359-375.

Riccomini, C.; Melo, M.S.; Coutinho, J.M.V. 1991. Late cretaceous-early tertiary ultrabasic magmatism in the western part of the state of Rio de Janeiro, II. Workshop on Mafic Dyke Swarms of Brazil, Brazil Boletim IG-USP. Publicação Especial 10: 77-84. doi: https://doi.org/10.11606/issn.2317-8078.v0i10p77-84

Rowan, C.J.; Rowley, D.B. 2014. Spreading behaviour of the Pacific-Farallon ridge system since 83 Ma. Geophysical Journal International 197 (3): 1273-1283. doi: https://doi.org/10.1093/gji/ggu056

Seton, M.; Müller, R.D.; Zahirovic, S.; Gaina, C.; Torsvik, T.; Shephard, G.; Talsma, A.; Gurnis, M.; Turner, Maus, S.; Chandler, M. 2012. Global continental and ocean basin reconstructions since 2000 Ma. Earth-Science Reviews 113 (3-4): 212-270. doi: https://doi.org/10.1016/j.earscirev.2012.03.002

Siebel, W.; Becchiob, R.; Volker, F.; Hansene, M.A.F.; Viramonte, J.; Trumbull, R.B.; Haase, G.; Zimmer, M. 2000. Trindade and Martin Vaz Islands, South Atlantic: Isotopic (Sr, Nd, Pb) and trace element constraints on plume related magmatism. Journal of South American Earth Sciences 13: 79-103. doi: https://doi.org/10.1016/S0895-9811(00)00015-8

Skolotnev, S.G.; Bylinskaya, M.E.; Golovina, L.A.; Ipat'eva, I.S. 2011. First data on the age of rocks from the central part of the Vitoria-Trindade Ridge (Brazil Basin, South Atlantic). Doklady Earth Sciences 437 (1): 316-322. doi: https://doi.org/10.1134/S1028334X11030093

Sonoki, I.K.; Garda, G.M. 1988. Idades K-Ar de rochas alcalinas do Brasil Meridional e Paraguai Oriental: compilação e adaptação às novas constantes de decaimento. Boletim IG-USP Série Científica 19: 63-85. doi: https://doi.org/10.11606/issn.2316-8986.v19i0p63-85

Souza, Z.S.; Vasconcelos, P.M.; Knesel, K.M.; da Silveira Dias, L.G.; Roesner, E.H.; Cordeiro de Farias, P.R.; de Morais Neto, J.M. 2013. The tectonic evolution of Cenozoic extensional basins, northeast Brazil: Geochronological constraints from continental basalt $^{40}Ar/^{39}Ar$ ages. Journal of South American Earth Sciences 48: 159-172. doi: https://doi.org/10.1016/j.jsames.2013.09.008

Tebbens, S.F.; Cande, S.C. 1997. Journal of Geophysical Research: Solid Earth, Southeast Pacific tectonic evolution from Early Oligocene to Present. Journal of Geophysical Research, Solid Earth 102 (B6): 12061-12084. doi: https://doi.org/10.1029/96JB02582

Torsvik, T.H.; Steinberger, B.; Shephard, G.E.; Doubrovine, P.V.; Gaina, C.; Domeier, M.; Carmen Gaina, C.; Domeier, M.; Conrad, C.P. 2019. Pacific-Panthalassic reconstructions: Overview, errata and the way forward. Geochemistry, Geophysics, Geosystems 20. doi: https://doi.org/10.1029/2019GC008402

Wessel, P.; Kroenke, L.W. 2008. Journal of Geophysical Research, Pacific absolute plate motions since 145 Ma. Journal of Geophysical Research 113 (B6): B06101. doi: https://doi.org/10.1029/2007JB005499

Wessel, P.; Harada, Y.; Kroenke, L.W. 2006. Toward a self-consistent, high-resolution absolute plate motion model for the Pacific. Geochemistry, Geophysics, Geosystems 7: Q03L12. doi: https://doi.org/10.1029/2005GC001000

Wilder, D.T. 2003. Relative motion history of the Pacific-Nazca (Farallon) plates since 30 million years ago. MSc Thesis (Unpublished), University of South Florida: 94 p.

Wright, N.; Müller, R.D.; Seton, M.; Williams, S. 2015. Revision of Paleogene plate motions in the Pacific and implications for the Hawaiian-Emperor bend. Geology 43 (5): 455-458. doi: https://doi.org/10.1130/G36303.1

Wright, N.; Müller, R.D.; Seton, M.; Williams, S. 2016, The Late Cretaceous to recent tectonic history of the Pacific Ocean basin. Earth-Science Reviews 154: 138-173. doi: https://doi.org/10.1016/j.earscirev.2015.11.015

Supplementary figures and tables

Pilger (2023)-Tracing hotspot traces in the Andes: supplementary data

Supplementary figures and tables
Figure S1. Map view of isotopic dates of Andean igneous rocks, 0-100 Ma
Figure S2A-H. Map views of isotopic dates of Andean igneous rocks in 10 Myr increments, 0-80 Ma
Figure S3. Plate-Hotspot models and East Africa magmatism
Table S1. Source plate-pair reconstruction parameters, timescale of Ogg (2020)
Table S2. Calculated reconstruction parameters at 1 Myr increments
Uncertainties in Global Plate Reconstructions-An Unsolved Problem

Separate file for display in Google Earth: Andes_Tracing_Traces_Supporting.kmz - Includes:
- Pacific Hotspot Dates
- Andes 0-100 Ma Silicic-Intermediate Igneous Dates
- Hawaiian Hotspot-Nazca Loci
- Brazil-Paraguay Igneous Dates and Loci (post Parana)
- South American Lithospheric Thickness
- East African (EAFR) Igneous Dates (Cenozoic)
- Tristan Hotspot Loci

FIG. S1. Map view of isotopic dates of igneous rocks, South American Andes, and adjacent areas, 0-100 Ma. Data accessible via GEOROC (see main text for details).

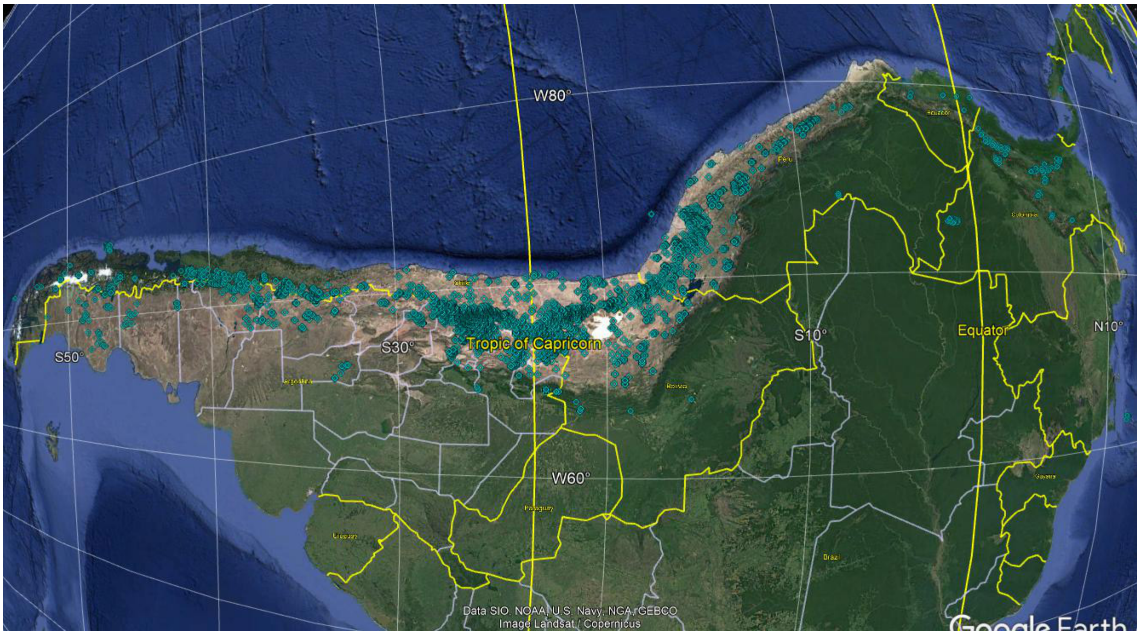

FIG. S2A. 0-10 Ma.

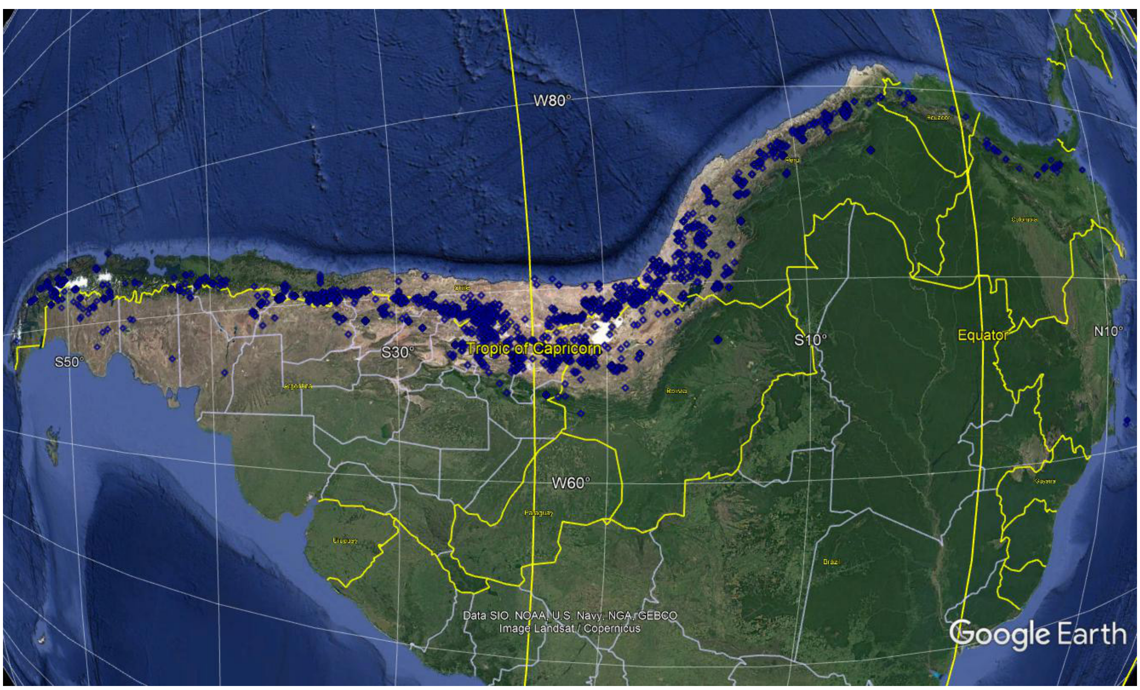

FIG. S2B. 10-20 Ma.

FIG. S2C. 20-30 Ma.

FIG. S2D. 30-40 Ma.

FIG. S2E. 40-50 Ma.

FIG. S2F. 50-60 Ma.

FIG. S2G. 60-70 Ma.

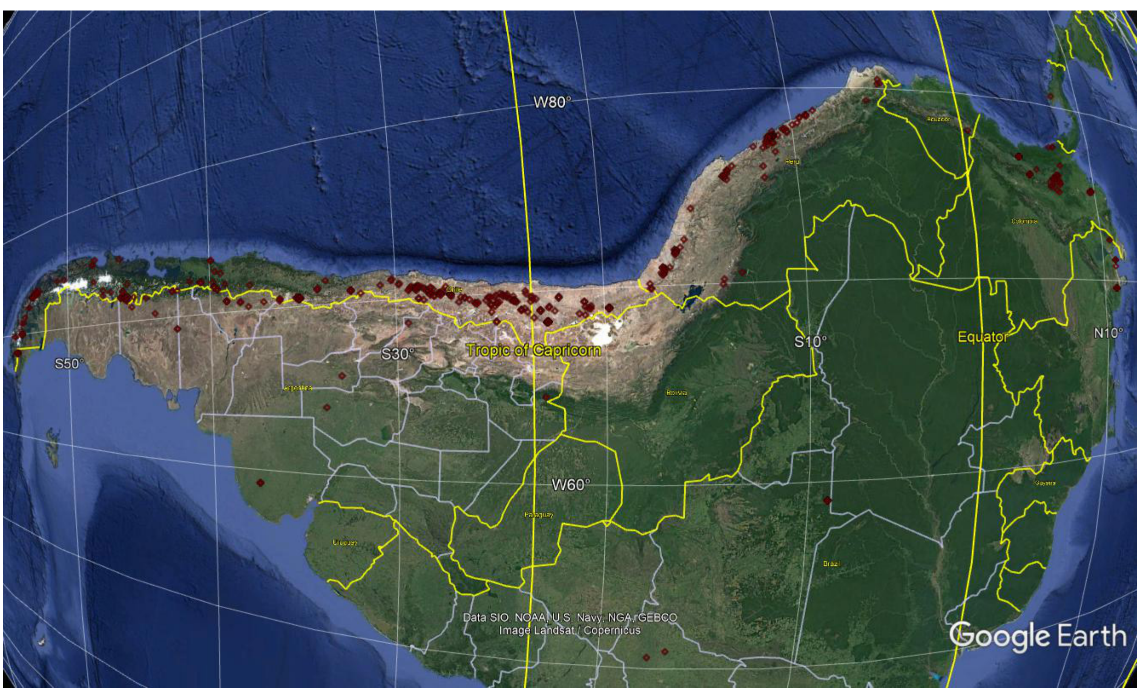

FIG. S2H. 70-80 Ma.

FIG. S2. Map views of isotopic dates of igneous rocks, 0-80 Ma, South American Andes, in 10 Myr Intervals. Data accessible via GEOROC (see main text for details). Data also included in the Google Earth file attached to this paper.

TABLE S1. SOURCE PLATE-PAIR RECONSTRUCTION PARAMETERS, TIMESCALE OF OGG (2020).

Reference Plate	Moving Plate	Latitude (°)	Longitude (°)	Rotation Angle (°)/ Rate (°/Myr) *	Age (Ma)	Reference
SOAM	AFRC	63.900	-34.300	*0.320	0.000	DeMets *et al*. (2010)
SOAM	AFRC	60.350	-38.740	0.221	0.774	DeMets and Merkouriev (2019)
SOAM	AFRC	60.600	-39.010	0.507	1.783	DeMets and Merkouriev (2019)
SOAM	AFRC	60.770	-39.200	0.741	2.595	DeMets and Merkouriev (2019)
SOAM	AFRC	60.940	-39.400	1.046	3.613	DeMets and Merkouriev (2019)
SOAM	AFRC	61.010	-39.480	1.227	4.194	DeMets and Merkouriev (2019)
SOAM	AFRC	61.090	-39.590	1.550	5.240	DeMets and Merkouriev (2019)
SOAM	AFRC	61.140	-39.650	1.798	6.188	DeMets and Merkouriev (2019)
SOAM	AFRC	61.170	-39.690	2.030	6.917	DeMets and Merkouriev (2019)
SOAM	AFRC	61.190	-39.720	2.312	7.601	DeMets and Merkouriev (2019)
SOAM	AFRC	61.200	-39.740	2.521	8.161	DeMets and Merkouriev (2019)
SOAM	AFRC	61.210	-39.740	2.881	9.187	DeMets and Merkouriev (2019)
SOAM	AFRC	61.210	-39.730	3.131	9.817	DeMets and Merkouriev (2019)
SOAM	AFRC	61.160	-39.650	3.621	11.149	DeMets and Merkouriev (2019)
SOAM	AFRC	61.050	-39.480	4.221	12.542	DeMets and Merkouriev (2019)
SOAM	AFRC	60.890	-39.260	4.773	13.763	DeMets and Merkouriev (2019)
SOAM	AFRC	60.760	-39.080	5.154	14.556	DeMets and Merkouriev (2019)
SOAM	AFRC	60.570	-38.810	5.752	16.026	DeMets and Merkouriev (2019)
SOAM	AFRC	60.390	-38.560	6.313	17.254	DeMets and Merkouriev (2019)
SOAM	AFRC	60.280	-38.400	6.692	17.816	DeMets and Merkouriev (2019)
SOAM	AFRC	60.170	-38.260	7.019	18.299	DeMets and Merkouriev (2019)
SOAM	AFRC	60.020	-38.040	7.485	18.987	DeMets and Merkouriev (2019)
SOAM	AFRC	59.820	-37.800	7.960	20.198	DeMets and Merkouriev (2019)
SOAM	AFRC	59.540	-37.480	8.463	21.202	DeMets and Merkouriev (2019)
SOAM	AFRC	58.790	-36.710	9.432	23.128	DeMets and Merkouriev (2019)
SOAM	AFRC	58.600	-36.520	9.649	23.635	DeMets and Merkouriev (2019)
SOAM	AFRC	58.380	-36.290	9.913	24.432	DeMets and Merkouriev (2019)
SOAM	AFRC	58.070	-35.980	10.287	25.310	DeMets and Merkouriev (2019)
SOAM	AFRC	57.930	-35.830	10.469	25.722	DeMets and Merkouriev (2019)
SOAM	AFRC	57.640	-35.510	10.897	26.797	DeMets and Merkouriev (2019)
SOAM	AFRC	57.550	-35.390	11.073	27.182	DeMets and Merkouriev (2019)
SOAM	AFRC	57.470	-35.290	11.249	27.769	DeMets and Merkouriev (2019)
SOAM	AFRC	57.350	-35.100	11.629	28.637	DeMets and Merkouriev (2019)
SOAM	AFRC	57.280	-34.970	11.959	29.627	DeMets and Merkouriev (2019)
SOAM	AFRC	57.230	-34.860	12.220	30.774	DeMets and Merkouriev (2019)
SOAM	AFRC	57.200	-34.790	12.407	31.057	DeMets and Merkouriev (2019)
SOAM	AFRC	57.060	-34.470	13.317	33.319	DeMets and Merkouriev (2019)
SOAM	AFRC	57.020	-34.380	13.551	33.894	DeMets and Merkouriev (2019)

table S1 continued.

Reference Plate	Moving Plate	Latitude (°)	Longitude (°)	Rotation Angle (°)/ Rate (°/Myr) *	Age (Ma)	Reference
SOAM	AFRC	56.190	-31.460	15.770	37.978	Pérez-Díaz and Eagles (2014)
SOAM	AFRC	57.020	-31.060	17.600	41.219	Pérez-Díaz and Eagles (2014)
SOAM	AFRC	58.270	-30.880	19.120	45.008	Pérez-Díaz and Eagles (2014)
SOAM	AFRC	61.280	-32.070	21.230	52.913	Pérez-Díaz and Eagles (2014)
SOAM	AFRC	62.210	-32.490	24.730	66.611	Pérez-Díaz and Eagles (2014)
SOAM	AFRC	61.850	-32.560	26.560	71.313	Pérez-Díaz and Eagles (2014)
SOAM	AFRC	61.640	-32.620	27.920	74.296	Pérez-Díaz and Eagles (2014)
SOAM	AFRC	61.140	-33.190	30.970	80.389	Pérez-Díaz and Eagles (2014)
SOAM	AFRC	60.740	-33.850	33.420	83.650	Pérez-Díaz and Eagles (2014)
SOAM	AFRC	59.960	-35.150	37.840	92.726	Pérez-Díaz and Eagles (2014)
SOAM	AFRC	61.560	-38.970	43.350	102.758	Pérez-Díaz and Eagles (2014)
SOAM	AFRC	58.830	-40.060	51.360	118.523	Pérez-Díaz and Eagles (2014)
SOAM	AFRC	57.400	-39.880	53.470	125.331	Pérez-Díaz and Eagles (2014)
SOAM	AFRC	57.360	-40.040	55.890	132.495	Pérez-Díaz and Eagles (2014)
SOAM	AFRC	56.230	-39.280	59.580	139.778	Pérez-Díaz and Eagles (2014)
SOAM	AFRC	56.230	-39.280	59.580	150.000	Pérez-Díaz and Eagles (2014)
EANT	AFRC	6.300	-51.690	*0.160	0.000	DeMets *et al*. (2010)
EANT	AFRC	-5.460	-34.420	0.112	0.773	DeMets *et al*. (2021)
EANT	AFRC	-4.110	-33.630	0.254	1.775	DeMets *et al*. (2021)
EANT	AFRC	-9.880	-30.260	0.372	2.595	DeMets *et al*. (2021)
EANT	AFRC	-13.380	-29.640	0.532	3.596	DeMets *et al*. (2021)
EANT	AFRC	-13.060	-28.870	0.633	4.187	DeMets *et al*. (2021)
EANT	AFRC	-11.110	-30.330	0.753	5.235	DeMets *et al*. (2021)
EANT	AFRC	-7.520	-31.960	0.834	6.023	DeMets *et al*. (2021)
EANT	AFRC	-4.330	-33.780	0.908	6.727	DeMets *et al*. (2021)
EANT	AFRC	-6.740	-31.530	1.046	7.537	DeMets *et al*. (2021)
EANT	AFRC	-5.680	-31.830	1.102	8.125	DeMets *et al*. (2021)
EANT	AFRC	-8.600	-29.430	1.321	9.105	DeMets *et al*. (2021)
EANT	AFRC	-5.760	-30.110	1.430	9.786	DeMets *et al*. (2021)
EANT	AFRC	-3.980	-31.010	1.601	11.056	DeMets *et al*. (2021)
EANT	AFRC	-4.570	-30.140	1.807	12.474	DeMets *et al*. (2021)
EANT	AFRC	-5.910	-29.150	2.059	13.739	DeMets *et al*. (2021)
EANT	AFRC	-6.090	-28.420	2.187	14.609	DeMets *et al*. (2021)
EANT	AFRC	-8.520	-26.670	2.500	15.974	DeMets *et al*. (2021)
EANT	AFRC	-5.710	-27.370	2.974	18.636	DeMets *et al*. (2021)
EANT	AFRC	12.000	-48.400	5.460	33.214	DeMets *et al*. (2021)
EANT	AFRC	12.190	-41.440	7.900	43.450	DeMets *et al*. (2021)
EANT	AFRC	10.000	-40.660	8.830	47.760	DeMets *et al*. (2021)
EANT	AFRC	8.020	-39.670	9.190	49.666	DeMets *et al*. (2021)

table S1 continued.

Reference Plate	Moving Plate	Latitude (°)	Longitude (°)	Rotation Angle (°)/ Rate (°/Myr) *	Age (Ma)	Reference
EANT	AFRC	7.610	-39.300	9.630	51.724	DeMets *et al*. (2021)
EANT	AFRC	7.600	-39.570	9.980	53.900	Cande and Patriat (2015)
EANT	AFRC	6.690	-42.740	10.580	57.101	Cande and Patriat (2015)
EANT	AFRC	3.810	-43.670	11.170	63.537	Cande and Patriat (2015)
EANT	AFRC	0.640	-43.290	11.980	68.351	Cande and Patriat (2015)
EANT	AFRC	-3.270	-41.140	12.830	71.451	Cande and Patriat (2015)
EANT	AFRC	-5.380	-39.540	13.910	74.201	Cande and Patriat (2015)
EANT	AFRC	-3.270	-39.790	15.980	79.900	Cande and Patriat (2015)
EANT	AFRC	-1.350	-39.520	17.820	83.650	Cande and Patriat (2015)
EANT	AFRC	-3.060	-33.490	26.800	99.892	Marks and Stock (2001)
EANT	AFRC	-10.360	-26.330	41.560	120.964	Müller *et al*. (2008)
EANT	AFRC	-9.450	-27.500	42.910	124.772	Müller *et al*. (2008)
EANT	AFRC	-9.300	-28.000	43.710	126.547	Müller *et al*. (2008)
EANT	AFRC	-8.630	-28.970	44.470	128.963	König and Jokat (2006)
EANT	AFRC	-8.500	-29.160	45.070	130.251	König and Jokat (2006)
EANT	AFRC	-8.270	-29.420	45.900	132.495	König and Jokat (2006)
EANT	AFRC	-7.970	-29.760	47.040	134.571	König and Jokat (2006)
EANT	AFRC	-7.750	-30.020	47.910	138.491	König and Jokat (2006)
EANT	AFRC	-7.810	-30.270	48.740	140.500	König and Jokat (2006)
EANT	AFRC	-7.290	-31.130	49.800	143.999	König and Jokat (2006)
EANT	AFRC	-6.900	-31.540	50.720	147.043	König and Jokat (2006)
EANT	AFRC	-6.690	-31.780	51.260	148.495	König and Jokat (2006)
EANT	AFRC	-6.690	-31.780	51.260	150.000	König and Jokat (2006)
EANT	WANT	67.050	-109.470	*0.000	0.000	Granot and Dyment (2018)
EANT	WANT	67.050	-109.470	0.000	5.019	Granot and Dyment (2018)
EANT	WANT	67.050	-109.470	0.000	11.056	Granot and Dyment (2018)
EANT	WANT	67.050	-109.470	0.570	25.987	Granot *et al*. (2013)
EANT	WANT	84.780	10.990	1.330	30.977	Granot *et al*. (2013)
EANT	WANT	85.870	40.490	4.480	40.073	Granot *et al*. (2013)
EANT	WANT	85.870	40.490	4.800	53.900	Granot *et al*. (2013)
EANT	WANT	85.870	40.490	6.200	62.530	Granot *et al*. (2013)
EANT	WANT	85.870	40.490	7.000	65.700	Granot *et al*. (2013)
EANT	WANT	85.870	40.490	7.500	71.451	Granot *et al*. (2013)
EANT	WANT	78.760	133.500	7.720	100.000	Matthews *et al*. (2015)
EANT	WANT	78.760	133.500	7.720	150.000	Matthews *et al*. (2015)
PCFC	WANT	33.100	-96.300	*0.477	0.000	DeMets *et al*. (2010)
PCFC	WANT	64.303	-81.212	0.676	0.773	Croon *et al*. (2008)
PCFC	WANT	64.901	-81.138	1.606	1.855	Croon *et al*. (2008)

table S1 continued.

Reference Plate	Moving Plate	Latitude (°)	Longitude (°)	Rotation Angle (°)/ Rate (°/Myr) *	Age (Ma)	Reference
PCFC	WANT	65.204	-81.225	2.227	2.595	Croon *et al*. (2008)
PCFC	WANT	65.897	-81.165	3.109	3.596	Croon *et al*. (2008)
PCFC	WANT	66.624	-80.533	3.702	4.244	Croon *et al*. (2008)
PCFC	WANT	66.909	-80.658	4.480	5.116	Croon *et al*. (2008)
PCFC	WANT	67.091	-81.081	5.211	6.148	Croon *et al*. (2008)
PCFC	WANT	67.331	-81.202	5.808	6.916	Croon *et al*. (2008)
PCFC	WANT	68.162	-80.540	6.830	7.913	Croon *et al*. (2008)
PCFC	WANT	68.833	-79.969	7.639	8.938	Croon *et al*. (2008)
PCFC	WANT	69.707	-78.566	8.417	9.786	Croon *et al*. (2008)
PCFC	WANT	70.356	-77.813	9.481	11.056	Croon *et al*. (2008)
PCFC	WANT	71.293	-76.115	10.631	12.373	Croon *et al*. (2008)
PCFC	WANT	71.746	-75.122	11.283	13.108	Croon *et al*. (2008)
PCFC	WANT	72.381	-73.576	12.420	14.386	Croon *et al*. (2008)
PCFC	WANT	72.601	-73.192	13.012	15.096	Croon *et al*. (2008)
PCFC	WANT	72.974	-72.498	13.948	16.121	Croon *et al*. (2008)
PCFC	WANT	73.181	-72.032	14.344	16.632	Croon *et al*. (2008)
PCFC	WANT	73.394	-71.580	14.929	17.393	Croon *et al*. (2008)
PCFC	WANT	73.617	-70.909	15.418	18.007	Croon *et al*. (2008)
PCFC	WANT	73.712	-70.936	15.946	18.636	Croon *et al*. (2008)
PCFC	WANT	74.001	-70.157	16.727	19.535	Croon *et al*. (2008)
PCFC	WANT	74.133	-70.089	17.381	20.607	Croon *et al*. (2008)
PCFC	WANT	74.385	-69.727	18.675	22.342	Croon *et al*. (2008)
PCFC	WANT	74.482	-69.581	19.347	23.265	Croon *et al*. (2008)
PCFC	WANT	74.509	-69.664	19.923	24.025	Croon *et al*. (2008)
PCFC	WANT	74.499	-69.836	20.625	25.099	Croon *et al*. (2008)
PCFC	WANT	74.511	-69.806	21.175	25.987	Croon *et al*. (2008)
PCFC	WANT	74.455	-69.900	21.531	26.420	Croon *et al*. (2008)
PCFC	WANT	74.401	-69.747	22.234	27.439	Croon *et al*. (2008)
PCFC	WANT	74.407	-69.504	22.575	27.859	Croon *et al*. (2008)
PCFC	WANT	74.330	-69.543	22.953	28.278	Croon *et al*. (2008)
PCFC	WANT	74.378	-68.714	23.662	29.183	Croon *et al*. (2008)
PCFC	WANT	74.329	-68.430	24.232	29.970	Croon *et al*. (2008)
PCFC	WANT	74.366	-67.750	24.708	30.591	Croon *et al*. (2008)
PCFC	WANT	74.320	-67.593	25.058	30.977	Croon *et al*. (2008)
PCFC	WANT	74.444	-64.739	26.969	33.214	Croon *et al*. (2008)
PCFC	WANT	74.479	-64.015	27.395	33.726	Croon *et al*. (2008)
PCFC	WANT	74.621	-61.886	28.395	35.102	Croon *et al*. (2008)
PCFC	WANT	74.634	-61.485	28.615	35.336	Croon *et al*. (2008)

table S1 continued.

Reference Plate	Moving Plate	Latitude (°)	Longitude (°)	Rotation Angle (°)/ Rate (°/Myr) *	Age (Ma)	Reference
PCFC	WANT	74.702	-60.180	29.234	35.774	Croon *et al*. (2008)
PCFC	WANT	74.750	-59.047	29.808	36.351	Croon *et al*. (2008)
PCFC	WANT	74.763	-58.638	30.049	36.573	Croon *et al*. (2008)
PCFC	WANT	74.816	-57.440	30.678	37.385	Croon *et al*. (2008)
PCFC	WANT	74.855	-56.211	31.411	38.398	Croon *et al*. (2008)
PCFC	WANT	74.868	-54.460	32.620	40.073	Croon *et al*. (2008)
PCFC	WANT	74.859	-53.254	33.532	41.105	Croon *et al*. (2008)
PCFC	WANT	74.856	-52.225	34.217	42.196	Croon *et al*. (2008)
PCFC	WANT	74.775	-51.610	35.288	43.450	Croon *et al*. (2008)
PCFC	WANT	74.430	-48.540	38.180	47.760	Wright *et al*. (2016)
PCFC	WANT	73.470	-52.080	40.100	53.900	Wright *et al*. (2016)
PCFC	WANT	72.630	-54.730	41.140	57.379	Wright *et al*. (2016)
PCFC	WANT	71.350	-54.160	45.500	62.530	Wright *et al*. (2016)
PCFC	WANT	68.940	-56.690	49.010	68.178	Wright *et al*. (2016)
PCFC	WANT	66.630	-57.360	52.780	74.201	Wright *et al*. (2016)
PCFC	WANT	64.800	-57.800	56.280	79.900	Wright *et al*. (2016)
PCFC	WANT	63.600	-58.100	58.800	83.650	Wright *et al*. (2016)
PCFC	WANT	63.600	-58.100	58.800	150.000	Wright *et al*. (2016)
PCFC	HSPT	60.200	-90.000	*0.932	0.000	Gripp and Gordon (2002)
PCFC	HSPT	73.250	-98.500	1.170	1.000	Interpolated
PCFC	HSPT	73.170	-97.500	2.300	2.000	Gaastra *et al*. (2022)
PCFC	HSPT	72.110	-100.500	3.420	3.000	Gaastra *et al*. (2022)
PCFC	HSPT	70.390	-105.600	4.550	4.000	Gaastra *et al*. (2022)
PCFC	HSPT	70.970	-102.600	5.550	5.000	Gaastra *et al*. (2022)
PCFC	HSPT	70.960	-101.600	6.540	6.000	Gaastra *et al*. (2022)
PCFC	HSPT	70.940	-100.600	7.500	7.000	Gaastra *et al*. (2022)
PCFC	HSPT	70.950	-99.500	8.430	8.000	Gaastra *et al*. (2022)
PCFC	HSPT	70.900	-98.610	9.330	9.000	Gaastra *et al*. (2022)
PCFC	HSPT	70.880	-97.610	10.210	10.000	Gaastra *et al*. (2022)
PCFC	HSPT	71.490	-99.740	11.540	11.200	Gaastra *et al*. (2022)
PCFC	HSPT	71.540	-98.180	12.380	12.400	Gaastra *et al*. (2022)
PCFC	HSPT	71.570	-96.650	13.200	13.600	Gaastra *et al*. (2022)
PCFC	HSPT	71.580	-95.140	14.000	14.800	Gaastra *et al*. (2022)
PCFC	HSPT	71.580	-93.640	14.780	16.000	Gaastra *et al*. (2022)
PCFC	HSPT	71.560	-92.210	15.540	17.200	Gaastra *et al*. (2022)
PCFC	HSPT	71.530	-90.790	16.290	18.400	Gaastra *et al*. (2022)
PCFC	HSPT	70.790	-71.770	17.570	25.000	Norton (2000)
PCFC	HSPT	68.648	-69.337	21.955	31.944	Norton (2000)

table S1 continued.

Reference Plate	Moving Plate	Latitude (°)	Longitude (°)	Rotation Angle (°)/ Rate (°/Myr) *	Age (Ma)	Reference
PCFC	HSPT	67.197	-67.953	26.362	38.889	Norton (2000)
PCFC	HSPT	66.150	-67.060	30.783	45.833	Norton (2000)
PCFC	HSPT	65.106	-57.707	31.951	49.960	Raymond *et al*. (2000)
PCFC	HSPT	64.437	-58.761	32.238	50.690	Raymond *et al*. (2000)
PCFC	HSPT	61.498	-62.740	33.597	54.600	Raymond *et al*. (2000)
PCFC	HSPT	57.769	-66.684	35.596	59.570	Raymond *et al*. (2000)
PCFC	HSPT	51.627	-71.516	39.761	67.040	Raymond *et al*. (2000)
PCFC	HSPT	48.535	-73.438	42.396	71.060	Raymond *et al*. (2000)
PCFC	HSPT	44.183	-75.755	46.932	79.590	Raymond *et al*. (2000)
PCFC	HSPT	52.550	-75.770	52.290	90.000	Torsvik *et al*. (2019)
PCFC	HSPT	52.290	-77.100	54.210	95.000	Torsvik *et al*. (2019)
PCFC	HSPT	54.170	-78.480	55.690	100.000	Torsvik *et al*. (2019)
PCFC	HSPT	56.580	-78.200	58.760	110.000	Torsvik *et al*. (2019)
PCFC	HSPT	57.850	-77.920	64.460	123.000	Torsvik *et al*. (2019)
PCFC	HSPT	57.610	-73.930	67.090	130.000	Torsvik *et al*. (2019)
PCFC	HSPT	57.500	-71.370	68.880	135.000	Torsvik *et al*. (2019)
PCFC	HSPT	61.600	-65.750	69.250	144.000	Torsvik *et al*. (2019)
PCFC	HSPT	64.140	-61.190	69.730	150.000	Torsvik *et al*. (2019)
PCFC	NAZC	55.900	-87.800	*1.311	0.000	DeMets *et al*. (2010)
PCFC	NAZC	57.506	-90.916	4.967	3.596	Tebbens and Cande (1997); Croon *et al*. (2008)
PCFC	NAZC	60.224	-91.067	7.173	5.116	Tebbens and Cande (1997); Croon *et al*. (2008)
PCFC	NAZC	54.380	-94.660	9.680	6.727	Wilder (2003)
PCFC	NAZC	58.230	-93.640	13.180	8.938	Wilder (2003)
PCFC	NAZC	60.010	-93.270	16.860	11.056	Wilder (2003)
PCFC	NAZC	62.000	-92.790	19.630	13.108	Wilder (2003)
PCFC	NAZC	64.520	-96.390	23.100	15.096	Wilder (2003)
PCFC	NAZC	59.680	-91.020	38.450	22.482	Wilder (2003)
PCFC	NAZC	65.600	-97.390	43.830	27.859	Wilder (2003)
PCFC	NAZC	70.065	-103.880	49.620	33.214	Rowan and Rowell (2014)
PCFC	NAZC	73.960	-110.185	53.970	36.573	Rowan and Rowell (2014)
PCFC	NAZC	76.181	-113.283	56.073	38.398	Rowan and Rowell (2014)
PCFC	NAZC	77.747	-117.394	58.232	40.073	Rowan and Rowell (2014)
PCFC	NAZC	79.132	-123.890	61.795	42.196	Rowan and Rowell (2014)
PCFC	NAZC	79.735	-127.584	63.662	43.450	Rowan and Rowell (2014)
PCFC	NAZC	82.402	-149.315	69.880	50.767	Rowan and Rowell (2014)
PCFC	NAZC	82.931	-159.470	72.233	53.900	Rowan and Rowell (2014)
PCFC	NAZC	83.167	170.027	80.229	65.700	Rowan and Rowell (2014)

table S1 continued.

Reference Plate	Moving Plate	Latitude (°)	Longitude (°)	Rotation Angle (°)/ Rate (°/Myr) *	Age (Ma)	Reference
PCFC	NAZC	82.414	151.315	86.587	74.201	Rowan and Rowell (2014)
PCFC	NAZC	80.497	126.564	93.180	83.650	Rowan and Rowell (2014)
PCFC	NAZC	77.529	116.637	126.972	110.000	Rowan and Rowell (2014)
PCFC	NAZC	72.707	105.553	134.001	120.964	Rowan and Rowell (2014)
PCFC	NAZC	69.393	102.143	138.369	126.514	Rowan and Rowell (2014)
PCFC	NAZC	66.714	100.108	142.052	132.552	Rowan and Rowell (2014)
PCFC	NAZC	64.052	101.641	147.561	140.186	Rowan and Rowell (2014)
PCFC	NAZC	61.239	102.978	153.588	147.009	Rowan and Rowell (2014)
PCFC	NAZC	59.189	103.793	158.123	153.442	Rowan and Rowell (2014)
PCFC	COCO	42.200	-112.800	*1.676	0.000	DeMets *et al*. (2010)
PCFC	COCO	39.130	-108.600	10.250	4.997	Wilson (1996)
PCFC	COCO	35.300	-105.600	25.080	9.984	Wilson (1996)
PCFC	COCO	36.000	-107.700	30.270	12.093	Wilson (1996)
PCFC	COCO	36.700	-109.100	32.660	13.032	Wilson (1996)
PCFC	COCO	38.300	-111.800	36.330	14.775	Wilson (1996)
PCFC	COCO	39.300	-114.900	42.450	17.235	Wilson (1996)
PCFC	COCO	40.420	-117.810	47.440	19.535	Wilson (1996)
PCFC	COCO	39.321	-119.770	53.956	22.342	Lonsdale (2005)
PCFC	COCO	46.474	-128.066	65.236	33.214	Lonsdale (2005); Wright *et al*. (2016)
PCFC	COCO	54.011	-138.364	68.849	40.073	Lonsdale (2005); Wright *et al*. (2016)
PCFC	COCO	56.143	-142.957	72.750	43.450	Lonsdale (2005); Wright *et al*. (2016)
PCFC	COCO	58.478	-148.648	75.308	47.760	Lonsdale (2005); Wright *et al*. (2016)
PCFC	COCO	59.152	-150.688	76.442	49.666	Lonsdale (2005); Wright *et al*. (2016)
PCFC	COCO	59.829	-152.990	77.995	52.540	Lonsdale (2005); Wright *et al*. (2016)
PCFC	COCO	60.885	-156.698	79.692	57.101	Lonsdale (2005); Wright *et al*. (2016)
PCFC	COCO	61.228	-158.000	80.372	58.959	Lonsdale (2005); Wright *et al*. (2016)
PCFC	COCO	61.866	-160.618	81.852	62.530	Lonsdale (2005); Wright *et al*. (2016)
PCFC	COCO	62.091	-161.589	82.205	63.537	Lonsdale (2005); Wright *et al*. (2016)
PCFC	COCO	62.798	-165.103	85.126	68.351	Lonsdale (2005); Wright *et al*. (2016)
PCFC	COCO	64.646	-174.986	90.255	79.900	Lonsdale (2005); Wright *et al*. (2016)
PCFC	COCO	65.248	-179.047	91.729	83.650	Lonsdale (2005); Wright *et al*. (2016)
PCFC	COCO	65.836	156.825	122.113	109.446	Lonsdale (2005); Seton *et al*. (2012); Wright *et al*. (2016)
PCFC	COCO	63.766	142.052	126.106	120.964	Lonsdale (2005); Seton *et al*. (2012); Wright *et al*. (2016)
PCFC	COCO	61.525	134.519	128.664	126.547	Lonsdale (2005); Seton *et al*. (2012); Wright *et al*. (2016)
PCFC	COCO	59.463	129.271	130.930	132.150	Lonsdale (2005); Seton *et al*. (2012); Wright *et al*. (2016)
PCFC	COCO	56.439	126.575	135.394	139.692	Lonsdale (2005); Seton *et al*. (2012); Wright *et al*. (2016)

table S1 continued.

Reference Plate	Moving Plate	Latitude (°)	Longitude (°)	Rotation Angle (°)/ Rate (°/Myr) *	Age (Ma)	Reference
PCFC	COCO	53.219	124.193	140.364	146.613	Lonsdale (2005); Seton *et al*. (2012); Wright *et al*. (2016)
PCFC	COCO	50.871	122.671	144.155	153.237	Lonsdale (2005); Seton *et al*. (2012); Wright *et al*. (2016)
AFRC	HSPT	-1.500	155.800	*0.134	0.000	Gripp and Gordon (2002)
AFRC	HSPT	-59.300	148.400	1.890	10.654	Müller *et al*. (1993)
AFRC	HSPT	-50.900	135.500	4.360	19.535	Müller *et al*. (1993)
AFRC	HSPT	-40.300	137.000	7.910	33.214	Müller *et al*. (1993)
AFRC	HSPT	-37.700	138.800	9.650	41.452	Müller *et al*. (1993)
AFRC	HSPT	-32.800	139.200	12.090	47.760	Müller *et al*. (1993)
AFRC	HSPT	-30.100	138.300	13.890	57.101	Müller *et al*. (1993)
AFRC	HSPT	-26.400	139.100	16.230	69.271	Müller *et al*. (1993)
AFRC	HSPT	-22.300	140.400	17.800	74.201	Müller *et al*. (1993)
AFRC	HSPT	-18.000	141.100	19.980	79.900	Müller *et al*. (1993)
AFRC	HSPT	-19.000	139.100	21.530	83.650	Müller *et al*. (1993)
AFRC	HSPT	-19.400	138.100	23.310	90.338	Müller *et al*. (1993)
AFRC	HSPT	-18.900	138.600	25.350	99.892	Müller *et al*. (1993)
AFRC	HSPT	-17.700	140.500	26.710	109.446	Müller *et al*. (1993)
AFRC	HSPT	-18.700	140.300	27.370	117.758	Müller *et al*. (1993)
AFRC	HSPT	-16.700	142.500	28.520	131.568	Müller *et al*. (1993)
AFRC	HSPT	-56.620	132.371	0.011	0.000	Maher *et al*. (2015)
AFRC	HSPT	-56.620	132.371	0.043	4.090	Maher *et al*. (2015)
AFRC	HSPT	-71.137	136.171	0.184	5.113	Maher *et al*. (2015)
AFRC	HSPT	-70.481	134.835	0.385	6.023	Maher *et al*. (2015)
AFRC	HSPT	-70.455	134.630	0.410	6.132	Maher *et al*. (2015)
AFRC	HSPT	-70.263	132.775	0.635	7.127	Maher *et al*. (2015)
AFRC	HSPT	-69.889	131.157	0.859	8.122	Maher *et al*. (2015)
AFRC	HSPT	-69.306	129.695	1.083	9.116	Maher *et al*. (2015)
AFRC	HSPT	-68.571	128.282	1.306	10.111	Maher *et al*. (2015)
AFRC	HSPT	-67.783	126.982	1.517	11.056	Maher *et al*. (2015)
AFRC	HSPT	-67.739	126.913	1.528	11.105	Maher *et al*. (2015)
AFRC	HSPT	-66.886	125.608	1.751	12.077	Maher *et al*. (2015)
AFRC	HSPT	-66.123	124.472	1.973	13.048	Maher *et al*. (2015)
AFRC	HSPT	-65.376	123.380	2.196	14.020	Maher *et al*. (2015)
AFRC	HSPT	-64.650	122.350	2.419	14.992	Maher *et al*. (2015)
AFRC	HSPT	-63.983	121.402	2.642	15.964	Maher *et al*. (2015)
AFRC	HSPT	-63.976	121.392	2.644	15.974	Maher *et al*. (2015)
AFRC	HSPT	-63.343	120.510	2.864	16.830	Maher *et al*. (2015)
AFRC	HSPT	-62.759	119.714	3.087	17.694	Maher *et al*. (2015)

table S1 continued.

Reference Plate	Moving Plate	Latitude (°)	Longitude (°)	Rotation Angle (°)/ Rate (°/Myr) *	Age (Ma)	Reference
AFRC	HSPT	-62.193	118.991	3.310	18.558	Maher *et al*. (2015)
AFRC	HSPT	-61.675	118.340	3.532	19.423	Maher *et al*. (2015)
AFRC	HSPT	-61.609	118.264	3.561	19.535	Maher *et al*. (2015)
AFRC	HSPT	-61.164	117.804	3.755	20.409	Maher *et al*. (2015)
AFRC	HSPT	-60.661	117.409	3.977	21.414	Maher *et al*. (2015)
AFRC	HSPT	-60.144	117.176	4.199	22.419	Maher *et al*. (2015)
AFRC	HSPT	-59.585	117.121	4.421	23.424	Maher *et al*. (2015)
AFRC	HSPT	-59.005	117.200	4.642	24.429	Maher *et al*. (2015)
AFRC	HSPT	-58.404	117.400	4.864	25.434	Maher *et al*. (2015)
AFRC	HSPT	-58.052	117.568	4.986	25.987	Maher *et al*. (2015)
AFRC	HSPT	-57.741	117.742	5.085	26.492	Maher *et al*. (2015)
AFRC	HSPT	-57.054	118.157	5.306	27.613	Maher *et al*. (2015)
AFRC	HSPT	-56.346	118.624	5.528	28.734	Maher *et al*. (2015)
AFRC	HSPT	-56.054	118.820	5.617	29.183	Maher *et al*. (2015)
AFRC	HSPT	-55.614	119.117	5.750	29.844	Maher *et al*. (2015)
AFRC	HSPT	-54.856	119.640	5.971	30.945	Maher *et al*. (2015)
AFRC	HSPT	-54.073	120.200	6.193	32.047	Maher *et al*. (2015)
AFRC	HSPT	-53.285	120.772	6.415	33.148	Maher *et al*. (2015)
AFRC	HSPT	-53.237	120.808	6.428	33.214	Maher *et al*. (2015)
AFRC	HSPT	-52.482	121.381	6.637	34.126	Maher *et al*. (2015)
AFRC	HSPT	-51.667	121.997	6.860	35.096	Maher *et al*. (2015)
AFRC	HSPT	-50.824	122.624	7.083	36.066	Maher *et al*. (2015)
AFRC	HSPT	-49.971	123.237	7.308	37.036	Maher *et al*. (2015)
AFRC	HSPT	-49.113	123.842	7.534	38.007	Maher *et al*. (2015)
AFRC	HSPT	-48.239	124.449	7.763	38.977	Maher *et al*. (2015)
AFRC	HSPT	-47.346	125.061	7.994	39.947	Maher *et al*. (2015)
AFRC	HSPT	-47.228	125.142	8.024	40.073	Maher *et al*. (2015)
AFRC	HSPT	-46.434	125.682	8.230	40.876	Maher *et al*. (2015)
AFRC	HSPT	-45.528	126.279	8.472	41.798	Maher *et al*. (2015)
AFRC	HSPT	-44.611	126.868	8.721	42.721	Maher *et al*. (2015)
AFRC	HSPT	-43.872	127.330	8.925	43.450	Maher *et al*. (2015)
AFRC	HSPT	-43.670	127.455	8.980	43.670	Maher *et al*. (2015)
AFRC	HSPT	-42.681	128.062	9.254	44.716	Maher *et al*. (2015)
AFRC	HSPT	-41.659	128.671	9.542	45.762	Maher *et al*. (2015)
AFRC	HSPT	-40.584	129.274	9.847	46.808	Maher *et al*. (2015)
AFRC	HSPT	-39.569	129.838	10.139	47.760	Maher *et al*. (2015)
AFRC	HSPT	-39.464	129.895	10.169	47.855	Maher *et al*. (2015)
AFRC	HSPT	-38.260	130.525	10.511	48.914	Maher *et al*. (2015)
AFRC	HSPT	-37.408	130.950	10.760	49.666	Maher *et al*. (2015)

table S1 continued.

Reference Plate	Moving Plate	Latitude (°)	Longitude (°)	Rotation Angle (°)/ Rate (°/Myr) *	Age (Ma)	Reference
AFRC	HSPT	-37.062	131.119	10.864	50.003	Maher *et al*. (2015)
AFRC	HSPT	-35.892	131.675	11.228	51.167	Maher *et al*. (2015)
AFRC	HSPT	-34.759	132.182	11.598	52.330	Maher *et al*. (2015)
AFRC	HSPT	-33.667	132.646	11.970	53.493	Maher *et al*. (2015)
AFRC	HSPT	-33.297	132.799	12.101	53.900	Maher *et al*. (2015)
AFRC	HSPT	-32.620	133.070	12.342	54.166	Maher *et al*. (2015)
AFRC	HSPT	-31.609	133.458	12.711	55.421	Maher *et al*. (2015)
AFRC	HSPT	-30.733	133.777	13.040	57.101	Maher *et al*. (2015)
AFRC	HSPT	-30.637	133.813	13.076	57.207	Maher *et al*. (2015)
AFRC	HSPT	-29.702	134.155	13.434	58.270	Maher *et al*. (2015)
AFRC	HSPT	-28.873	134.459	13.757	59.237	Maher *et al*. (2015)
AFRC	HSPT	-28.792	134.489	13.788	59.321	Maher *et al*. (2015)
AFRC	HSPT	-27.909	134.819	14.137	60.252	Maher *et al*. (2015)
AFRC	HSPT	-27.053	135.139	14.483	61.184	Maher *et al*. (2015)
AFRC	HSPT	-26.211	135.464	14.824	62.115	Maher *et al*. (2015)
AFRC	HSPT	-25.381	135.795	15.158	63.047	Maher *et al*. (2015)
AFRC	HSPT	-24.567	136.125	15.486	63.979	Maher *et al*. (2015)
AFRC	HSPT	-23.772	136.451	15.808	64.910	Maher *et al*. (2015)
AFRC	HSPT	-23.002	136.773	16.119	65.842	Maher *et al*. (2015)
AFRC	HSPT	-22.497	136.987	16.324	66.380	Maher *et al*. (2015)
AFRC	HSPT	-22.266	137.084	16.420	66.770	Maher *et al*. (2015)
AFRC	HSPT	-21.578	137.371	16.710	67.693	Maher *et al*. (2015)
AFRC	HSPT	-20.986	137.609	16.991	68.616	Maher *et al*. (2015)
AFRC	HSPT	-20.681	137.687	17.258	69.540	Maher *et al*. (2015)
AFRC	HSPT	-20.935	137.424	17.508	70.463	Maher *et al*. (2015)
AFRC	HSPT	-21.694	136.848	17.742	71.386	Maher *et al*. (2015)
AFRC	HSPT	-21.768	136.794	17.757	71.451	Maher *et al*. (2015)
AFRC	HSPT	-22.934	135.959	17.959	72.454	Maher *et al*. (2015)
AFRC	HSPT	-24.441	134.879	18.167	73.532	Maher *et al*. (2015)
AFRC	HSPT	-25.487	134.131	18.288	74.201	Maher *et al*. (2015)
AFRC	HSPT	-26.146	133.660	18.362	74.598	Maher *et al*. (2015)
AFRC	HSPT	-27.923	132.405	18.557	75.641	Maher *et al*. (2015)
AFRC	HSPT	-29.726	131.136	18.759	76.685	Maher *et al*. (2015)
AFRC	HSPT	-31.262	130.085	18.972	77.729	Maher *et al*. (2015)
AFRC	HSPT	-32.104	129.600	19.209	78.773	Maher *et al*. (2015)
AFRC	HSPT	-31.997	129.935	19.470	79.816	Maher *et al*. (2015)
AFRC	HSPT	-31.924	130.019	19.493	79.900	Maher *et al*. (2015)
AFRC	HSPT	-30.689	131.373	19.770	80.657	Maher *et al*. (2015)

table S1 continued.

Reference Plate	Moving Plate	Latitude (°)	Longitude (°)	Rotation Angle (°)/ Rate (°/Myr) *	Age (Ma)	Reference
AFRC	HSPT	-29.096	133.058	20.088	81.479	Maher *et al*. (2015)
AFRC	HSPT	-27.512	134.714	20.395	82.301	Maher *et al*. (2015)
AFRC	HSPT	-26.092	136.170	20.689	83.124	Maher *et al*. (2015)
AFRC	HSPT	-25.268	136.999	20.876	83.650	Maher *et al*. (2015)
AFRC	HSPT	-28.553	125.940	22.042	85.000	Maher *et al*. (2015)
AFRC	HSPT	-27.093	127.042	24.145	90.000	Maher *et al*. (2015)
AFRC	HSPT	-25.897	129.121	26.545	95.000	Maher *et al*. (2015)
AFRC	HSPT	-24.850	130.640	28.990	100.000	Maher *et al*. (2015)
AFRC	HSPT	-24.175	133.162	31.067	105.000	Maher *et al*. (2015)
AFRC	HSPT	-23.550	135.350	33.190	110.000	Maher *et al*. (2015)
AFRC	HSPT	-22.699	137.354	35.036	115.000	Maher *et al*. (2015)
AFRC	HSPT	-21.910	139.140	36.920	120.000	Maher *et al*. (2015)
AFRC	HSPT	-21.667	139.223	38.270	125.000	Maher *et al*. (2015)
AFRC	HSPT	-21.440	139.300	39.620	130.000	Maher *et al*. (2015)
AFRC	HSPT	-21.841	139.592	40.774	135.000	Maher *et al*. (2015)
AFRC	HSPT	-22.220	139.870	41.930	140.000	Maher *et al*. (2015)
AFRC	HSPT	-22.022	139.728	42.535	145.000	Maher *et al*. (2015)
AFRC	HSPT	-21.830	139.590	43.140	150.000	Maher *et al*. (2015)

Key: **AFRC:** African, **COCO:** Cocos, **EANT:** East Antarctica, **HSPT:** Hotspot reference frame, **NAZC:** Nazca, **PCFC:** Pacific, **SOAM:** South American, **WANT:** West Antarctica.

TABLE S2. CALCULATED RECONSTRUCTION PARAMETERS AT 1 MYR INCREMENTS.

Plate 1	Plate 2	Age (Ma)	Longitude (º)	Latitude (º)	Angle (º)/ Rate (º/Myr)*
SOAM	NAZC	0	-34.3	63.9	*2.6
SOAM	NAZC	1	-99.7	51.5	0.7
SOAM	NAZC	2	-99.2	54.5	1.5
SOAM	NAZC	3	-100.5	55.5	2.3
SOAM	NAZC	4	-101.6	59.1	3.2
SOAM	NAZC	5	-101.7	61.3	4.0
SOAM	NAZC	6	-101.9	55.1	5.0
SOAM	NAZC	7	-102.0	49.8	6.0
SOAM	NAZC	8	-101.3	51.4	7.0
SOAM	NAZC	9	-101.4	55.9	8.2
SOAM	NAZC	10	-101.3	56.9	9.3
SOAM	NAZC	11	-100.5	57.2	10.5
SOAM	NAZC	12	-99.5	57.5	11.4

table S2 continued.

Plate 1	Plate 2	Age (Ma)	Longitude (º)	Latitude (º)	Angle (º)/ Rate (º/Myr)*
SOAM	NAZC	13	-100.2	58.8	12.3
SOAM	NAZC	14	-103.7	60.8	13.5
SOAM	NAZC	15	-106.0	61.7	15.0
SOAM	NAZC	16	-104.3	60.4	16.4
SOAM	NAZC	17	-102.2	59.1	18.0
SOAM	NAZC	18	-99.4	58.1	20.0
SOAM	NAZC	19	-96.5	57.2	22.5
SOAM	NAZC	20	-95.1	56.4	24.2
SOAM	NAZC	21	-93.9	56.1	25.4
SOAM	NAZC	22	-92.3	55.7	27.2
SOAM	NAZC	23	-91.2	55.5	28.5
SOAM	NAZC	24	-91.2	56.3	29.3
SOAM	NAZC	25	-92.1	58.0	29.8
SOAM	NAZC	26	-93.7	60.2	30.2
SOAM	NAZC	27	-95.9	62.6	30.4
SOAM	NAZC	28	-98.6	64.7	30.6
SOAM	NAZC	29	-100.8	66.4	31.0
SOAM	NAZC	30	-103.3	67.7	31.5
SOAM	NAZC	31	-105.4	68.8	32.1
SOAM	NAZC	32	-107.3	69.9	33.0
SOAM	NAZC	33	-110.3	70.8	33.9
SOAM	NAZC	34	-114.1	71.9	34.9
SOAM	NAZC	35	-118.5	73.1	36.2
SOAM	NAZC	36	-123.7	74.2	37.2
SOAM	NAZC	37	-129.0	75.4	38.3
SOAM	NAZC	38	-134.2	76.6	39.6
SOAM	NAZC	39	-140.2	77.4	41.0
SOAM	NAZC	40	-146.4	77.7	42.5
SOAM	NAZC	41	-152.2	77.6	44.1
SOAM	NAZC	42	-156.9	77.4	45.9
SOAM	NAZC	43	-161.4	77.2	47.3
SOAM	NAZC	44	-165.6	76.8	48.4
SOAM	NAZC	45	-169.3	76.3	49.3
SOAM	NAZC	46	-172.5	75.9	50.1
SOAM	NAZC	47	-175.6	75.5	50.9
SOAM	NAZC	48	-178.4	75.1	51.6

table S2 continued.

Plate 1	Plate 2	Age (Ma)	Longitude (º)	Latitude (º)	Angle (º)/ Rate (º/Myr)*
SOAM	NAZC	49	178.8	74.6	52.4
SOAM	NAZC	50	176.0	74.2	53.2
SOAM	NAZC	51	173.3	73.8	53.9
SOAM	NAZC	52	170.8	73.4	54.7
SOAM	NAZC	53	168.4	73.0	55.6
SOAM	NAZC	54	166.0	72.7	56.5
SOAM	NAZC	55	163.3	72.4	57.5
SOAM	NAZC	56	160.8	72.0	58.4
SOAM	NAZC	57	158.5	71.6	59.2
SOAM	NAZC	58	156.8	71.1	59.9
SOAM	NAZC	59	155.5	70.6	60.5
SOAM	NAZC	60	154.6	70.1	61.0
SOAM	NAZC	61	153.9	69.5	61.5
SOAM	NAZC	62	153.1	69.0	62.0
SOAM	NAZC	63	152.3	68.5	62.7
SOAM	NAZC	64	151.3	68.0	63.4
SOAM	NAZC	65	150.2	67.5	64.3
SOAM	NAZC	66	149.0	67.1	65.3
SOAM	NAZC	67	148.0	66.6	66.4
SOAM	NAZC	68	147.2	66.1	67.5
SOAM	NAZC	69	146.5	65.6	68.6
SOAM	NAZC	70	146.0	65.1	69.8
SOAM	NAZC	71	145.5	64.6	71.0
SOAM	NAZC	72	145.0	64.1	72.2
SOAM	NAZC	73	144.6	63.5	73.4
SOAM	NAZC	74	144.0	63.0	74.5
SOAM	NAZC	75	143.3	62.4	75.5
SOAM	NAZC	76	142.6	61.8	76.4
SOAM	NAZC	77	141.8	61.2	77.3
SOAM	NAZC	78	140.9	60.6	78.1
SOAM	NAZC	79	140.1	59.9	79.0
SOAM	NAZC	80	139.4	59.2	79.8
NAZC	HSPT	0	92.2	-55.9	*2.6
NAZC	HSPT	1	98.5	3.1	0.4
NAZC	HSPT	2	96.0	-1.7	0.9

table S2 continued.

Plate 1	Plate 2	Age (Ma)	Longitude (º)	Latitude (º)	Angle (º)/ Rate (º/Myr)*
NAZC	HSPT	3	98.5	-7.7	1.3
NAZC	HSPT	4	106.7	-17.6	1.5
NAZC	HSPT	5	103.6	-26.2	1.9
NAZC	HSPT	6	96.4	-21.2	2.7
NAZC	HSPT	7	92.3	-17.6	3.7
NAZC	HSPT	8	92.4	-23.4	4.2
NAZC	HSPT	9	93.7	-32.7	4.7
NAZC	HSPT	10	93.4	-38.4	5.4
NAZC	HSPT	11	95.3	-38.7	6.1
NAZC	HSPT	12	96.2	-40.6	6.7
NAZC	HSPT	13	95.0	-44.8	7.2
NAZC	HSPT	14	90.5	-50.2	8.0
NAZC	HSPT	15	86.1	-53.5	9.1
NAZC	HSPT	16	87.2	-52.5	10.3
NAZC	HSPT	17	88.5	-51.5	11.7
NAZC	HSPT	18	89.7	-50.8	13.3
NAZC	HSPT	19	90.7	-50.5	15.7
NAZC	HSPT	20	90.8	-50.2	17.6
NAZC	HSPT	21	90.2	-49.9	18.8
NAZC	HSPT	22	89.9	-49.8	21.0
NAZC	HSPT	23	89.2	-49.9	22.7
NAZC	HSPT	24	87.3	-50.9	23.9
NAZC	HSPT	25	84.6	-52.5	24.7
NAZC	HSPT	26	81.1	-54.5	25.2
NAZC	HSPT	27	77.0	-56.6	25.4
NAZC	HSPT	28	72.9	-58.4	25.6
NAZC	HSPT	29	69.3	-59.7	25.9
NAZC	HSPT	30	66.3	-60.7	26.2
NAZC	HSPT	31	63.6	-61.5	26.5
NAZC	HSPT	32	61.0	-62.2	26.9
NAZC	HSPT	33	57.9	-63.0	27.5
NAZC	HSPT	34	54.0	-63.9	28.3
NAZC	HSPT	35	49.3	-64.8	29.1
NAZC	HSPT	36	44.2	-65.8	30.0
NAZC	HSPT	37	38.9	-66.8	30.8

table S2 continued.

Plate 1	Plate 2	Age (Ma)	Longitude (º)	Latitude (º)	Angle (º)/ Rate (º/Myr)*
NAZC	HSPT	38	33.6	-67.7	31.5
NAZC	HSPT	39	28.3	-68.3	32.3
NAZC	HSPT	40	23.1	-68.5	33.2
NAZC	HSPT	41	18.5	-68.5	34.3
NAZC	HSPT	42	14.7	-68.4	35.6
NAZC	HSPT	43	11.6	-68.1	36.7
NAZC	HSPT	44	9.1	-67.6	37.7
NAZC	HSPT	45	7.4	-67.1	38.6
NAZC	HSPT	46	6.6	-66.5	39.4
NAZC	HSPT	47	6.5	-65.9	40.3
NAZC	HSPT	48	6.5	-65.3	41.1
NAZC	HSPT	49	5.9	-64.7	41.9
NAZC	HSPT	50	4.0	-64.2	42.7
NAZC	HSPT	51	0.8	-63.8	43.4
NAZC	HSPT	52	-1.9	-63.3	44.3
NAZC	HSPT	53	-4.0	-62.9	45.1
NAZC	HSPT	54	-5.9	-62.4	46.0
NAZC	HSPT	55	-7.6	-62.0	46.9
NAZC	HSPT	56	-9.3	-61.5	47.7
NAZC	HSPT	57	-10.9	-61.0	48.5
NAZC	HSPT	58	-12.4	-60.5	49.3
NAZC	HSPT	59	-13.8	-59.9	50.2
NAZC	HSPT	60	-15.2	-59.3	51.0
NAZC	HSPT	61	-16.4	-58.7	51.8
NAZC	HSPT	62	-17.6	-58.0	52.7
NAZC	HSPT	63	-18.7	-57.4	53.5
NAZC	HSPT	64	-19.7	-56.7	54.4
NAZC	HSPT	65	-20.6	-56.0	55.3
NAZC	HSPT	66	-21.4	-55.4	56.3
NAZC	HSPT	67	-22.2	-54.7	57.2
NAZC	HSPT	68	-22.8	-54.0	58.2
NAZC	HSPT	69	-23.5	-53.4	59.3
NAZC	HSPT	70	-24.1	-52.7	60.3
NAZC	HSPT	71	-24.8	-52.1	61.4
NAZC	HSPT	72	-25.4	-51.6	62.6

table S2 continued.

Plate 1	Plate 2	Age (Ma)	Longitude (º)	Latitude (º)	Angle (º)/ Rate (º/Myr)*
NAZC	HSPT	73	-26.0	-51.0	63.9
NAZC	HSPT	74	-26.7	-50.5	65.1
NAZC	HSPT	75	-27.3	-50.0	66.3
NAZC	HSPT	76	-28.0	-49.5	67.4
NAZC	HSPT	77	-28.6	-49.1	68.4
NAZC	HSPT	78	-29.3	-48.7	69.4
NAZC	HSPT	79	-29.8	-48.4	70.1
NAZC	HSPT	80	-30.3	-48.1	70.7
NAZC	HSPT	81	-30.6	-47.9	71.1
NAZC	HSPT	82	-30.9	-47.7	71.3
NAZC	HSPT	83	-31.1	-47.6	71.4
NAZC	HSPT	84	-31.2	-47.5	71.5
NAZC	HSPT	85	-31.2	-47.5	71.5
NAZC	HSPT	86	-31.0	-47.5	71.6
NAZC	HSPT	87	-30.9	-47.6	71.7
NAZC	HSPT	88	-30.7	-47.7	71.9
NAZC	HSPT	89	-30.4	-47.8	72.4
NAZC	HSPT	90	-30.2	-47.9	73.0
NAZC	HSPT	91	-30.0	-48.0	74.0
NAZC	HSPT	92	-29.7	-48.1	75.1
NAZC	HSPT	93	-29.5	-48.3	76.3
NAZC	HSPT	94	-29.2	-48.4	77.6
NAZC	HSPT	95	-28.9	-48.6	78.8
NAZC	HSPT	96	-28.6	-48.9	79.8
NAZC	HSPT	97	-28.3	-49.2	80.7
NAZC	HSPT	98	-28.0	-49.6	81.5
NAZC	HSPT	99	-27.6	-50.0	82.3
NAZC	HSPT	100	-27.3	-50.3	83.0
NAZC	HSPT	101	-26.9	-50.7	83.9
NAZC	HSPT	102	-26.5	-51.0	84.7
NAZC	HSPT	103	-26.1	-51.2	85.6
NAZC	HSPT	104	-25.7	-51.5	86.5
NAZC	HSPT	105	-25.3	-51.7	87.5
NAZC	HSPT	106	-25.1	-51.8	88.4
NAZC	HSPT	107	-24.8	-52.0	89.3

table S2 continued.

Plate 1	Plate 2	Age (Ma)	Longitude (º)	Latitude (º)	Angle (º)/ Rate (º/Myr)*
NAZC	HSPT	108	-24.7	-52.0	90.1
NAZC	HSPT	109	-24.6	-52.0	91.0
NAZC	HSPT	110	-24.7	-51.9	91.7
NAZC	HSPT	111	-24.9	-51.8	92.5
NAZC	HSPT	112	-25.2	-51.6	93.1
NAZC	HSPT	113	-25.6	-51.4	93.7
NAZC	HSPT	114	-26.0	-51.1	94.3
NAZC	HSPT	115	-26.5	-50.7	94.9
NAZC	HSPT	116	-27.0	-50.3	95.6
NAZC	HSPT	117	-27.5	-49.9	96.2
NAZC	HSPT	118	-28.1	-49.4	96.9
NAZC	HSPT	119	-28.5	-49.0	97.6
NAZC	HSPT	120	-29.0	-48.5	98.5
NAZC	HSPT	121	-29.4	-48.1	99.4
NAZC	HSPT	122	-29.7	-47.7	100.4
NAZC	HSPT	123	-29.9	-47.3	101.5
NAZC	HSPT	124	-30.1	-46.9	102.6
NAZC	HSPT	125	-30.2	-46.6	103.8
NAZC	HSPT	126	-30.2	-46.3	104.9
NAZC	HSPT	127	-30.2	-46.1	106.0
NAZC	HSPT	128	-30.2	-45.8	107.0
NAZC	HSPT	129	-30.2	-45.6	107.9
NAZC	HSPT	130	-30.1	-45.4	108.8
NAZC	HSPT	131	-30.0	-45.2	109.6
NAZC	HSPT	132	-29.8	-45.0	110.4
NAZC	HSPT	133	-29.6	-44.8	111.2
NAZC	HSPT	134	-29.3	-44.6	112.0
NAZC	HSPT	135	-29.0	-44.5	112.7
NAZC	HSPT	136	-28.7	-44.4	113.3
NAZC	HSPT	137	-28.5	-44.4	113.9
NAZC	HSPT	138	-28.2	-44.5	114.4
NAZC	HSPT	139	-28.0	-44.5	114.9
NAZC	HSPT	140	-27.8	-44.6	115.4
NAZC	HSPT	141	-27.6	-44.7	116.0
NAZC	HSPT	142	-27.5	-44.8	116.5

table S2 continued.

Plate 1	Plate 2	Age (Ma)	Longitude (º)	Latitude (º)	Angle (º)/ Rate (º/Myr)*
NAZC	HSPT	143	-27.4	-44.9	117.1
NAZC	HSPT	144	-27.3	-45.0	117.7
NAZC	HSPT	145	-27.2	-45.1	118.4
NAZC	HSPT	146	-27.1	-45.2	119.0
NAZC	HSPT	147	-27.0	-45.3	119.6
NAZC	HSPT	148	-26.9	-45.3	120.2
NAZC	HSPT	149	-26.8	-45.4	120.7
NAZC	HSPT	150	-26.6	-45.5	121.1

Key: **HSPT:** Hotspot reference frame; either Pacific or Atlantic-Indian Ocean, **NAZC:** Nazca, **SOAM:** South American.

Uncertainties in global plate reconstructions - an unsolved problem

The conventional method of derivation of relative plate reconstructions of corresponding magnetic isochrons and fracture zone offsets is that of Hellinger (1981; *e.g.*, Kirkwood *et al.*, 1999). Three unknown parameters are sought: the latitude and longitude of the finite pole of rotation, and the counterclockwise angle of rotation. However, additional parameters are required, defining great circle segments which fit separate clusters of magnetic isochron, and fracture zone offset identifications. Each segment requires two parameters, for example the latitude and longitude of the pole to its fitted great circle. Thus, the reconstruction produces three plus two times the number of great circle segments; a typical reconstruction might involve ten segments, thus requiring 23 parameters. (Each segment must have a minimum of three distinct identifications to produce a unique great circle fit.) The fitting criterion is minimization of the sum of the squared distance of each data point from its corresponding great circle segment as a function of the parameters. The problem includes non-linear components and, therefore, an iterative process of searching out the optimal solution.

If uncertainties in the location of each data point are available, the algorithm can incorporate the uncertainties as weights in the least-squares solution. Conventional applications produce “estimates” of the rotation parameters plus uncertainties, including variances and covariances, from which ellipsoids of uncertainty can be constructed for the three parameters. What are the sources of uncertainty in individual identifications? Navigation, modeling of isochrons, and width of fracture zones are most relevant, recognizing that the obliquity of the navigation to the linear feature contributes to the uncertainty. (Further, note that the uncertainty is measured in distance units, not age) The non-linearity of the problem means that the ellipsoid of uncertainty is itself an approximation of error. More importantly, however, note that the uncertainties in the great circle segment parameters are largely ignored and treated as nuisance factors.

The calculation of global reconstructions by composing plate-pair reconstructions, including uncertainties, is straightforward if the ages across each pair are all the same. However, should ages of reconstructions vary among the plate pairs, interpolation is required. Conventional interpolation assumes constant finite difference poles and rotation rates between finite rotations. Alternatively, spline interpolation of pseudovectors representing the rotation parameters (with magnitude equal to rotation rate) may be utilized. The latter may be more realistic in that the conventional approach forces changes in rotations to correspond with the finite reconstruction isochrons, which are usually most confidently identified for near-constant spreading directions, not times of significant rotation changes. In either case, interpolation of uncertainties is indeterminant, since the source uncertainties are measured in distance, not time; interpolation necessarily involves rates, therefore time, as well as distance.

Various studies which include interpolation may report uncertainties, but their meaning is itself uncertain. The finite rotation parameterization assumption is kinematic rigidity of plates, a tested keystone of the theory of plate tectonics. However, there is no geologically meaningful consensus on parameterizing motions *between* finite reconstructions. Consequently, there is no clear rationale for any uncertainty interpolation method. Further, neglecting uncertainties in great circle segment poles as "nuisance parameters" lacks any rationale, beyond convenience, as well.

Plate-Hotspot models and East Africa magmatism

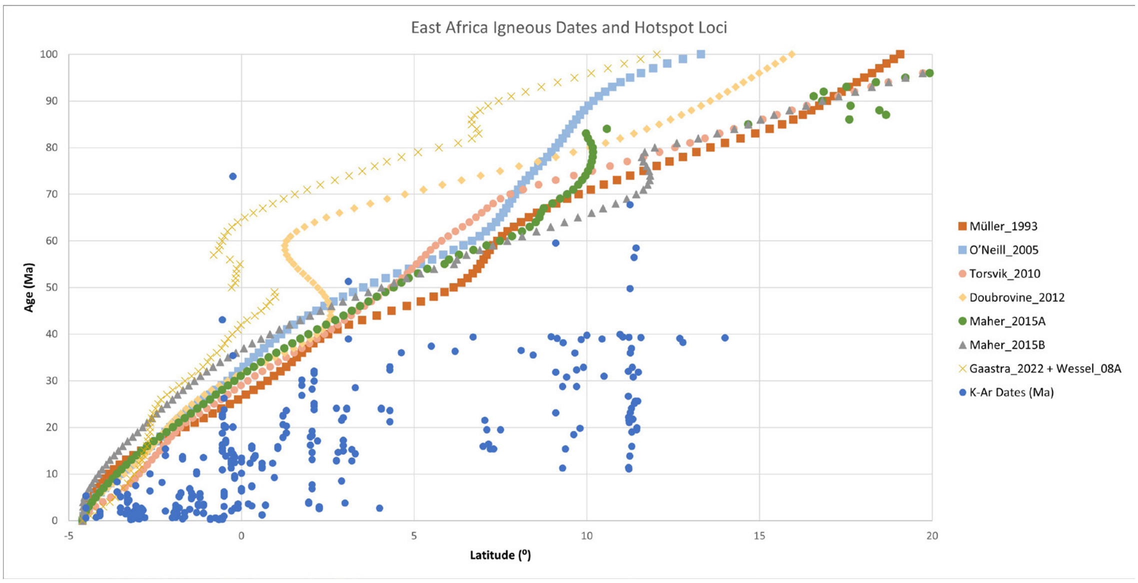

FIG. S3. Plot of isotopic dates from igneous rocks, East Africa (compilation of Pilger, 2003) versus latitude, plus calculated loci of hypothetical hotspot, arbitrarily located at 33ºE and -4.6ºS. Loci are based on reconstruction models from Muller *et al*. (1993, 2019), O'Neill *et al*. (2005); Torsvik *et al*. (2010); Doubrovine *et al*. (2012); Maher *et al*. (2015); Gaastra *et al*. (2022).

Supplementary References

Cande, S.C.; Patriat, P. 2015. The anticorrelated velocities of Africa and India in the Late Cretaceous and early Cenozoic. Geophysical Journal International 200 (1): 227-243. doi: https://doi.org/10.1093/gji/ggu392

Croon, M.B.; Cande, S.C.; Stock, J.M. 2008. Revised Pacific-Antarctic plate motions and geophysics of the Menard Fracture Zone. Geochemistry, Geophysics, Geosystems 9 (7): Q07001. doi: https://doi.org/10.1029/2008GC002019

DeMets, C.; Merkouriev, S. 2019. High-resolution reconstructions of Nubia, North America, and Antarctic plate motions relative to South America: 34 Ma to present. Geophysical Journal International 217 (3): 1821-1853. doi: https://doi.org/10.1093/gji/ggz087

DeMets, C.; Gordon, R.G.; Argus, D.F. 2010. Geologically current plate motions. Geophysical Journal International 181 (1): 1-80. doi: https://doi.org/10.1111/j.1365-246X.2009.04491.x

DeMets, C.; Merkouriev, S.; Sauter, D. 2021. High resolution reconstructions of the Southwest Indian Ridge, 52 Ma to present: implications for the breakup and absolute motion of the Africa plate. Geophysical Journal International 226 (3): 1461-1497. doi: https://doi.org/10.1093/gji/ggab107

Doubrovine, P.V.; Steinberger, B.; Torsvik, T.H. 2012. Absolute plate motions in a reference frame defined by moving hotspots in the Pacific, Atlantic and Indian Oceans. Journal of Geophysical Research 117: B09101. doi. https://doi.org/10.1029/2011JB009072

Gaastra, K.M.; Gordon, R.G.; Woodworth, D.T. 2022. Quantification of Pacific Plate hotspot tracks since 80 Ma. Tectonics 41(7): e2021TC006772. doi: https://doi.org/10.1029/2021TC006772

Granot, R.; Dyment, J. 2018. Late Cenozoic unification of East and West Antarctica. Nature Communications 9: 3189. doi: https://doi.org/10.1038/s41467-018-05270-w

Granot, R.; Cande, S.C.; Stock, J.M.; Damaske, D. 2013. Revised Eocene-Oligocene kinematics for the West Antarctic rift system. Geophysical Research Letters 40 (2): 279-284. doi: https://doi.org/10.1029/2012GL054181

Gripp, A.E.; Gordon, R.G. 2002. Young tracks of hotspots and current plate velocities. Geophysical Journal International 150 (2): 321-361. doi: https://doi.org/10.1046/j.1365-246X.2002.01627.x

Hellinger, S.J. 1981. The uncertainties of finite rotations in plate tectonics, Journal of Geophysical Research 86 (B10): 9312-9318. doi: https://doi.org/10.1029/JB086iB10p09312

Kirkwood, B.H.; Royer, J.-Y.; Chang, T.C.; Gordon, R.G. 1999. Statistical tools for estimating and combining finite rotations and their uncertainties. Geophysical Journal International 137 (2): 408-428. doi: https://doi.org/10.1046/j.1365-246X.1999.00787.x

König, M.; Jokat, W. 2006. The Mesozoic breakup of the Weddell Sea. Journal of Geophysical Research 111: B12102, doi: https://doi.org/10.1029/2005JB004035

Lonsdale, P. 2005. Creation of the Cocos and Nazca plates by fission of the Farallon plate. Tectonophysics 404(3): 237-264. doi: https://doi.org/10.1016/j.tecto.2005.05.011

Maher, S.M.; Wessel, P.; Müller, R.D.; Williams, S.E.; Harada, Y. 2015. Absolute plate motion of Africa around Hawaii-Emperor bend time. Geophysical Journal International 201 (3): 1743-1764. doi: https://doi.org/10.1093/gji/ggv104

Marks, K.; Stock, J. 2001. Evolution of the Malvinas plate south of Africa. Marine Geophysical Researches 22: 289-302. doi: https://doi.org/10.1023/A:1014638325616

Matthews, K.J.; Williams, S.E.; Whittaker, J.M.; Müller, R.D.; Seton, M.; Clarke, G.L. 2015. Geologic and kinematic constraints on Late Cretaceous to mid Eocene plate boundaries in the southwest Pacific. Earth-Science Reviews 140: 72-107. doi: https://doi.org/10.1016/j.Earscirev.2014.10.008

Müller, R.D.; Royer, J.-Y.; Lawver, L.A. 1993. Revised plate motions relative to the hotspots from combined Atlantic and Indian Ocean hotspot tracks. Geology 21 (3): 275-278. doi: https://doi.org/10.1130/0091-7613(1993)021%3C0275:RPMRTT%3E2.3.CO;2

Müller, R.D.; Sdrolias, M.; Gaina, C.; Roest, W.R. 2008. Age, spreading rates, and spreading asymmetry of the world's ocean crust. Geochemistry, Geophysics, Geosystems 9 (4). doi: https://doi.org/10.1029/2007GC001743

Müller, R.D.; Zahirovic, S.; Williams, S.E.; Cannon, J.; Seton, M.; Bower, D.J.; Tetley, M.G.; Heine1, C.; Le Breton, E.; Liu, S.; Russell, S.H.J.; Yang, T.; Leonard, J.; Gurnis, M. 2019. A global plate model including lithospheric deformation along major rifts and orogens since the Triassic. Tectonics 38 (6): 1884-1907. doi: https://doi.org/10.1029/2018TC005462

Norton, I.O. 2000. Global hotspot reference frames and plate motion. *In* The history and dynamics of global plate motions (Richards, M.A; Gordon, R.G.; van der Hilst, R.D.; editors). American Geophysical Union, Geophysical Monograph 121: 339-357.

Ogg, J.G. 2020. Geomagnetic Polarity Time Scale. *In* Geologic Time Scale 2020 (Gradstein, F.M.; Ogg, J.G.; Schmitz, M.D.; Ogg, G.M.; editors). Elsevier 1: 159-192. Amsterdam.

O'Neill, C.; Müller, R.D.; Steinberger, B. 2005. On the uncertainties in hot spot reconstructions and the significance of moving hot spot reference frames. Geochemistry, Geophysics, Geosystems 6 (4): Q04003. doi: https://doi.org/10.1029/2004GC000784

Pérez-Díaz, L.; Eagles, G. 2014. Constraining South Atlantic growth with seafloor spreading data. Tectonics 33 (9): 1848-1873. doi: https://doi.org/10.1002/2014TC003644

Pilger, R.H.Jr. 2003. Geokinematics - Prelude to Geodynamics. Springer, New York. doi: https://doi.org/10.1007/978-3-662-07439-8.

Raymond, C.A.; Stock, J.M.; Cande, S.C. 2000. Fast Paleogene motion of the Pacific hotspots from revised global plate circuit constraints. In the history and dynamics of global plate motions (Richards, M.A.; Gordon, R.G.; van der Hilst, R.D.; editors). American Geophysical Union, Geophysical Monograph 121: 359-375.

Rowan, C.J.; Rowley, D.B. 2014. Spreading behaviour of the Pacific-Farallon ridge system since 83 Ma. Geophysical Journal International 197 (3): 1273-1283. doi: https://doi.org/10.1093/gji/ggu056

Seton, M.; Müller, R.D.; Zahirovic, S.; Gaina, C.; Torsvik, T.; Shephard, G.; Talsma, A.; Gurnis, M.; Turner, M.; Maus, S.; Chandler, M. 2012. Global continental and ocean basin reconstructions since 2000 Ma. Earth-Science Reviews 113 (3-4): 212-270. doi: https://doi.org/10.1016/j.earscirev.2012.03.002

Tebbens, S.F.; Cande, S.C. 1997. Southeast Pacific tectonic evolution from Early Oligocene to Present. Journal of Geophysical Research, Solid Earth 102 (B6): 12061-12084. doi: https://doi.org/10.1029/96JB02582

Torsvik, T.H.; Steinberger, B.; Gurnis, M.; Gaina, C. 2010. Plate tectonics and net lithosphere rotation over the past 150 My. Earth and Planetary Science Letters 291: 106-112. doi: https://doi.org/10.1016/j.epsl.2009.12.055

Torsvik, T.H.; Steinberger, B.; Shephard, G.E.; Doubrovine, P.V.; Gaina, C.; Domeier, M.; Conrad, C.P.; Sager, W.W. 2019. Pacific-Panthalassic reconstructions: Overview, errata and the way forward. Geochemistry, Geophysics, Geosystems 20 (7): 3659-3689. doi: https://doi.org/10.1029/2019GC008402

Wilder, D.T. 2003. Relative motion history of the Pacific-Nazca (Farallon) plates since 30 million years ago. M.Sc. Thesis (Unpublished), University of South Florida: 94 p.

Wilson, D.S. 1996. Fastest known spreading on the Miocene Cocos-Pacific Plate Boundary. Geophysical Research Letters 23 (21): 3003-3006. doi: https://doi.org/10.1029/96GL02893

Wright, N.; Müller, R.D.; Seton, M.; Williams, S. 2016. The Late Cretaceous to recent tectonic history of the Pacific Ocean basin. Earth-Science Reviews 154: 138-173. doi: https://doi.org/10.1016/j.earscirev.2015.11.015